# Processing of local features in the zebrafish optic tectum

**By:**

Katharina Bergmann

A thesis submitted in partial fulfilment of the requirements for the degree of
Doctor of Philosophy

The University of Sheffield
Faculty of Science
Department of Biomedical Science

Submission Date: July 2018

# Acknowledgements

First, I would like to thank my supervisor, Anton, for his support and enthusiasm throughout my PhD. I would also like to thank my advisors, Vincent and Walter, who were always supportive, encouraging and ready with advice.

I am very grateful for having found so many good friends in BMS; thank you Montse, Elvira, Xiaoming, Eleni, Rike and Ciara, for your help and friendship over the years, for much-needed coffee breaks and sharing the ups and downs of our PhD/Postdoc journeys.

I am forever grateful to my parents and sister who have done everything to support me and have always believed in me.

Finally, Haris and Chris - you drive me mad, you make me laugh; you are my life.

# Declaration

Part of the work presented in this thesis has been published prior to submission: "Imaging Neuronal Activity in the Optic Tectum of Late Stage Larval Zebrafish, Journal of Developmental Biology 2018".

The article has been published under the Creative Commons Attribution License (CC BY 4.0) and the copyright retained with the authors.

# Table of contents

# Table of Figures

# Abstract

The optic tectum is the main visual processing area in zebrafish and is involved in a variety of visually-driven behaviours. A key question is how information about the visual environment is processed and integrated in order to generate guided behaviour. The aim of this study was to explore the response properties of tectal neurons, i.e., their preference for certain features of the visual input. To do this, I developed a custom set-up for calcium imaging and simultaneous visual stimulation in older zebrafish larvae, up to the age of 21 dpf. First, this set-up was employed to measure the spatial receptive fields of tectal neurons with small moving spots. Notably, the results suggested that receptive field development is not completed by 9 dpf as previously believed; instead, receptive field refinement continues beyond this age. The results also confirmed that receptive fields in the optic tectum were relatively large in older larvae. Based on this, I formulated the hypothesis that tectal neurons might process multiple local features simultaneously. To test how the optic tectum encodes local features, I used small, moving oriented bars and combinations of bars, i.e., angles. Tectal responses to these stimuli suggested that, not only does the optic tectum encode local features, but is also tuned to horizontal-oriented local stimuli. Finally, I used a set of moving stimuli, consisting of simple features (i.e., lines and angles) and a composite feature (i.e. square) to test how information about multiple local features was integrated by tectal neurons. The results indicated that local features are spatially integrated in a sublinear fashion. The outcomes of the work presented in this thesis add to our understanding of how visual information provided by the retina is processed within the optic tectum.

# Abbreviations

| | |
|---|---|
| AC | Amacrine cell |
| AF | Arborisation field |
| ANOVA | Analysis Of Variance |
| BC | Bipolar cell |
| CB | Cell bodies |
| cpd | cycles per degree |
| $\Delta F/F_0$ | Relative change of fluorescence signal |
| Dpf | Days-post-fertilisation |
| DS | Direction selectivity/selective |
| DSGC | Direction selective ganglion cell |
| GABA | gamma-Aminobutyric Acid |
| GC | Ganglion cell |
| GCL | Ganglion cell layer |
| GFP | Green fluorescent protein |
| HC | Horizontal cell |
| INL | Inner nuclear layer |
| IPL | Inner plexiform layer |
| LGN | Lateral geniculate nucleus |
| NBT | Neural-specific beta tubulin |
| NP | Neuropil |
| OKR | Optokinetic response |
| OMR | Optomotor response |
| ONL | Outer nuclear layer |
| OPL | Outer plexiform layer |
| OS | Orientation selectivity/selective |
| OSGC | Orientation selective ganglion cell |
| OSI | Orientation selectivity index |
| OT | Optic tectum |
| PVN | Periventricular neuron |
| RGC | Retinal ganglion cell |
| RF | Receptive field |

| | |
|---|---|
| ROI | Region of interest |
| SAC | Stratum album central |
| SD | Standard deviation |
| SEM | Standard error of the mean |
| SFGS | Stratum fibrosum et griseum |
| SIN | Superficial interneuron |
| SM | Stratum marginale |
| SO | Stratum opticum |
| SPV | Stratum periventriculare |

# Chapter 1

# Introduction

Vision is a key survival factor for many organisms. It allows the animal to effectively interact with its environment and appropriately respond to changes within this environment, e.g., escape a looming predator. Visual perception arises from a complex, multi-step process. Objects in the surrounding environment of an animal reflect light; the eye captures this light and photoreceptors in the retina transduce the incoming photons into electrical signals. Within the retina, a highly organised network of cells processes this signal to extract information. Ganglion cells, the output neurons of the retina, then transmit this information to the brain. In mammals, the majority of retinal fibres project to the thalamus, which relays information to the visual cortex. From there, the signal flows along two different pathways, the dorsal 'where' pathway and the ventral 'what' pathway, to two highly specialised areas in the neocortex, where cells respond to very complex visual stimuli. In lower vertebrates, the majority of retinal projections terminate in the optic tectum, which is regarded as the main visual processing centre in the absence of a neocortex.

In order to understand how visual perception arises, it is essential to determine what kind of information is extracted from the visual input, and how this information is processed along the visual pathway. Contemporary research in the field of visual neuroscience focuses on the circuitry behind the generation of visual perception in the brain and the zebrafish model is particularly well-suited for this (Friedrich et al., 2010). Zebrafish are small and translucent and provide easy (optical) access to the brain. They are highly visually-guided animals and, although they do not have a neocortex, they perform complex visual behaviours and display remarkable learning abilities (Kalueff et al., 2013; Roberts et al., 2013).

One of the most influential concepts in visual neuroscience is the concept of receptive fields. The receptive field of a cell provides a description of its response properties, i.e., the nature and position of a stimulus that excites the cell (Hartline, 1938). Measuring receptive fields in a population of cells can be used to determine what features, i.e., the basic units of visual information, are extracted at a particular stage of the visual pathway. Although a large body of literature on the properties of receptive fields in the retina, thalamus, and visual cortex exists, the precise role of the early visual system has yet to be fully understood (Carandini, 2005).

This introductory chapter sets the scene for the research presented in this thesis. Firstly, this chapter outlines the organisation and function of the zebrafish visual system. As the present study investigates visual processing in the optic tectum, particular emphasis will be placed on the zebrafish retino-tectal system. Secondly, it outlines the rationale behind the concept of receptive fields, with a focus on the early years and its role as feature detectors. A more detailed description of the spatial receptive fields in zebrafish is presented in Chapter 4. The spatio-temporal aspect and mathematical models of receptive fields are not discussed here, as they are beyond the scope of the research presented in this thesis. Finally, at the end of this chapter, the aim of this Ph.D. study is presented.

# 1.1 Processing of visual information in zebrafish

Zebrafish have become a popular model for studying the visual system (Saszik and Bilotta, 1999; Neuhauss, 2003). The development of their brain and nervous system, including the retina, is similar to most other vertebrates (Kimmel, 1993; Schmitt and Dowling, 1999). However, in contrast to well-established mammalian model organisms, the small size, easy (optical) accessibility and genetic amenability of zebrafish makes them ideal for the use of state-of-the-art *in vivo* microscopy and optogenetics (Friedrich et al., 2010; Del Bene and Wyart, 2011; Ahrens et al., 2013; Feierstein et al., 2015). Importantly, the behaviour of zebrafish is highly visually guided. Their visually-evoked behaviours range from relatively simple responses to light changes, e.g., visual startle (Easter and Nicola, 1996), to more elaborate directed behaviours, such as phototaxis (Burgess et al., 2010) and highly complex performances, e.g., prey capture (Gahtan, 2005), kin recognition (Hinz et al., 2013) and shoaling (Gerlai, 2014), which require a high degree of visual processing. Moreover, visual behaviour in zebrafish emerges early in development. Visual startle and eye tracking movements, also known as optokinetic response (OKR), have been observed as early as 68 hpf and 73 hpf, respectively (Easter and Nicola, 1996). Zebrafish larvae feed independently from 4–5 days-postfertilisation (dpf) onward (Clark, 1981), which suggests that by this time their visual system is already fully functional.

## 1.1.1 Vision begins in the retina

The vertebrate retina, located at the back of the eye, is a relatively small structure, compared to structures in other brain areas. Nerve cell bodies and synaptic areas in the retina are precisely organised in five distinct layers (Wässle, 2004) (Figure 1.1): i) the outer nuclear layer (ONL) consisting of the cell bodies of the photoreceptors (rods and cones); ii) the outer plexiform layer (OPL) consisting of synaptic connections between photoreceptors, bipolar, and horizontal cells; iii) the inner nuclear layer (INL) consisting of the cell bodies of horizontal, bipolar and amacrine cells, and the retinal ganglion cell somata form the ganglion cell layer (the dendrites and axons are organised in the plexiform layers, which are located between the nuclear layers); iv) the inner plexiform layer (IPL), consisting of connections between

bipolar, amacrine and ganglion cells; v) the ganglion cell layer (GCL) where the cell bodies of the ganglion cells

Information in the retina flows from the outer to the inner levels. Photoreceptors located in the outer retina transduce the incoming light into electrochemical signals. An intricate network of horizontal cells, bipolar cells and amacrine cells then processes the information, before retinal ganglion cells transmit feature-specific information (e.g., direction of movement or orientation of a stimulus) along multiple parallel channels to higher visual areas (Wässle, 2004; Masland, 2012a). While it remains unknown how many different retinal feature channels exist, and what exactly they encode, it is clear that retinal processing is far more complex than previously thought (Gollisch and Meister, 2010; Baden et al., 2016)Although, more than 60 years ago, Lettvin (1959) and Maturana (1960) noted that the complex structure of the retina should be reflected in its function, a simplistic model of retinal function prevailed for many decades. Because of the presence of simple centre-surround receptive fields in retinal ganglion cells, the role of the retina was reduced to light adaptation and contrast enhancement via lateral inhibition (Gollisch and Meister, 2010).
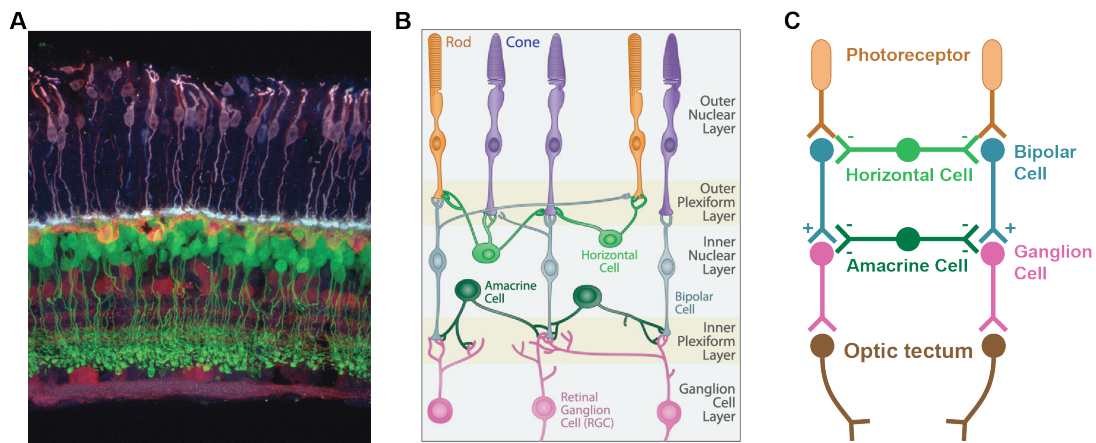
**Figure 1.1 Cellular organisation and synaptic connections of the vertebrate retina.** (**A**) Vertical section of the mouse retina with immunostaining for cones (purple), horizontal cells (orange), bipolar cells (green), amacrine and ganglion cells (magenta). Image by Josh Morgan (Rachel Wong Lab). (**B**) Schematic diagram of the vertebrate retina. The retina contains five types of neurons, and both cell bodies and neurites are precisely organised in distinct layers. (**C**) Schematic of synaptic connections in the retina. Excitatory synapses are indicated by '+' and inhibitory synapses by '-'. Panels (B) and (C) were slightly adapted from Sanes and Zipursky (2010).

## Photoreceptors transduce light into electrical signals and provide information on colour and light levels

The vertebrate retina contains two basic classes of photoreceptors; rods, which have a long integration time and mediate vision at low light levels, and cones, which function at higher light levels, respond much faster and mediate colour vision. The incoming light is absorbed by visual pigments, which are located in the outer segments of rods and cones. The visual pigments have a highly conserved structure and consist of a chromophore and an opsin; the wavelength specificity of photoreceptors depends on the type of opsin.

The zebrafish retina contains four types of cones, with different wavelength sensitivities (Branchek and Bremiller, 1984; Nawrocki et al., 1985), which are evenly distributed across the retina and organised in a mosaic pattern (Engström, 1960). Short single cones are sensitive to ultraviolet light (UV-cones), long single cones are sensitive to short wavelengths (S-cones), and double cones contain either a pigment sensitive to middle-range wavelengths (M-cone) or to long wavelengths (L-cones). Usually, individual cones express only a single opsin type, but in zebrafish the M-cones have been found to have two different 'green' opsins (Vihtelic et al., 1999).

Like in other vertebrates, only one type of rods exists in the zebrafish retina. In contrast to cones, which express one of several opsins, rods express only rhodopsin under normal conditions (Saszik and Bilotta, 1999). Rods are also organised in a

specific pattern and are arranged regularly around each UV-cone (Fadool, 2003). Photoreceptor spacing also defines the physical limit of visual acuity, i.e., the ability to resolve two separate objects at a certain distance. In order to distinguish two separate objects, the critical, also called Nyquist frequency, should not exceed $\frac{1}{2}$ s, where s is the spacing between photoreceptors (reviewed in: Haug et al., 2010). In larval zebrafish (5 dpf) the distance between double cones sets the physical resolution limit at 0.24 cpd (minimum separable angle 2.1°) (Haug et al., 2010). However, it appears that in the developing visual system the maximal spatial information cannot yet be fully utilised: The visual acuity determined by the optokinetic response (OKR) was 0.16 cpd (3.1°) and therefore slightly lower than the maximal possible value (Haug et al., 2010). Visual acuity increases during development and using a modified version of the optomotor response (OMR), Tappeiner and colleagues (2012) measured visual acuity values between 0.56 to 0.58 cpd for adult zebrafish.

## Horizontal cells adapt signals for processing in the inner retina

Photoreceptors are connected to two types of neurons in the retina; horizontal and bipolar cells. Both cell types extend processes into the ONL, directed towards invaginations of photoreceptor terminals where synaptic connections are formed (Masland, 2012a).

Horizontal cells mediate lateral connections in the OPL and provide a mechanism for local gain control in the retina by adjusting the photoreceptor signal for processing in the inner retina. Horizontal cells, sample input from a wide range of rods and cones. Depending on local average illumination levels they then provide inhibitory feedback to rods and cones, ensuring that input to the inner retina stays within operating range. Hence, horizontal cells prevent saturation by a single bright object, which is particularly useful in the natural world, where brightness levels can vary significantly within the same scene (Masland, 2012a). Horizontal cells also contribute to the generation of centre-surround receptive fields observed in the retina (Kuffler, 1953). Because horizontal cells are widely spreading along the ONL, their feedback signal extends beyond the borders of the bright object and also reduces the signals evoked by nearby objects (reviewed in: Diamond, 2017 and Masland, 2012a). Horizontal cells have also been shown to provide feedforward

inhibition onto bipolar cells, a process, which is not yet well understood (Diamond, 2017).

Connaughton et al., (2004) identified three types of horizontal cells in zebrafish, according to morphology and the presence or absence of an axon, i.e., $H_A$ -1, $H_A$-2, and $H_B$. A more recent study (Song et al., 2008) classified horizontal cells into H1/2 cells, which differ in size, and are probably the same as the previously described $H_A$-2 cells; and H3 cells, which have a laminar morphology and branch widely. H3 cells, probably include the $H_B$ cells described previously and are thought to be chromatic horizontal cells, which selectively connect to photoreceptor types. Also, in contrast to the findings by Connaughton et al., (2004) all horizontal cells identified by Song et al., (2008) had axons.

## Bipolar cells provide a link between the outer and inner retina

Like horizontal cells, bipolar cells receive direct input from photoreceptors; however, instead of providing feedback to the photoreceptors, the excitatory bipolar cells transmit information to amacrine cells and ganglion cells (Masland, 2012a). Photoreceptors hyperpolarise in response to light increments, which results in a decrease of glutamate release; conversely, light decrements lead to a depolarisation of photoreceptors and an increase in glutamate release. In bipolar cells, at the postsynaptic side, glutamate can have differential effects, depending on the type of glutamate receptors they express. ON bipolar cells are activated by light because the presence of glutamate has an inhibitory effect, mediated by metabotropic glutamate receptors. OFF bipolar cells, on the other hand, express ionotropic glutamate receptors and are excited by glutamate, therefore, they respond to a decrease in light. The axons of ON- and OFF- bipolar cells terminate separately in the inner and outer part of the IPL, respectively (Famiglietti et al., 1977; Wässle, 2004). Thus, parallel channels of ON and OFF responses are created at the first synapse in the retinal circuit (Wässle, 2004).

In zebrafish 17 bipolar cell subtypes have been identified (Connaughton et al., 2004). However, their classification is not straightforward and a recent study (Li et al., 2012) proposed there are at least 33 subtypes, based on photoreceptor connectivity and axonal stratification. The axonal arbors of bipolar cells in the IPL of zebrafish can be either mono- or multi-stratified (Connaughton et al., 2004), unlike in mouse models, where each bipolar cell type projects to a specific layer in the IPL (reviewed

in: Euler et al., 2014). In zebrafish, bipolar cells receive cone or rod-and-cone input (Connaughton et al., 2004; Li et al., 2012) but there is no type receiving only rod input, as it happens in the mammalian retina (Wässle et al., 1991). It is believed that the different bipolar cell types act as different channels, which transmit specific information, such as polarity (ON, OFF), colour, or kinetics from the photoreceptors to the inner retina (Euler et al., 2014).

## Amacrine cells form inhibitory synapses with bipolar and ganglion cells

Amacrine cells are a very diverse group of cells, widely varying in morphology, connectivity, and neurotransmitter expression. Generally, they provide direct feedforward input to ganglion cells, feedback to bipolar cells, and form synapses with other amacrine cells (Masland, 2012a). Overall, the role of amacrine cells in the retina is to modulate and refine visual information flowing vertically through the retina, from the photoreceptors to the ganglion cells; this is key in shaping the precise response properties of retinal ganglion cells (Masland, 2012b)

Like in other vertebrates, amacrine cells in zebrafish mainly express the inhibitory neurotransmitters GABA and glycine (Connaughton et al., 1999), although excitatory neurotransmitters, such as acetylcholine, can also be expressed by some amacrine cells (Arenzana et al., 2005). Additionally, amacrine cells can provide synaptic input onto other cells via gap junctions. Interestingly, narrow-field amacrine cells can provide excitatory outputs via electrical synapses and inhibitory output via chemical synapses. The mammalian AII amacrine cell, for example, contributes to the transmission of rod information to retinal ganglion cells by making sign conserving connections (electrical) with ON bipolar cells, and sign inverting connections (chemical) with OFF cone bipolar cells (reviewed in: Bloomfield and Völgyi, 2009).

Morphologically, amacrine cells can be characterised by the extent of their dendritic field, i.e., 'narrow', 'medium' and 'widefield'; and by the stratification pattern of their neurites in the IPL, i.e., 'diffuse', 'mono-', or 'multistratified' neurites. Early morphological studies identified 29 types of amacrine cells in the mammalian retina (MacNeil et al., 1999; MacNeil and Masland, 1998). More recently, a 3D reconstruction of the IPL from electron microscopy data revealed 45 different amacrine cell types (Helmstaedter et al., 2013).

In zebrafish, Connaughton et al., (2004) identified seven types of amacrine cells, classified into three categories, i.e., $A_{on}$, $A_{off}$, and $A_{diffuse}$. A more recent study by Jusuf et al., (2011) reported 28 types of amacrine cells. Generally, amacrine cells in zebrafish seem to have smaller dendritic arbors than in other species (Connaughton et al., 2004).

The exact functions carried out by the various amacrine cells types have not yet been fully characterised. It is clear, however, that amacrine cells perform essential computations on the signal provided by photoreceptors, modulating and shaping the output of the retina. While most bipolar cells and ganglion cells extend neurites into only one or two strata of the IPL, many narrow amacrine cells extend their processes vertically, spanning several strata. Wide-field amacrine cells, on the other hand, are thinly stratified and extend neurites horizontally. There are three principles underpinning the function of amacrine cells. First, via lateral inhibition, medium- and wide-field amacrine cells introduce contextual effects to the ganglion cell response, such as the inhibitory surround of the receptive field; other examples include motion detection and anticipation (reviewed in: Gollisch and Meister, 2010). Second, narrow- and medium-field amacrine cells perform vertical integration of the signal, mainly in the form of crossover inhibition; amacrine cells, which extend branches into several or all layers of the IPL, transmit information between ON and OFF sublayers (reviewed in: Masland, 2012; Werblin, 2011). Third, certain types of amacrine cells, such as starburst amacrine cells (SAC) or AII amacrine cells carry out very specific tasks; e.g., SACs mediate direction selectivity (DS) via functionally isolated units within their dendritic arbors, which selectively connect to individual DS ganglion cells.

## Retinal ganglion cells project feature-specific information to higher visual areas

Retinal ganglion cells (RGCs) integrate multiple excitatory and inhibitory inputs from bipolar and amacrine cells and are the only output neurons in the retina; their axons form the optic nerve and transmit information from the retina to the brain (Masland, 2012a). The response properties of RGCs and their fibres have long been of interest to vision scientists, and early studies on RGCs led to the discovery and description of receptive fields (Hartline, 1938; Kuffler, 1953; Barlow, 1953). RGCs have relatively simple centre-surround receptive fields (Kuffler, 1953) and can be divided into three groups, i.e., ON, ON-OFF and OFF (Hartline, 1938; Barlow, 1953; Kuffler, 1953). However, Barlow (1953) and later Lettvin et al., (1959), observed that some RGCs selectively respond to complex stimulus features, a finding which could not be explained by linear summation within the spatial receptive field, such as stimulus movement or shape. These discoveries led to the idea that receptive fields act as feature detectors and that RGCs transmit feature-specific information in parallel channels to the brain; rather than just conveying a light-adapted, pixel-by-pixel representation of the visual scene. In the following years, direction- (Barlow et al., 1964) and orientation-selective ganglion cells (OSGCs) were identified together with cells which act as local edge detectors and uniformity detectors (Levick, 1967). The variety of functional response profiles in RGCs is also represented in their heterogeneous morphologies. Although different functional types correspond to certain morphological types (Cleland et al., 1975; Baden et al., 2016), a definitive classification of RGCs has been difficult to be agreed upon, mainly due to the fact that the exact nature of visual information extracted in the retina is still under debate (Carandini, 2005; Masland, 2012a; Baden et al., 2016).

A recent study by Baden et al., (2016) combined functional imaging with electrophysiological, immunohistochemical and morphological studies, resulting in the identification of at least 32 unique functional RGC types in the mouse retina. In zebrafish, 11 morphological RGC types have been identified, based on the size of their somata and the stratification and branching patterns of their dendritic trees (Mangrum et al., 2002; Ott et al., 2007). When axonal projections patterns are taken into account, more than 50 structural RGC types can be identified (Robles et al., 2014). This is important, given that different functional RGC types have been shown to terminate in separate layers in the optic tectum, which represents the main retino-

recipient area in lower vertebrates (in frogs: Maturana, 1960; in zebrafish: Del Bene et al., 2010; Nikolaou et al., 2012; Robles et al., 2013). There is mounting evidence that the different types of RGCs form precisely coordinated projection patterns in retino-recipient brain areas, such as the optic tectum. These so-called RGC maps, create brain-area-specific representations of the visual scene (Robles et al., 2014, 2013). Understanding where feature-specific RGCs terminate, and what connections they make, could provide valuable insight into how feature-specific information is processed in the brain and how visual behaviour arises (reviewed in: Dhande and Huberman, 2014; Dhande et al.,2015).

## 1.1.2 Visual computations in the retina

While there seem to exist 'pixel sensor' RGCs (X cells in cat; Enroth-Cugell et al., 1983), it is now known that the majority of RGCs types convey to the brain feature-specific information, e.g., about object motion, direction of movement, orientation of an object or looming stimuli (reviewed in: Roska and Meister, 2014). In contrast to bipolar cells, which have simple ON or OFF receptive fields, RGCs selectively respond to complex stimulus features, such as the orientation of an elongated object. This feature-selectivity emerges in the inner retina and is the result of highly organised connections and intricate interactions between distinct bipolar, amacrine and ganglion cell types (Briggman et al., 2011; Helmstaedter et al., 2013).

Part of this thesis focuses on local orientations and how they are represented in the optic tectum. As orientation selectivity in the optic tectum seems to be inherited from the retinotectal projections (Hunter et al., 2013a), the next section expands on the mechanisms which underlie the generation of orientation selectivity in the retina.

## Orientation selectivity

Neurons, which respond maximally to an elongated object in a certain orientation, and minimally (or not at all) to an object in the orthogonal orientation, are called orientation-selective (OS). Orientation selective cells were first described in the mammalian visual cortex by Hubel and Wiesel (1959). Shortly afterwards, orientation selective RGCs were identified in the retina of birds (Maturana and Frenk, 1963) and mammals (Levick, 1967). Orientation-selective retinal ganglion cells (OSGCs) have now been described in almost all vertebrates, including zebrafish (Nikolaou et al., 2012; reviewed in: Antinucci and Hindges, 2018). More recently, Antinucci et al., (2016) discovered two types of OS amacrine cells in the retina of zebrafish; a monostratified type, which extends neurites into the OFF layer of the IPL, and a bistratified type, which also reaches into the IPL ON layer. Based on this finding, they proposed a putative mechanism of how orientation tuning is generated in the retina. Orientation tuning in amacrine cells, in the zebrafish retina, appears to be determined by their morphology. Both types have highly elongated dendritic fields and their orientation matches their preferred stimulus orientation. Additionally, the degree of orientation tuning seems to be determined by the extent of dendritic tree elongation. Building on the observation that inhibitory GABAergic output of OS amacrine cells is required for normal orientation tuning in RGCs, Antinucci et al., (2016) proposed a new model, according to which in the presence of an orthogonally orientated stimulus, OS amacrine cells release GABA and provide weak orthogonally-oriented inhibitory input to RGCs and presumably the bipolar cell presynapse, thereby modulating the bipolar output to ganglion cells. Consequently, orientation tuning in RGCs arises from excitatory preferred-orientation tuned input from bipolar cells and orthogonally tuned inhibitory input from OS amacrine cells (Antinucci et al., 2016; Figure 1.2B).

Both amacrine cells and OSGCs in zebrafish show tuning to four orientations, i.e., the horizontal and the vertical, as well as two oblique orientations (Lowe et al., 2013; Antinucci et al., 2016). OSGCs mainly project to the tectal neuropil, where input from the four OSGC types terminates in distinct layers. Orientation tuning in the developing retino-tectal system appears to be a highly dynamic process, which greatly relies on visual experience in order to form four distinct OSGC populations (Lowe et al., 2013).

Neurons in the optic tectum seem to inherit their orientation tuning from the retinal input and no emergent OS populations have been found so far (Hunter et al., 2013a).
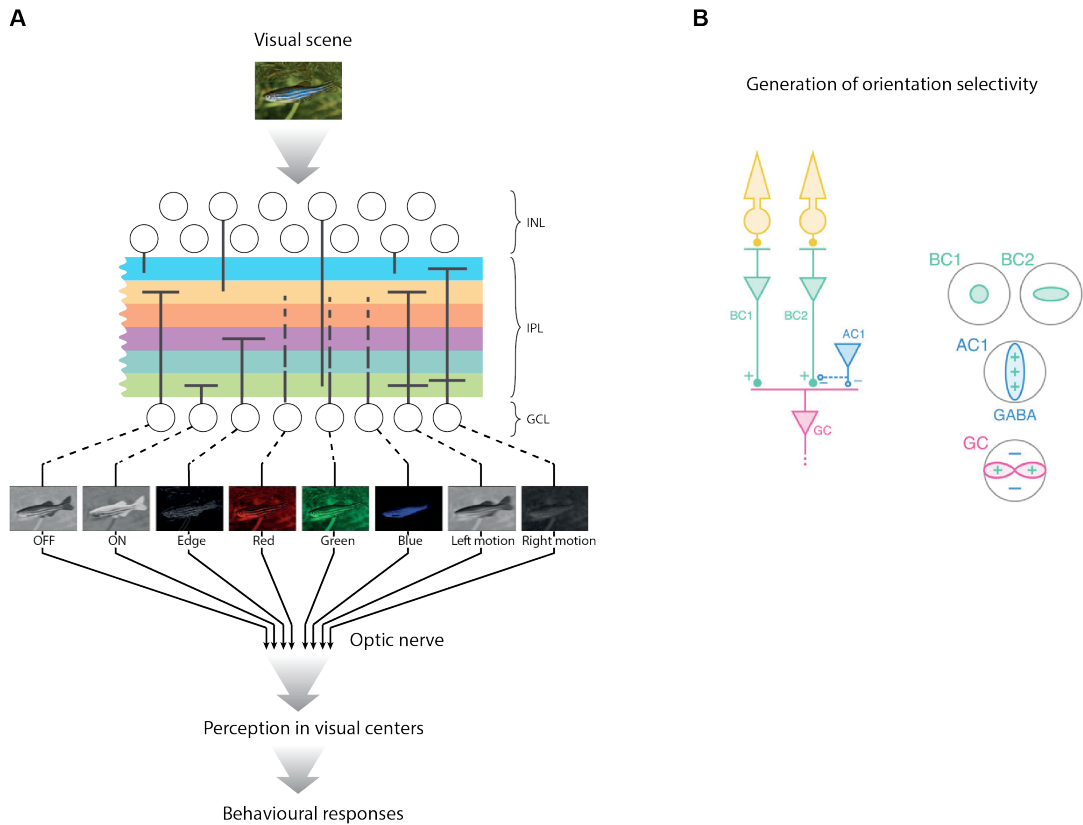


**Figure 1.2 Optic flow and retinal computations in the retina.** (**A**) Distinct ganglion cell types process individual visual features such as changes of light levels (OFF, ON), high contrast contours (Edge), chromatic information (Red, Green, and Blue), or direction of motion, in parallel. The feature selectivity of ganglion cells is the result of highly specific inputs from bipolar and amacrine cells, which form synapses with ganglion cells in the IPL. Ganglion cells are the only output neurons of the retina and their axons form the optic nerve, which projects to the optic tectum and a variety of extra-tectal visual brain areas. The combined activity of these brain areas generates visual perception and visually-guided behaviours. Abbreviations: INL, inner nuclear layer; IPL, inner plexiform layer; GCL, ganglion cell layer. Image extracted from Baier (2013). (**B**) Generation of orientation selectivity in the zebrafish retina. Left: proposed circuit underlying the firing selectivity of OS ganglion cells. Photoreceptors are shown in yellow; bipolar cells (BCs) in green; amacrine cells (ACs) in blue and ganglion cells (GCs) in red. Right: Response profiles of cell types to oriented visual stimuli. Excitatory synapses are indicated by '+' and inhibitory synapses by '-'. Extracted from Antinucci and Hindges (2018).

## 1.1.3 Retinal connections

RGCs and their projections provide the only output from the retina, therefore, the ability of the brain to generate visual perception, relies entirely on the information provided via retinal projections.

In teleost fish, like in other lower vertebrates, the majority of retinofugal projections terminate in the optic tectum (OT), a large layered structure in the mesencephalon equivalent to the mammalian superior colliculus, which is considered to be the main visual processing centre in lower vertebrates (Northcutt and Wullimann, 1988). However, there are also several diencephalic nuclei, which receive direct retinal input as well as various nuclei in the mesencephalon and telencephalon, which are innervated by other visual structures, mainly the optic tectum. In zebrafish, retinofugal projections terminate in ten arborisation fields (AF-1 to AF-10), with AF-10, the optic tectum, being the largest (Burrill and Easter, 1994).

Retinal connections also include projections to the retina itself. The majority of these retinopetal fibers arise from the terminal nerve (TN) ganglion (reviewed in: Behrens and Wagner, 2004), a structure that has been described as the primary chemosensory centre (Demski and Northcutt, 1983). In zebrafish, the TN has only recently been identified (Pinelli et al., 2000) and reported to mediate olfactory input to the retina and to modulate retinal function, e.g., increasing the visual sensitivity (Maaswinkel, 2003; Huang et al., 2005; Esposti et al., 2013).

## 1.1.4 Non-tectal visual processing

Non-tectal visual processing structures can be separated into two groups according to the origin of their visual input. In zebrafish, similar to other teleost fishes, the optic tectum, as well as several nuclei in the diencephalon, receive direct retinal input (Northcutt and Wullimann, 1988; Burrill and Easter, 1994). While the optic tectum receives the majority of retinal inputs (> 97%), only a small number of RGC types exclusively targets the optic tectum (Robles, 2017). The majority of RGC types innervate multiple brain areas in parallel (Robles et al., 2014; reviewed in: Robles, 2017). Despite receiving direct visual input and being reciprocally connected with the optic tectum, little is known about the diencephalon's role in vision. The role of the thalamus as the main visual relay station, as described in mammals, could also not be confirmed (Mueller, 2012).

A recent study in zebrafish by Semmelhack et al., (2014) however, reported that a pretectal nucleus (parvocellular superficial pretectal nucleus, PSp), which was previously identified as AF-7 plays an important role in the detection of prey. AF-7 receives topographically organised input from RGCs in the temporal retina (Robles et al., 2014) and neurons in AF-7 project to the optic tectum as well as to reticulospinal neurons, which are involved in swim orientation and speed.

On the other hand, telencephalic nuclei, and tegmental nuclei in the mesencephalon receive indirect visual input mainly via the optic tectum and pretectal nuclei (Schellart, 1990). The mesencephalic nuclei are widely connected, receive multimodal as well as motor input, and have been shown to participate in oculomotor behaviour (Schellart, 1990). The dorsal telencephalon is homologous to the pallium in mammals and ablation studies in goldfish suggest that it is involved in spatial and emotional learning, similar to the hippocampus and amygdala (Portavella et al., 2002; Durán et al., 2010). Recent studies have also linked the cerebellum to visually-driven associative learning (Aizenberg and Schuman, 2011) and spatial cognition (Durán et al., 2014), although, it has been traditionally linked to motor control.
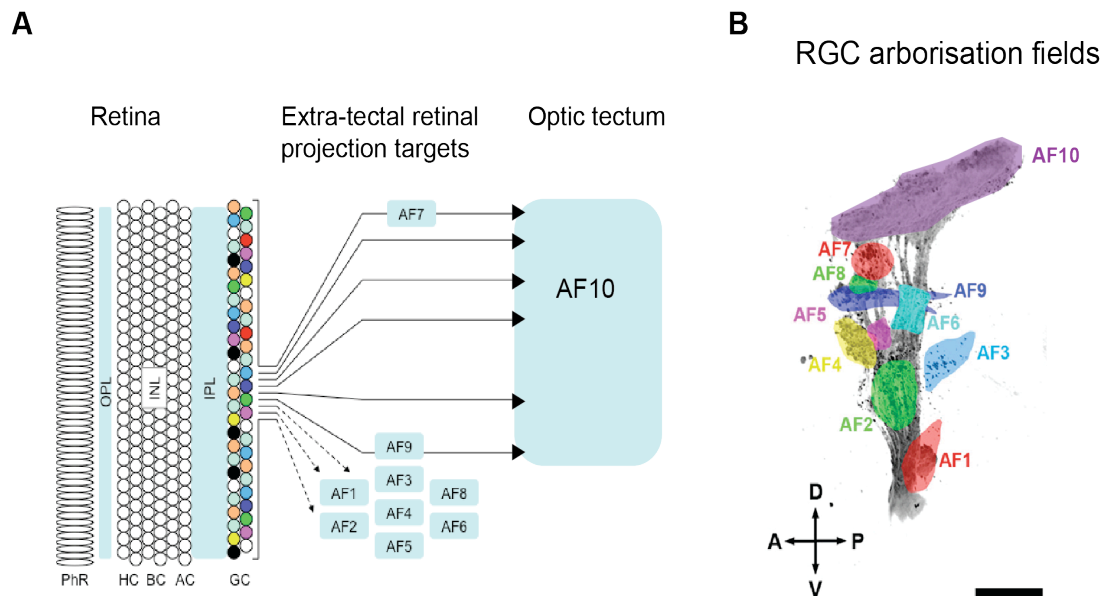


**Figure 1.3 Retinal projections.** (**A**) Diagram of retinal projections targets in zebrafish. The axons of ganglion cells terminate in 10 arborisations fields AF1-10. The majority of retinal projections terminates in the optic tectum. Phr, Photoreceptors; HC, horizontal cells; BC, bipolar cells; AC, amacrine cells; GC, ganglion cells; ONL, outer nuclear layer; INL, inner nuclear layer; IPL, inner plexiform layer. Image slightly modified from Nevin (2010). (**B**) Lateral view of the optic tract. AF1-10 are highlighted in different colours. Scale bar 50 μm. Image slightly modified from Robles (2014).

## 1.1.5 Visual processing in the optic tectum

The optic tectum is by far the best-characterised retinorecipient area in the zebrafish brain; a large layered structure just below the skin, easy to identify and access. It can be divided into six main layers (from superficial to deep): the *stratum marginale* (SM); the *stratum opticum* (SO); the *stratum fibrosum et griseum superficiale* (SFGS); the *stratum griseum centrale* (SGC); the *stratum album centrale* (SAC); and the *stratum perievntriculare* (SPV) (Vanegas and Ito, 1983; Meek, 1990). The optic tectum can roughly be divided into two parts: a superficial neuropil area (SM, SO, SFGS, SGC, and SAC) which contains both afferent axons as well as the dendrites and axons of tectal neurons and a small number of interneurons, and a deep cell body layer (SPV).

Retinal projections enter the superficial neuropil from the anterior side and terminate in four major laminae of the neuropil: the SO, the SFGS (where the majority of retinal afferents terminates), the SGC, and a lamina located between SAC and SPV (Xiao, 2005) (Figure 1.4A). Within these four layers, the retinotectal projection is further divided functionally and anatomically, as groups of axons costratify and precisely form ten retinorecipient sublaminae (Robles et al., 2013). These sublaminae appear to be hardwired (present *ab initio*) and represent the visual scene in parallel retinotopic maps (Robles et al., 2013) (Figure 1.4B, left). In zebrafish, unlike in other teleosts, the SM, i.e., the most superficial layer, does not contain retinal axons but is composed of afferent fibres from the *torus longitudinalis*, in the mesencephalon (Meek, 1990). The optic tectum receives significant input from other visual brain areas such as the pretectum and other sensory modalities e.g., lateral line input via *torus semicircularis* (Meek, 1990). Together with the dendrites and axons of tectal neurons, these non-retinal afferents occupy the space in between the retinorecipient layers in the neuropil.

The first evidence of the existence of a layer-specific functional organisation in the zebrafish tectum came from Del Bene and colleagues (2010), who reported that deeper layers in the neuropil respond best to small stimuli, whereas superficial layers seem to be tuned to large stimuli. This preference for small stimuli was proposed to be the result of feedforward inhibition by a population of inhibitory interneurons located in the superficial neuropil (SINs), which are tuned to large stimuli (Del Bene et al., 2010). However, in a later study Preuss et al., (2014) argued that the optic tectum already receives size tuned input from the retina and that small-size selective

RGCs predominantly innervate the superficial neuropil, whereas large-size selective RGCs terminate in deeper layers. Furthermore, SINs do not seem to be generally tuned to large stimuli, but can also be tuned to small stimuli, depending on the stratification of their dendritic trees. SINs with dendritic arbours in the SO receive predominantly small-size tuned excitatory input, whereas SINs with dendritic arbours in the SFGS sample large-size tuned RGC input. PVN cells can be either selective for small or large size stimuli, presumably depending on the stratification pattern of their dendritic tree (Preuss et al., 2014).

Feature-selective input to the optic tectum is not limited to stimulus size. Two subsequent studies by Meyer and colleagues (Nikolaou et al., 2012; Lowe et al., 2013) concluded that retinotectal projections provide orientation- and direction-selective (DS) input to the optic tectum and that OSGCs and DSGCs innervate distinct tectal layers according to their tuning profile (Figure 1.4B, right). While OS tuning is highly dynamic during development, DS responses appear to be invariant and hardwired (Lowe et al., 2013). This is supported by the fact that tectal cells exhibit near-mature DS tuning as early as 78 hpf and that normal DS tuning is not dependent on sensory experience (Niell and Smith, 2005). Two studies by Engert and colleagues (Ramdya and Engert, 2008; Grama and Engert, 2012) produced evidence that direction selectivity is generated in a tectum-intrinsic mechanism, and arises from a combination of excitatory non-DS retinal input and recurrent inhibition tuned to the orthogonal (null) direction via a tectal interneuron. This model contradicts the findings of Nikolaou et al., (2012) and Lowe et al., (2013), which clearly showed DS tuned retinal input to the optic tectum. At the same time, Gabriel et al., (2012) proposed that direction tuning in the optic tectum arises from a combination of excitatory retinal input tuned to the preferred orientation, and inhibitory input by tectal interneurons tuned to the null-direction (orthogonal). Interestingly, both models appear to be valid and represent two complementary mechanisms of DS processing in the optic tectum (Hunter et al., 2013a). Following up on the description of DSGC populations (Nikolaou et al., 2012; Lowe et al., 2013), Hunter et al., (2013a) set out to provide a detailed description of OS and DS tectal cell populations and identified five DS populations; three of which corresponded to the previously described retinal DS input and two emergent DS populations, which are likely generated by an intrinsic tectal circuit, mediated by inhibitory input tuned to the null direction.

**A**



**B**



**C**
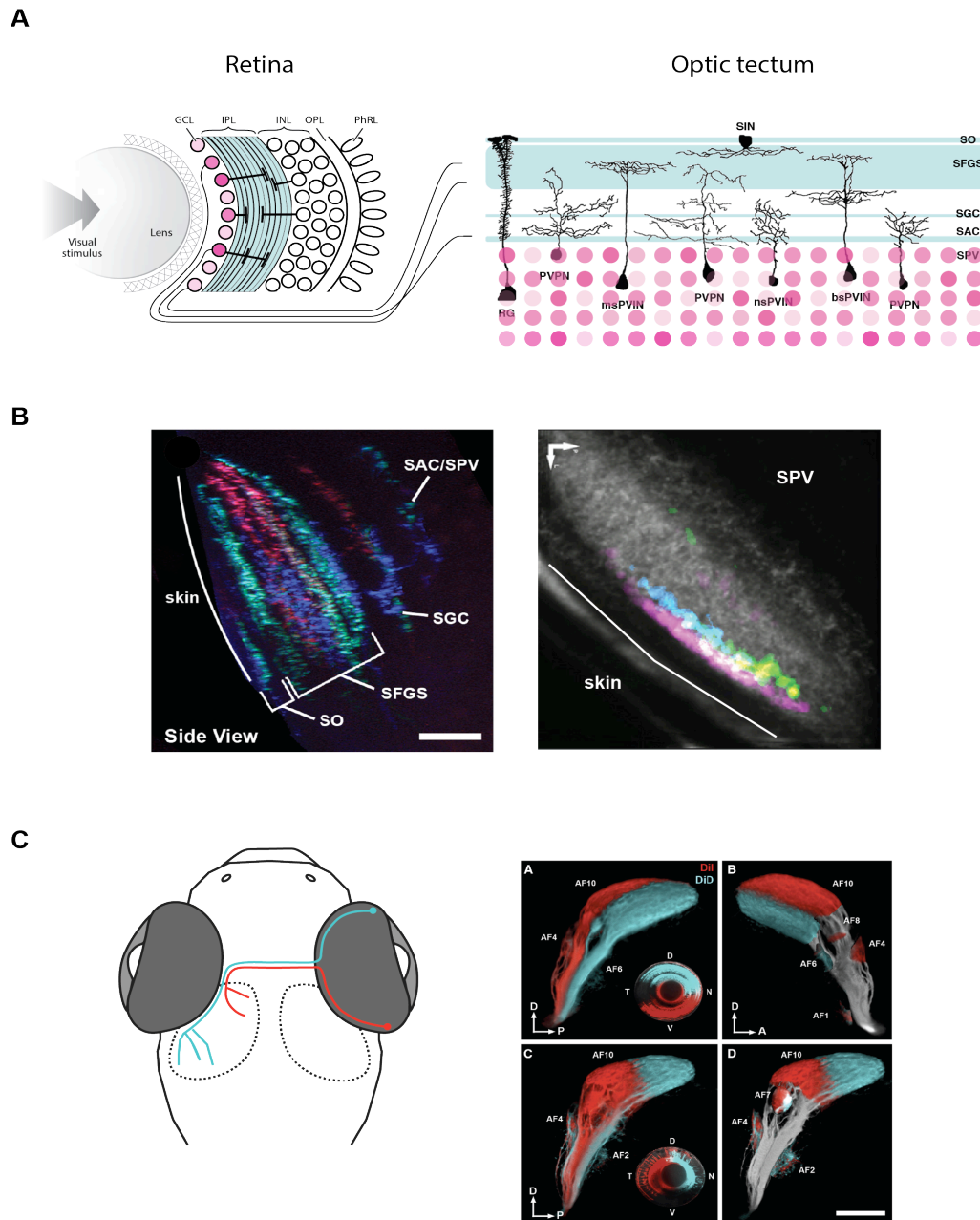


**Figure 1.4 Retinal input to the optic tectum is highly organised.** (**A**) Left: Visual information is processed in the retina and transmitted to the optic tectum via the axons of ganglion cells, which terminate in the tectal neuropil. Right: Morphological types of tectal cells: Radial glia (RG), periventricular projection neurons (PVPNs), periventricular interneurons (PVINs) and superficial interneurons (SINs). Adapted from Baier (2013) and Nevin (2010). (**B**) Retinal afferents form precise sublaminae within the four main layers of the tectal neuropil. Left: Multicolour brainbow labelling of retinal axons in the tectal neuropil. Image from Robles (2013). Right: Individual laminae receive feature-specific input, e.g., input tuned to different directions of motion. Image from Nikolaou (2012). (**C**) Input to the optic tectum is organised retinotopically, i.e., ganglion cells in the dorsal retina terminate in the ventral part of the optic tectum and vice versa. Similarly, ganglion cells from the nasal part of the retina project to the posterior optic tectum and vice versa. Right image extracted from Robles (2014).

The organisation of synaptic connections in precise, parallel laminae is one of the most striking features of the optic tectum. The arrangement of axonal arbours in fine layers appears to be hardwired and is independent of both spontaneous activity, such as retinal waves and sensory experience (Nevin et al., 2008). Synapses arranged in precise layers is not a feature exclusive to the optic tectum, but rather represents a common organising principle in the central nervous system across classes (reviewed in: Sanes and Zipursky, 2010). While the arrangement of axonal arbours within laminae undergoes continuous activity-dependent refinement during development (Schmidt et al., 2000; Gnuegge et al., 2001; Hua et al., 2005; Smear et al., 2007; Ben Fredj et al., 2010), lamination itself is precise from the earliest developmental stages. Several cellular and molecular mechanisms underlying this laminar pattern have been identified (reviewed in: Baier, 2013): 1) Intrinsic regulation of branching patterns via transcription factors, non-coding RNA or epigenetic marks. 2) Neurite guidance via secreted (e.g., hedgehog or netrins) or transmembrane molecules (e.g., semaphorins) or molecules located in the extracellular matrix (e.g., Slit). 3) Cell-cell recognition via adhesion molecules e.g., of the immunoglobulin superfamily.

Presumably, all three classes significantly contribute to the development of synaptic laminae in the visual system. Based on the ubiquitous presence of synaptic laminae in the nervous system, it has been suggested that wiring specificity, i.e., the need for highly connected neurons to be located closely together, has been suggested as a general underlying principle for lamination (reviewed in: Baier, 2013). More robust evidence comes from a study by Nikolaou and Meyer (2015), which showed that the laminar organisation of the tectum is necessary for a fast assembly of visual circuits.

Retinal input to the optic tectum is not only organised in a laminar manner but also topographically. Topographic maps provide an orderly representation of the sensory input, and in this case, of the visual world, to the brain. In the retinotectal system, neighbouring cells in the retina, project to neighbouring places in the optic tectum (Figure 1.4C). In detail, the anterior retina projects to the posterior optic tectum and vice versa. Similarly, projections from the dorsal and ventral retina terminate in the ventral and dorsal tectum, respectively (Stuermer, 1988; Robles et al., 2013). Retinotopic maps are crucial for directional behaviours, such as prey capture, which require that the exact stimulus position in the visual scene is conserved in the optic tectum.

Information in the optic tectum generally flows from superficial to deep layers. The majority of afferent fibres enter the optic tectum via the superficial neuropil layers, where they form excitatory connections upon the dendritic arbours of tectal interneurons. Information then flows to deeper layers along the vertically oriented dendritic trees of periventricular neurons. In the deeper layers, information is, in turn, conveyed to either tectal projections neurons or other tectal interneurons. Here, the efferent fibres of periventricular projection neurons also leave the optic tectum mainly bound for pretectal areas in the diencephalon and premotor areas in the mesencephalon and rhombencephalon. The vast majority of cells in the optic tectum have cell bodies located in the SPV and are therefore called periventricular neurons (PVNs) (reviewed in: Nevin et al., 2010). About 25% of these neurons are interneurons (PVINs), which primarily express GABA and have a local axon. These neurons can be divided into three groups according to the stratification pattern of their dendritic arbour, monostratified, bistratified or non-stratified. The majority of PVNs, however, have axons, which leave the optic tectum and project to the reticular formation, medulla or Raphe nucleus; these neurons are therefore termed periventricular projection neurons (PVPN). A small number of cell bodies can also be found between SO and SFGS. These are superficial inhibitory neurons (SINs), which express GABA and have been implicated in mediating size tuning in the optic tectum (Del Bene et al., 2010; Preuss et al., 2014). The majority of visual processing is thought to take place in the tectal neuropil, where retinal axons and dendritic dendrites form extensive connections. The vast majority of tectal cell bodies, on the other hand, are spatially removed from the actual site of processing due to the monopolar morphology of tectal neurons; the dendritic and axonal segments are contiguous and therefore the cell body does not seem to be required to mediate input and output of the cell (Nevin et al., 2010).

The optic tectum is involved in a variety of behaviours, in particular those that rely on a precise map of the visual world, such as phototaxis (Burgess et al., 2010), prey capture (Gahtan, 2005; Muto et al., 2013; Semmelhack et al., 2014; Bianco and Engert, 2015; Filosa et al., 2016) or escape responses (Temizer et al., 2015; Dunn et al., 2016; Filosa et al., 2016). Evidence from studies in birds and other teleost fish, suggests that in the absence of a neocortex, the optic tectum might be also performing more complex visual processing tasks such as pop-out visual search (Ben-Tov et al., 2015) and object recognition, which are traditionally thought to take place in the visual cortex.

## 1.2 Receptive fields

### 1.2.1 Discovery and definition of the visual receptive field

To understand how vision works it is imperative to investigate the nature of the visual information being transmitted from the eye, along the visual pathway, to the brain. As early as 1927, physiologists recorded impulses from the optic nerve of vertebrates (Adrian and Matthews, 1927). However, it was not until another decade that Keffer Hartline (1938), in a pioneering study, first recorded from a single optic nerve fibre. His results were strikingly different from previous recordings of the whole nerve, which were characterised by a strong burst of responses shortly after the light came on, followed by continuous low-rate spiking while the light was on and another burst when the light was switched off, which then gradually subsided (Hartline, 1938). By shining a small spot of light onto the isolated retina of a bullfrog, Hartline (1938) was the first to study the response properties of single optic nerve fibres in a precise and systematic manner. He observed that individual fibres could be excited by a light stimulus falling on a small area of the retina and respond differently to changes in illumination; some responded only when the light came on, others when the light went off, and a third group both times. He named these fibres *on-*, *off-* and *on-off-fibres*.

He also noted:

> "No description of the optic responses in single fibers would be complete
> without a description of the region of the retina which must be illuminated in
> order to obtain a response in any given fiber. This region will be termed the
> receptive field of the fiber." (Hartline, 1938 p. 410)

The term *receptive field* had been introduced 30 years earlier by Sherrington (1906),
who originally used it in a tactile context to describe the area on the skin, where a
scratch reflex could be evoked. Hartline (1938) however, was the first to apply the
term *receptive field* to describe the visual response properties of a neuron.

## 1.2.2 (Lateral) Inhibition and receptive field structure

The cells in the retina are highly interconnected and retinal interneurons (horizontal
and amacrine cells) provide inhibitory input to photoreceptors, bipolar cells and
ganglion cells (Masland, 2012a). Hartline (1938) similarly to Adrian and Matthews
(1927) took into consideration that the discharge patterns of retinal ganglion cell
fibres were likely the result of multiple inhibitory and excitatory inputs. While certain
aspects of Hartline's seminal study indicated the presence of inhibitory mechanisms
on the light response, he only recorded excitatory responses from ganglion cell fibres
and did not directly observe any inhibition within the receptive field.

Inhibitory mechanisms within the receptive field were first described in the 1950s,
independently, by Barlow and Kuffler and provided the first evidence of lateral
inhibition in the vertebrate retina: Barlow (1953) who had set out to repeat
Hartline's experiments in isolated retinae of frogs, provided the first description of
surround inhibition in *ex vivo* preparations of ganglion cell fibres. Kuffler (1953)
translated Hartline's (1938) research on receptive fields to the mammalian visual
system and independently discovered the presence of an inhibitory surround in the
ganglion cell receptive fields of cats. While Hartline (1940) had reported that the
response of an optic nerve fibre was proportional to the quantity of light falling onto
its receptive field, Barlow (1953) noticed that for *on-off* cells the sensitivity to light
spots decreased as the spot size increased. Barlow (1953) attributed this effect to the
presence of inhibitory action onto the receptive field centre and, to directly confirm
this hypothesis, he used a second light spot placed outside the receptive field centre.
Kuffler (1953), on the other hand, observed that in the cat retina, the response types

were not fixed like they were in frogs (Hartline, 1938) and that *on*, *on-off* and *off* responses could be found within the same receptive field, when illuminating specific areas within. Kuffler (1953) also extended the definition of the term receptive field to include all areas, which have excitatory or inhibitory effects on the cell. This observation led him to describe, what is still referred to today, as the classic organisation of the retinal ganglion cell receptive field, that is a concentric structure with one centre and an antagonistic surround (Figure 1.5A, top). Like Barlow (1953), he also placed a second light spot in the periphery, the antagonistic surround as he described it, to investigate interactions between different areas within the RF and to directly confirm the presence of inhibition (Kuffler, 1953).

Both Barlow and Kuffler came to the conclusion that inhibition likely plays a role in contrast enhancement and visual acuity (Barlow, 1953; Kuffler, 1953). Hartline and Ratliff (1958) were the first to provide a complete description of lateral inhibition between neighbouring ommatidia in the compound eye of the horseshoe crab. Lateral inhibition is the process whereby excitation of one neuron suppresses the activity of cells in its surround via an interneuron. In the retina, surround inhibition is generated by lateral inhibition at two stages: (i) horizontal cells provide lateral inhibition at the first synapse in the retina between photoreceptors and bipolar cells and (ii) amacrine cells at the second synapse between bipolar cells and ganglion cells.

## 1.2.3 Receptive fields as feature detectors

In his 1953 paper on summation and inhibition in the frog's retina, Barlow reported another important observation. He related the receptive field properties of ganglion cells to behaviour in frogs and in particular the fact that any small moving object can evoke a prey capture response (Yerkes, 1903). He noted that:

> "The receptive field of an 'on-off' unit would be nicely filled by the image of a fly at 2 in. distance and it is difficult to avoid the conclusion that the 'on-off' units are matched to this stimulus and act as 'fly detectors'." (Barlow, 1953 p. 86)

This idea was later revisited by Lettvin and colleagues (Lettvin et al., 1959), who in their seminal paper titled 'What the Frog's Eye Tells the Frog's Brain' provided a direct link between single retinal units and behaviourally relevant aspects of visual perception. A more detailed description of their findings was presented to the physiological community one year later (Maturana, 1960).

Influenced by McCulloch's and Pitts' study (1947) on the recognition of 'universals' or 'invariants' as they were called by Maturana (1960), and inspired by the fact that the frog's choice of food was seemingly only influenced by the size and movement of an object, Lettvin (1959) and his colleagues took an unusual approach. They suggested that the bright spot of light used to define RFs in the past (Barlow, 1953; Hartline, 1938; Kuffler, 1953) did not only convey information about the change in illumination but also about the size, shape, contrast and the presence of edges of an object. Given the intricate structure of the retina, Lettvin et al., (1959) postulated that the role of the retina was not to simply convey information about illumination levels on a point-by-point basis, but rather to detect complex patterns of light, such as the aforementioned features. To test this, Lettvin and colleagues (1959) used a variety of visual stimuli, including naturalistic ones, which resembled prey or enemies hoping to evoke capture or escape responses.

Recording from single fibres in the optic nerve and from the superficial layer of the tectal neuropil, where these fibres terminate, Lettvin et al., (1959) and Maturana (1960) described five operations which are applied to the retinal representation of the image:

1) *Sustained contrast detectors*, which respond when the edge of an object enters the receptive field and correspond to the *on* fibres previously described by Hartline (1938).

2) *Net convexity detect*ors, which respond to a small curved object moving through the receptive field. Fibres in the first two classes also frequently exhibit directionality, i.e., maximal response to an object moving in one direction and minimal or absent response to movement in the opposite direction.

3) *Moving edge detectors,* which correspond to previously identified *on-off* fibres (Barlow, 1953; Hartline, 1938) and respond to any edge moving through its receptive field.

4) *Net dimming detectors*, which are the same as *off* fibres (Barlow, 1953; Hartline, 1938) and respond to a sudden drop in light levels.

5) *Darkness detectors*, which are continually active, but respond to increasing levels of darkness and are insensitive to motion.

While several of these feature detectors are similar to the previously described *on*, *on-off*, and *off* responses (Barlow, 1953; Hartline, 1938) and can be explained by the underlying receptive field structure, the most unexpected finding of Lettvin et al. (1959) was that of the net convexity detector: This stimulus preference cannot easily be predicted by linear summation or inhibition within the receptive field.

Lettvin et al., (1959) reported that fibres from each operational group terminated in a spatially restricted space, i.e., separate layers of the tectal neuropil and that this order was reconstituted after severing the optic nerve. This confirmed an earlier similar observation by Sperry (1951) whose work focused on optic nerve regeneration. Lettvin and colleagues (1959), like Barlow (1953), directly related their findings to visual perception and the resulting visually evoked behaviours and suggested that the convexity detectors might, in fact, be used as 'bug perceivers' by the frog. Soon after feature detectors were discovered in frogs, Barlow, Hill, and Levick (1964) established that the remarkably complex operations on visual input described for lower vertebrates (Lettvin et al., 1959; Maturana, 1960), also occur in the mammalian retina. Further investigations on the rabbit retina by Levick (1967) revealed the presence of units detecting local edges and uniformity.

A different approach for the understanding of the mechanisms underlying feature detection was employed by Hubel and Wiesel (1959, 1962). Their landmark studies (Hubel and Wiesel, 1959, 1962) on receptive fields in the visual cortex of cats set the foundations for further research work in the field of visual neuroscience. Hubel (1959) had previously established recordings from single units in the visual cortex of awake cats and observed that while most units were spontaneously active in darkness and insensitive to overall changes in illumination, they responded well to a small spot of light, either stationary or moving and sometimes even displayed directional preferences. Shortly after, Hubel and Wiesel (1959) extended Hartline's concept of the receptive field to neurons of the cortex and provided a detailed description of cortical receptive fields in the anesthetised cat. Similar to the receptive fields of retinal ganglion cells (Kuffler, 1953), neurons in the lateral geniculate body (LGN) and the visual cortex, were divided into excitatory and inhibitory subfields, i.e., *on* and *off* regions. The shape of the receptive fields, however, was strikingly different: While cells in the retina (Kuffler, 1953) and LGN are more or less round, cortical receptive fields are elongated and oriented vertically, horizontally or obliquely; and *on* and *off* areas lie side by side. Hubel and Wiesel (1959) discovered that although

some cortical neurons responded to a single spot of light, the majority of them were maximally activated by a moving edge (i.e., a slit-shaped spot of light), oriented the same way as the receptive field (the response of these cells to an edge with orthogonal orientation was either minimal, or not existent at all). These receptive fields are often referred to as bar or edge detectors. Not long after this discovery in the visual cortex, orientation selectivity, and edge detectors were also found at the level of the retina in birds and mammals (Levick, 1967; Maturana and Frenk, 1963). Hubel (1959), and Hubel and Wiesel (1959) reported that many cells in the visual cortex exhibit a directional preference; this could often be attributed to asymmetries in the receptive field organisation, namely the flanking regions. In a later study, Hubel and Wiesel (1965), described what they called hypercomplex cells, which can detect the curvature of an object, similar to Lettvin's bug perceiver (Lettvin et al., 1959). However, in contrast to Barlow (1953) and Lettvin et al., (1959) who proposed that the retina encodes features of direct ethological relevance, Hubel and Wiesel (1965) avoided assigning specific functions to different cell types and suggested that the visual system encodes features for general use. By bringing together the findings of their previous work that cortical cells exhibit orientation tuning (Hubel and Wiesel, 1959, 1962, 1965), Hubel and Wiesel (1968a) suggested that neurons in the visual cortex perform contour analysis.

At the same time, the mid-1960s saw the rise of a completely novel approach to vision science: the mathematical modeling of receptive fields (reviewed in: Ringach, 2004). Driven by the idea to formalise the recent discoveries of receptive fields, the original concept of feature detectors (Barlow, 1953; Lettvin et al., 1959; Maturana, 1960) was soon surpassed by the concept that receptive fields act as linear spatiotemporal filters (Enroth-Cugell and Robson, 1966; Rodieck and Stone, 1965a, 1965b). The naturalistic stimuli, proposed by Lettvin and Maturana (1959), were substituted by 'richer' and more objective stimuli such as sine gratings (Enroth-Cugell and Robson, 1966) and white noise (Jones and Palmer, 1987). Together with Hubel and Wiesel's concept of hierarchical processing of visual information which will be described in more detailed in the next section, the advances in linear receptive field modelling led to the classic textbook view of retinal ganglion cell receptive fields: simple, with a concentric centre-surround organisation. While early studies on ganglion cell receptive fields (Lettvin et al., 1959; Levick, 1967; Maturana and Frenk, 1963) suggested that complex visual processing may already start in the

retina, this idea has been neglected for many decades and often referred to as a special case limited to simpler animals (Gollisch and Meister, 2010). Important visual computations such as object recognition, however, are highly nonlinear and feature detectors can provide valuable insight into how the brain achieves this task (Barlow, 2001).

## 1.2.4 Simple and complex cells and the concept of hierarchical processing

Hubel and Wiesel (1959, 1962) were the first to describe the receptive field properties of cells in the visual cortex. While for most cells stimulus preferences, such as size, shape or orientation could be understood as a result of summation and antagonism within the receptive field, Hubel and Wiesel (1959) also encountered cells where this was not possible. In 1962, they published a follow-up paper, which further explored the different receptive field properties of cortical cells and their putative role in visual processing. Hubel and Wiesel (1962) loosely divided the cortical cells into two groups: (i) simple cells which, like retinal ganglion cells and cells in LGN, have clearly defined *on* and *off* subdivisions where summation and antagonism occur, and (ii) complex cells, where these principles do not apply and whose stimulus preference cannot easily be predicted from their receptive field organisation. It was reported, however, by Hubel and Wiesel (1962) that both groups of cells responded best to bar stimuli in a certain orientation, i.e., they are orientation selective. This observation introduced a fundamental change in how visual information is represented. While cells in the LGN are insensitive to orientation, cortical cells only respond to a narrow range of stimulus orientations around their receptive field axis (Hubel and Wiesel, 1962). Hubel and Wiesel (1962) described how orientation-selectivity in the visual cortex could arise from LGN input. This idea is also referred to as the 'feedforward model of orientation selectivity' based on their following observations: 1) The LGN provides the main visual input to the visual cortex, and its cells have concentric, centre-surround receptive fields. 2) The receptive field properties in the two structures differ considerably; these differences must, therefore, arise from integrative mechanisms within the visual cortex. 3) Due to their simpler receptive field structure (compared to complex cells) which follows a similar organisation as LGN receptive fields, cortical simple cells likely represent an early stage of cortical processing and may

receive direct input from LGN afferents. Hubel and Wiesel (1962), therefore, proposed that the elongated and oriented receptive field of a simple cell may arise from the combined input of several LGN receptive fields, which are spatially offset along the receptive field axis of the simple cell (Figure 1.5A, bottom).

On the other hand, the response properties of complex cells cannot easily be predicted by LGN input. Based on the observation that complex cells exhibit a preference for bars of specific orientations (as simple cells do), and supported by the fact that cells (both simple and complex) with the same receptive field axis orientation are spatially organised in cortical columns, Hubel and Wiesel (1962) suggested that complex cells may receive input from multiple simple cells with identical axis orientations, but from different positions on the retina. The gradual increase in complexity from LGN to simple and complex cortical cells, as well as the fact that complex cells on average have larger receptive fields than simple cells, laid the foundations for the creation of the classical concept of hierarchical processing along the visual pathway (Hubel and Wiesel, 1962, 1968). This concept, that the anatomical hierarchy of the visual system is also reflected at the functional level, quickly spread within the scientific community.

Early studies on brain lesions in monkeys have led to the hypothesis of two discrete visual pathways originating in the occipital lobe (Ungerleider and Mishkin, 1982; Goodale and Milner, 1992). The ventral stream also referred to as the 'what' pathway, leads from visual area 1 (V1), through visual areas 2 and 4 (V2, V4) towards the temporal cortex, and is involved in object recognition. The dorsal stream, also referred to as the 'where' pathway, leads from V1 through visual areas 5 and 6 (V5, V6) and towards the parietal cortex and processes spatial vision (Goodale and Milner, 1992). Along the 'what' pathway, increasingly complex representations of visual information and an approximately 3-fold increase in receptive field size have been reported (Wilson and Wilkinson, 2015). Cells in V1 process simple contours and are tuned to orientation and direction (Hubel and Wiesel, 1968), whereas cells in cortical V2 have been shown to respond to combinations of orientations, such as complex and illusionary contours (Hegdé and Essen, 2003; Anzai et al., 2007). Neurons in V4 are selective for intermediate complex geometrical shapes (Desimone and Schein, 1987; Gallant et al., 1996) and at the top of the pathway, in the inferior temporal cortex (IT), cells respond selectively to hands and faces (Gross et al., 1972; Perrett et al., 1982; Desimone et al., 1984).
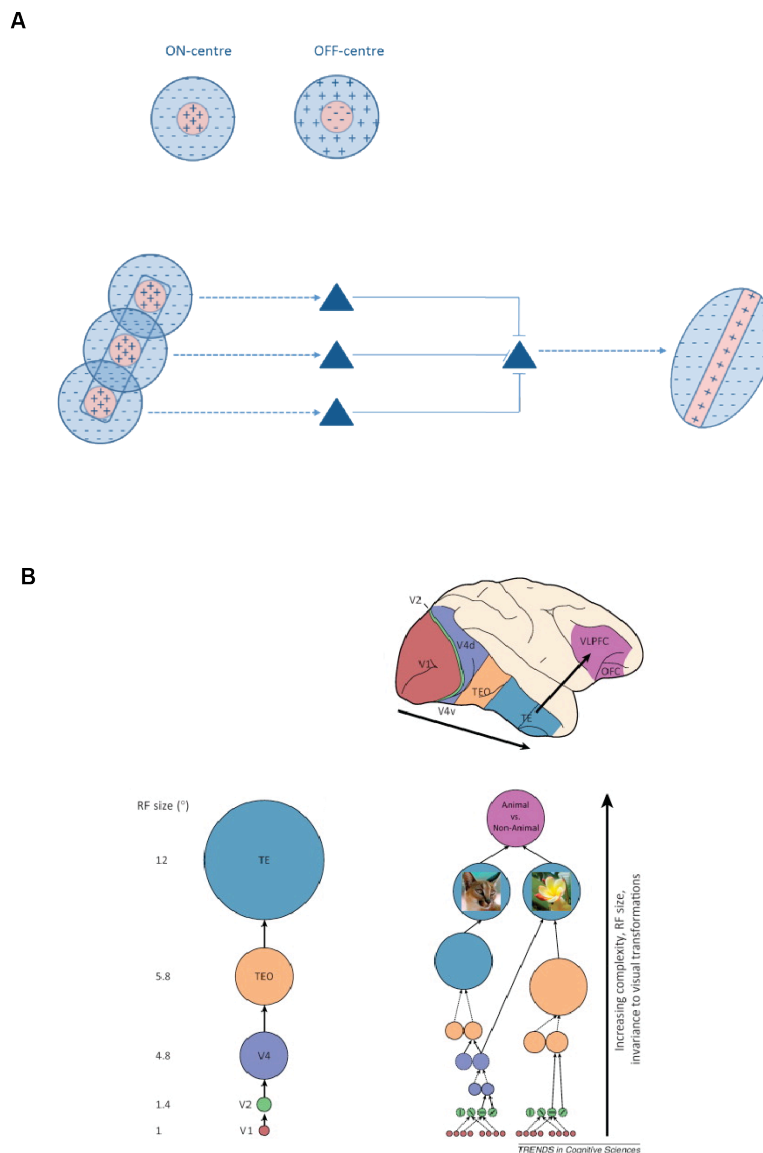
**Figure 1.5 Receptive field structure and hierarchical processing of visual information**. (**A**) Top: Concentric centre-surround ON and OFF receptive fields in retina. Adapted from Kuffler (1953) p.49. Bottom: Elongated receptive field of a simple cell in V1 created by hierarchical convergence of multiple concentric receptive fields in the LGN. Adapted from Hubel and Wiesel (1962) p. 142. (**B**) The ventral 'what' pathway in monkeys leads from V1 to area TE in the inferior temporal cortex to the ventrolaterral prefrontal cortex (VLPFC). Receptive fields along this pathway increase in size and complexity. Modified from Kravitz (2013).

In their original argument, Hubel and Wiesel (1962), however, had remarked that hierarchical processing might present an oversimplified model of cortical visual processing. Indeed, recently it has been suggested that while some hierarchical processing occurs along the visual pathway, this is oversimplified and does not take into account or explain the presence of 1) recurrent processing, such as feedback and lateral connections; 2) cortico-thalamo-cortical pathways; 3) the dynamic properties of neurons; and 4) the influence of other modalities on visual perception (reviewed in: Hegdé and Felleman, 2007). Mechler and Ringach (2002) have questioned the original classification of V1 cortical cells into separate simple and complex cell populations. They argue, alternatively, that simple and complex cells may represent two ends of a continuum, suggesting that cortical architecture is more uniform than previously thought.

## 1.2.5 Receptive field plasticity and maturation

In addition to their pioneering work on receptive field properties in the cortex, Hubel and Wiesel (1959, 1962) also significantly contributed to our understanding of how vision develops. In 1963, shortly after their discovery of simple and complex cells, Wiesel and Hubel published a series of papers, in which they described the response properties of cells along the visual pathway, following visual deprivation (Wiesel and Hubel, 1963a, 1963b) and prior to the onset of vision (Hubel and Wiesel, 1963).

Although connections in the visual system are remarkably precise and seemingly hardwired early in development (see Sperry 1959, 1963) i.e., before the onset of vision, Hubel and Wiesel (1963a, 1963b) highlighted the importance of visual experience for the correct development of visual function. For example, young kittens reared with one eye closed presented a stark reduction of binocular cells in V1 and completely lacked depth perception (Wiesel and Hubel, 1963b). Subsequent studies by Hirsch and Spinelli (1970) and Blakemore and Cooper (1970) demonstrated that other receptive field properties, in particular, orientation selectivity, can also be altered by abnormal visual input. Kittens, who were exposed to an abnormal visual environment containing only horizontal or vertical stripes, were virtually blind to orientations orthogonal to the one they had been exposed to (Blakemore and Cooper, 1970). This was also reflected in the response properties of neurons in the cortices of these animals. While the cells' responses were overall

similar to those in a normal animal, the distribution of preferred orientations was highly skewed towards the orientation the animal had been exposed to. Specifically, none of the recorded cells showed selectivity for the orthogonal orientation or any orientations within 20° of the orthogonal orientation (Blakemore and Cooper, 1970). The receptive fields of immature neurons are less well defined, usually larger (Derrington and Fuchs, 1981; Braastad and Heggelund, 1985) and undergo progressive refinement during development (Sanes and Constantine-Paton, 1985; Fagiolini et al., 1994; Tavazoie and Reid, 2000). Morphological studies examining axonal arbours of LGN afferents in the visual cortex have provided evidence that excitatory connections which are initially broad and diffuse, are being refined during development (Antonini and Stryker, 1993; McLaughlin et al., 2003). This process, which is often referred to as synaptic pruning, is based on the selective elimination of imprecise connections; at the same time, correct synaptic connections are strengthened and maintained (Simon and O'Leary, 1992; Katz and Shatz, 1996; Ruthazer and Cline, 2004). A recent study by Tschetter et al., (2018) demonstrated, that in the LGN of mice, the elimination of excitatory synapses is accompanied by an increase in feedforward inhibitory connections between interneurons and relay neurons in LGN. Together these processes lead to the functional refinement of receptive fields (Tschetter et al., 2018).

While studies on sensory deprivation and immature neuronal circuits highlighted the importance of visual input for normal vision, it became increasingly evident that essential features of the developing mammalian visual system, e.g., ocular dominance columns, are present before the onset of vision (Rakic, 1976; Godement et al., 1984; Horton and Hocking, 1996). This discrepancy led to the idea that spontaneous activity in the visual system, and in particular the retina, could drive anatomical and functional refinement of neuronal circuits prior to sensory experience (Galli and Maffei, 1988; Shatz and Stryker, 1988). Spontaneous activity and its importance for circuit development have been demonstrated for different stages of the visual system (reviewed in: Huberman et al., 2008); in fact, retinal waves coordinate patterned activity throughout the developing visual system (Ackman et al., 2012). On the other hand, molecules such as pentraxins, which can mediate synaptic refinement by translating activity into structural changes have been discovered (Bjartmar et al., 2006; Koch and Ullian, 2010). The relative contributions of sensory experience,

spontaneous activity and molecular guidance for the refinement of visual circuits and ultimately the refinement of receptive fields remain unclear.

# 1.3 Thesis aim

The aim of this Ph.D. study was to explore how visual information about local object features is represented in the zebrafish optic tectum. To achieve this aim, the following steps were undertaken: 1) Development of a set-up to conduct confocal calcium imaging and simultaneous visual stimulation in older zebrafish larvae, i.e., aged up to 21 dpf. 2) Generation of various sets of visual stimuli to observe the activity of tectal neurons. 3) Development of a pipeline for semi-automated analysis of confocal time-series. 4) Mapping of the spatial receptive fields of tectal neurons with flashing bars and small moving spots. 5) Testing of how local features are processed by tectal neurons.

Chapter 3 provides a detailed description of the process of setting up the experimental paradigm and provides information about the new transgenic zebrafish line (NBT:GCaMP3) used in this study. Chapter 4 describes how the spatial receptive fields of tectal neurons were mapped using two different stimuli. The findings of Chapter 4 led to the formulation of the hypothesis that tectal neurons may need to process multiple local features (belonging to one or more objects) at the same time. The research described in Chapter 5 addressed this question and used a variety of small moving stimuli to test how local features are processed and integrated by the optic tectum. The findings of this work are presented in a manuscript with the title: Processing and nonlinear integration of local features by zebrafish optic tectum. This manuscript is intended for submission for publication. In Chapter 6, I summarise the findings and present the conclusions of the work presented here. Moreover, implications and interesting questions for future research are discussed.

# Chapter 2

# Materials and methods

All experimental procedures were performed according to UK Home Office regulations (Animals (Scientific Procedures) Act 1986) and approved by the Ethical Review Committee at the University of Sheffield.

## 2.1 Zebrafish husbandry

Imaging of neural activity was carried out on zebrafish of the *nacre* mutant, which lack melanophores throughout development; the retinal pigment epithelium which is required for normal vision, is not affected (Lister et al., 1999). The calcium reporter GCaMP3 (Tian et al., 2009) was expressed under the control of the Xenopus neuronal beta-tubulin (NBT) promoter (Bronchain et al., 1999). NBT:GCaMP3 fish were kindly provided by Vincent Cunliffe, University of Sheffield. Zebrafish were bred using a marbling procedure and embryos were collected the next morning and raised in E3 embryo medium (E3 in mM: 5 NaCl, 0.17 KCl, 0.33 $CaCl_2$, 0.33 $MgSO_4$) at 28°C. Embryos were sorted for GFP fluorescence on day 2 post-fertilisation. At 5 dpf, larvae were moved to a Tecniplast system (Tecniplast S.p.A., Buguggiate, Italy), where they were kept under 14/10 hours light/dark cycles and fed twice a day, including the day of the experiment (Filosa et al., 2016). No more than 40 fish were housed per tank.

## 2.2 Confocal calcium imaging

### 2.2.1 Experimental setup

The imaging setup (**Figure 2.1**) used in this study was based on the setup described by Nikolaou et al. (2012) but has been modified to allow imaging of larger, i.e., 14-21 dpf larvae. Fish were immobilised in 3.5 % low-melting-point agarose (BioGene, Huntingdon, UK), which was sufficient to restrain larvae up to the age of 21 dpf. For fish >18 dpf, the agarose was carefully removed around the gills (on one or both sides) to allow movement and therefore increase oxygen supply. Fish were mounted dorsal side up on a plastic coverslip (Agar Scientific Ltd, Stansted, UK), which was then fixed with blu tack (Bostik, Stafford, UK) onto a removable, raised glass stage within the custom-made chamber. The experimental chamber was manufactured from Perspex (CBE workshop, University of Sheffield) and measured 90mm x 70mm x 15mm; wall thickness was 3mm. A diffusive filter (Cinegel #3026, Rosco EMEA, London, UK) was attached to one wall of the chamber, serving as a projector screen while the rest of the walls were covered with black insulation tape, to reduce unwanted visual cues. Fish faced the screen with either the left or the right eye. Eye-level was roughly in the middle of the screen and the eye-to-screen distance was either 1.3 cm for RF mapping with small spots or 2.4 cm for all other experiments. The projected image filled the entire screen, covering a visual field of approximately 124° by 35° or 155° by 74° (for 1.3 cm distance). The chamber was filled with imaging solution: Aquarium water was filtered through Grade 1 Whatman filter paper (GE Healthcare UK Limited, Little Chalfont, UK), buffered in 1.2 mM $NaH_2PO_4$ and 23 mM $NaHCO_3$ (Sigma-Aldrich, St. Louis, MO), and then aerated with a 95% $O_2$ and 5% $CO_2$ mix for at least 30 minutes to increase the level of oxygen in the solution and thereby facilitate oxygen absorption through the skin during the experiment. The pH of the solution was tested prior to the experiment to ensure a physiological pH, ranging between 7.0 and 7.5. The modifications described above made it possible to image 14-21 dpf fish for up to 3 hours with no oxygenation applied during the experiment.

Imaging of neural activity in the OT was performed using a FV1000 confocal microscope (Olympus, Tokyo, Japan) at the Wolfson imaging facility (The University of Sheffield), fitted with a 40x (NA 0.8) LUMPlan objective (Olympus). Sampling

frequency was 2.3 Hz. Imaging of the eye was performed on 10 dpf casper mutants expressing NBT:GCaMP3, which were additionally treated with 200 μM 1-phenyl-2-thiourea (PTU, Acros Organics, Geel, Belgium) from 1-10 dpf to avoid pigment formation (older fish were not studied, due to the detrimental effect of PTU on the health of zebrafish). Fish were mounted sideways and immobilized in 1.5 % agarose for confocal imaging
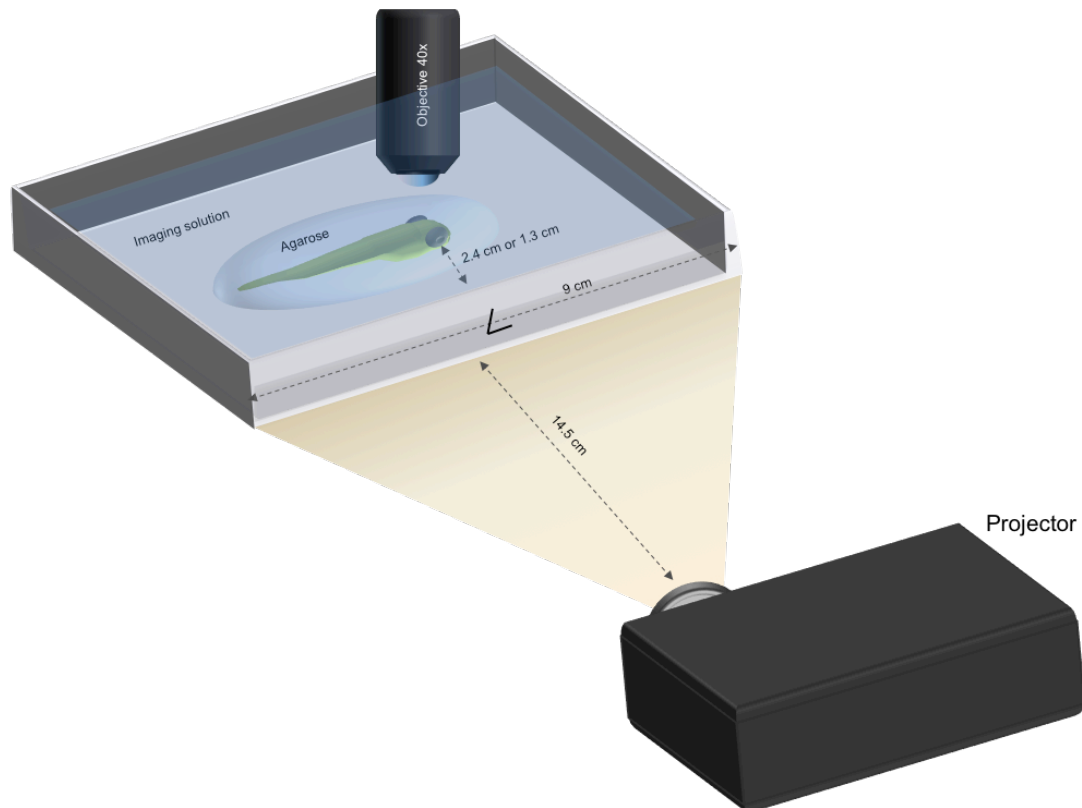


## 2.2.2 Visual stimulation

**Figure 2.1 Experimental setup.** Zebrafish larvae (12-21dpf) expressing GCaMP3 panneuronally under the NBT promoter, were immobilized in agarose and mounted on a custom made chamber. The chamber was fitted with an opaque screen (124° x 35° or 155° x 74° for 1 cm distance) onto which the visual stimulations were projected. Neural activity was monitored simultaneously via confocal imaging.

All stimulation scripts were custom-written using the Psychophysics toolbox (Brainard, 1997; Kleiner et al., 2007; Pelli, 1997) for Matlab (The MathWorks, Inc. Natick, MA). Stimuli were presented using a DLP Pico Projector PK320 (refresh rate: 60Hz, Optoma, Watford, UK) placed at a distance of 14.5 cm from the screen. Brightness and contrast levels were set to minimum and LED mode was set to ECO, eliminating the need for a notch filter and to avoid blinding the fish. The onset of

stimulation and imaging was synchronised via a TTL pulse transmitted by a LabJack (LabJack Corporation, Lakewood, CO).

All stimulations started with a 240 s wait to allow for the neural response to the laser return to baseline levels; followed by 60 s of an empty, bright screen, to let the fish adjust to the change in light intensity; and 10 s of a dark screen at the end of each experiment. Stimuli (angles, lines, square) moved horizontally across the screen, both rostro-caudally and caudo-rostrally (5 s wait in-between), at a speed of 35°/s, thereby reducing bias by some stimuli being closer to the RF centre (along the horizontal axis) than others. Stimuli were always presented in the middle (along the vertical axis) of the screen.

**i.   Angles** This stimulation was used to test whether tectal neurons exhibit tuning to complex local features, such as combinations of orientations e.g., angles. The visual stimulation consisted of a set of five angles (30°, 60°, 90°, 120°, 150°) presented at a pseudorandom order, in three different orientations (0°, 240°, 120°, **Figure 2.2**). Angles consisted of two thin, black lines, which had a size of 0.7° × 8.9° Angles moved horizontally across the screen as described above. The inter-stimulus-interval (ISI) between different angles was 20 s to allow for the GCaMP3 signal to return to baseline before the next stimulus. The complete set of fifteen angles was repeated three times.
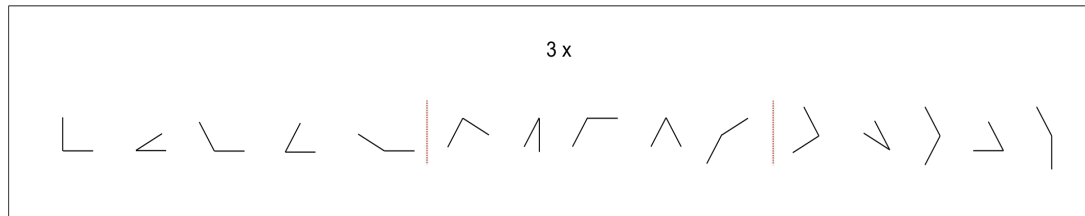


**Figure 2.2 Visual stimulation with angles.** Five angles (30°, 60°, 90°, 120°, 150°) at three different orientations moved horizontally along the screen in a pseudorandom order. The whole stimulus set was repeated three times.

**ii. Angles and bars** This stimulation script was designed to investigate tectal tuning to local orientations. It consisted of one repetition of angles (**Figure 2.2**) followed by three repetitions of a set of 12 single lines (0° - 330°, **Figure 2.3**) in six different orientations and two different positions. The lines had a size of 0.7° × 8.9°. ISI was 20 s.
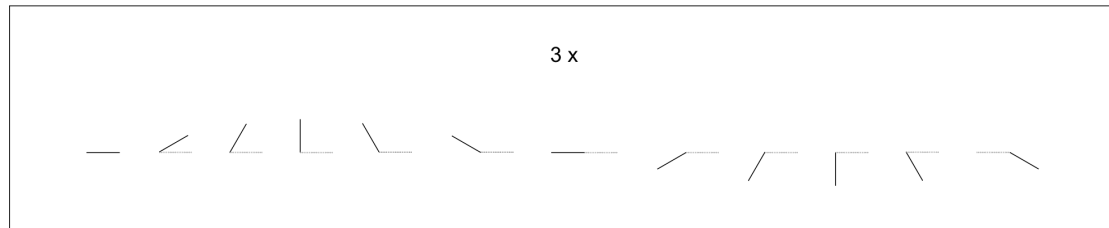


**Figure 2.3 Visual stimulation with angles and bars.** Set of 12 lines at different orientations. Single stimuli moved horizontally across the screen.

**iii. Linear combination test** This stimulation script was designed to test whether information about local features (lines, angles) is integrated in a linear or nonlinear manner within the tectal neuropil. The stimulation consisted of a composite feature i.e., square contour and two sets of simple features i.e., horizontal and vertical lines as well as corners (90° angles, Figure 2.4). The lines had a size of 0.7° x 11.8° or 0.7° x 5.9° (for corners). ISI was 20 s.
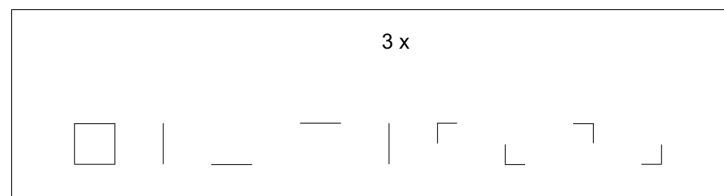


**Figure 2.4 Linear combination test**. The stimulation consisted of a composite feature (square) and two sets of simple features moving horizontally along the screen and was repeated three times.

**iv. RF measurement with flashing bars** This stimulation script was used to estimate receptive field sizes (RF) in the tectal neuropil. To test the dimension of the RFs along the horizontal axis, a flickering vertical black bar was presented at different positions along the width of the screen (Figure 2.5A). Due to the low height of the screen, the vertical dimension of the RFs could not be measured reliably. However, a flickering horizontal black bar was used to confirm the height of the screen was smaller than the average RF (Figure 2.5B), and therefore, a stimulus presented at any position along the vertical axis would fall into the average RF. Flicker frequency was 2 Hz and bar dimensions were 6° x 35° (vertical bars) or 124° x 6° (horizontal bars).
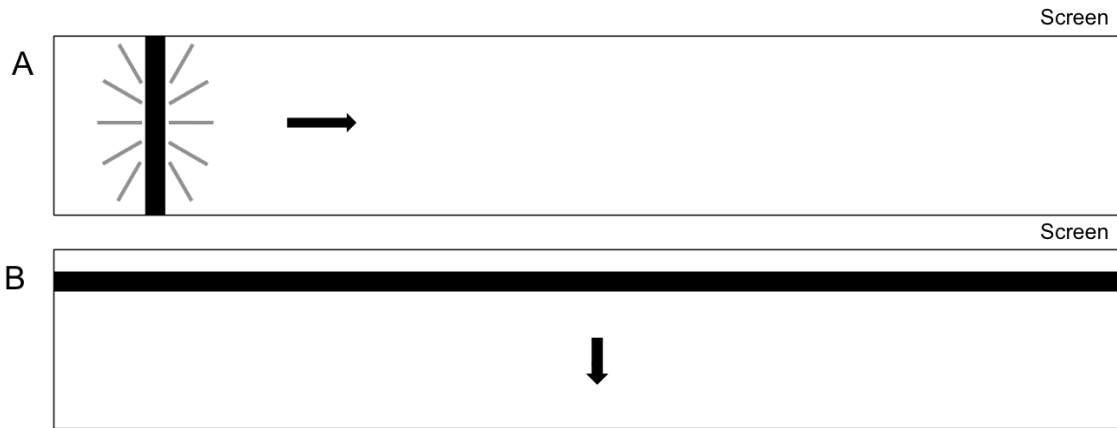
**Figure 2.5 RF measurement with flashing bars.** (**A**) A flickering vertical bar was presented at different positions along the horizontal axis to estimate the horizontal dimension of RFs in the optic tectum. (**B),** A flickering horizontal bar was presented at different positions along the vertical axis to confirm whether the vertical dimension of RF size is bigger than the apparent height of the screen.

**v. RF measurement with sweeping spots** In order to map the receptive field of tectal cells in a more detailed manner, small moving spots were used as stimuli, similar to previous experiments (Niell and Smith, 2005; Sajovic and Levinthal, 1982a). A small spot, 4.9° in diameter moved at 9.5°/s along the middle part of the screen (49°); first, the spot moved left to right at 10 different y-axis positions (pseudorandom); then the spot moved top to bottom at 10 different x-axis positions (pseudorandom, Figure 2.6). ISI was 5 s. Spots were either black on a white background or white on a grey background.
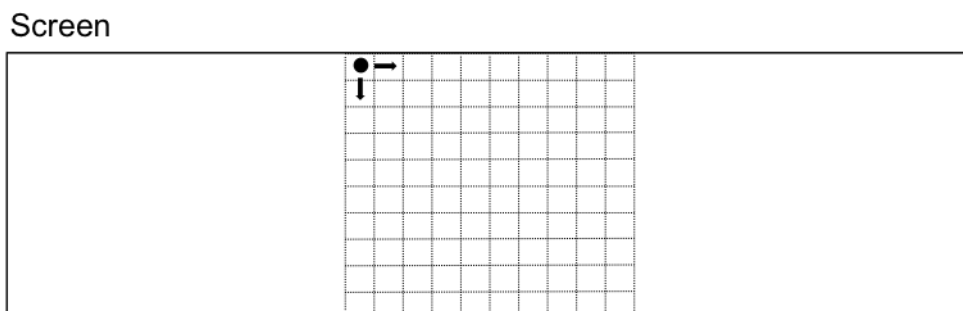


**Figure 2.6 RF measurement with sweeping spots.** A small spot first moved horizontally along the screen at 10 different y- axis positions; then the spot moved top to bottom at 10 different x-axis positions.

## 2.2.3 Data analysis

Two different approaches were used to analyse confocal imaging data in this thesis. In both cases, confocal time-series were corrected for motion using a rigid-body algorithm (TurboReg for ImageJ, (Thévenaz et al., 1998)) prior to image analysis. All further image analysis was performed in Igor Pro (WaveMetrics, Lake Oswego, OR), using SARFIA (Dorostkar et al., 2010a), a set of software tools for Igor Pro, as well as additional, custom-written scripts. Time series were not aligned to a reference brain, due to the differences in size and age across the fish used in this study.

### Data analysis for Chapter 5

#### Image segmentation

Cell bodies and small structures within the neuropil where identified using an automated segmentation algorithm (part of SARFIA). Confocal time-series were first mean filtered (kernel size $= 3 \times 3$) and then averaged over time. The resulting average images were then transformed using the Laplace operator. Individual regions of interest (ROIs) were defined by applying variable threshold levels (in negative standard deviations) on the Laplace operator of the average image. In the present study, a threshold of 0.4 was used. Figure 2.7 (right) shows an example of an ROI mask generated using the segmentation process described above. The ROI mask was then compared with the average image by eye and ROIs were separated manually where necessary.

#### ROI position

The position of ROIs was determined using an in-built feature in SARFIA: First, ROIs were divided into 'cell bodies' and 'neuropil' by manually outlining the neuropil area of the OT. Then, the superficial border of the neuropil was defined as 100% and the lower border as 0%; the centre of mass of each ROI determined the position of the ROI within the neuropil. Based on size and position, each ROI in the neuropil was likely to represent a fragment of one or several dendrites.
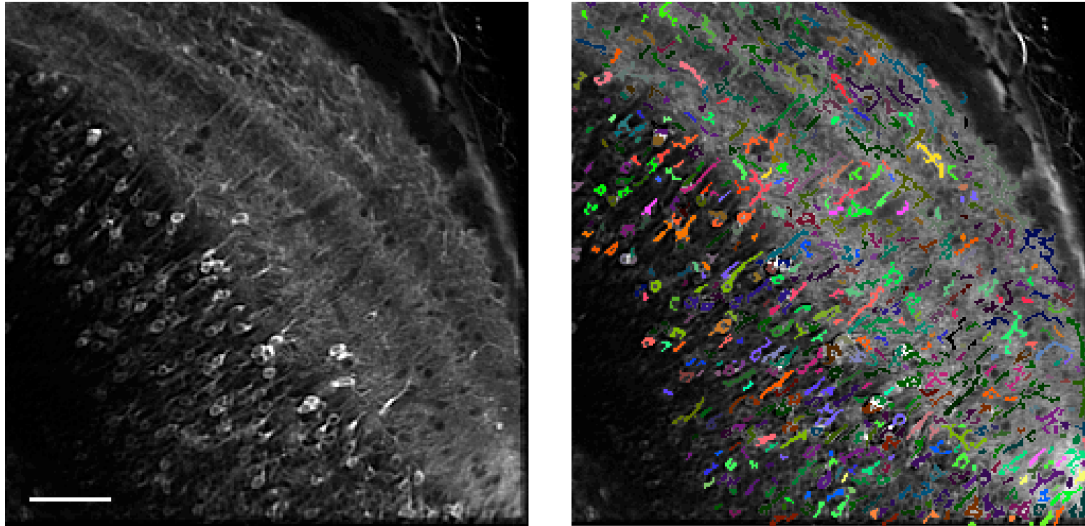
**Figure 2.7 Analysis of confocal time-series with SARFIA and Igor Pro.** The left panel shows a representative average image of a confocal time-series after registration. The right panel shows the ROI mask generated by thresholding the Laplace operator of the average image (593 ROIs randomly colour-coded). Scale bar: 50 µm

## Neuronal activity

Signal intensity changes for each ROI were measured as $\Delta F/F0$, where F0 was the mean intensity of the ROI during the 5s (12 frames) before the stimulation started. $\Delta F/F0$ values were then averaged across three stimulus presentations. To identify responding ROIs in an unbiased manner, the distribution of $\Delta F/F0$ for each ROI was tested for kurtosis. Kurtosis can be regarded as the 'tailedness' of a distribution and therefore provides a measure of outliers (Westfall, 2014); responding traces with many small values around the baseline and few responses (outliers) have higher kurtosis values than non-responding traces where values are relatively similar (Figure 2.8). Here, only traces with excess kurtosis > 1 were considered as visually responsive. This approach effectively separated non-responding, noisy traces from traces, which exhibited transient fluorescence changes in response to visual stimulation. A single response metric, $R$, was defined as the maximum signal amplitude during each stimulus interval.

**Calculation of orientation selectivity**

The orientation selectivity (OS) of responding ROIs was calculated from the average response $R$ to 2 moving bars of the same orientation at different positions. OS was determined using an OS index (Niell and Stryker, 2008):

$OSI = (R_{pref} - R_{ortho}) / (R_{pref} + R_{ortho})$, where $\theta_{pref}$ was defined as the orientation which caused the maximum response and $\theta_{ortho} = \theta_{pref} + \pi/2$. ROIs with an OSI >0.5 were regarded as orientation selective (Hunter et al., 2013b).

# Data analysis for Chapter 4

For the results presented in Chapter 4, the neuropil and cell body data were analysed separately.

**Image segmentation**

Cell bodies were identified in a similar manner as described for Chapter 5. However, several minor changes were applied to improve the result of the segmentation: The Laplace operator was applied to the raw average image, instead of the filtered image. Also, a lower threshold with values ranging between 0.1 and 0.3 was used and ROIs that consisted of less than 10 pixels were removed. ROI masks were manually inspected and ROIs separated where necessary.

For the neuropil, I used a voxel-wise approach. For this, the registered time-series was pre-processed in FIJI (Schindelin et al., 2012) as follows: To improve the signal-to-noise ratio, the time-series was median filtered (kernel size = $3 \times 3$) and spatially smoothed with a bivariate Gaussian function (kernel size = $5 \times 5$). Then, the area of the neuropil was outlined manually and saved as a separate file.

## Neuronal activity

Fluorescence signals were extracted on a voxel-wise basis for the neuropil and based on ROI segmentation for the cell bodies. Signal traces were normalised ($\Delta$F/F0, F0 was mean signal intensity in the 5s before stimulation started) and averaged across three repetitions. Visually responsive traces were identified by calculating the skewness of the distribution curve for each voxel or ROI (Figure 2.8). Skewness is a measure of symmetry; non-responding traces with values around the baseline have skewness around 0, whereas responding traces, with many small values around baseline and few higher values are positively skewed. Here, traces with skewness >1.4 (neuropil) and skewness >0.9 (cell bodies) were regarded as responsive and included in further analysis. Threshold levels were derived empirically and efficiently distinguished between visually responsive and unresponsive, noisy traces. A single response metric, $R$, was defined as the maximum signal amplitude during each stimulus interval.
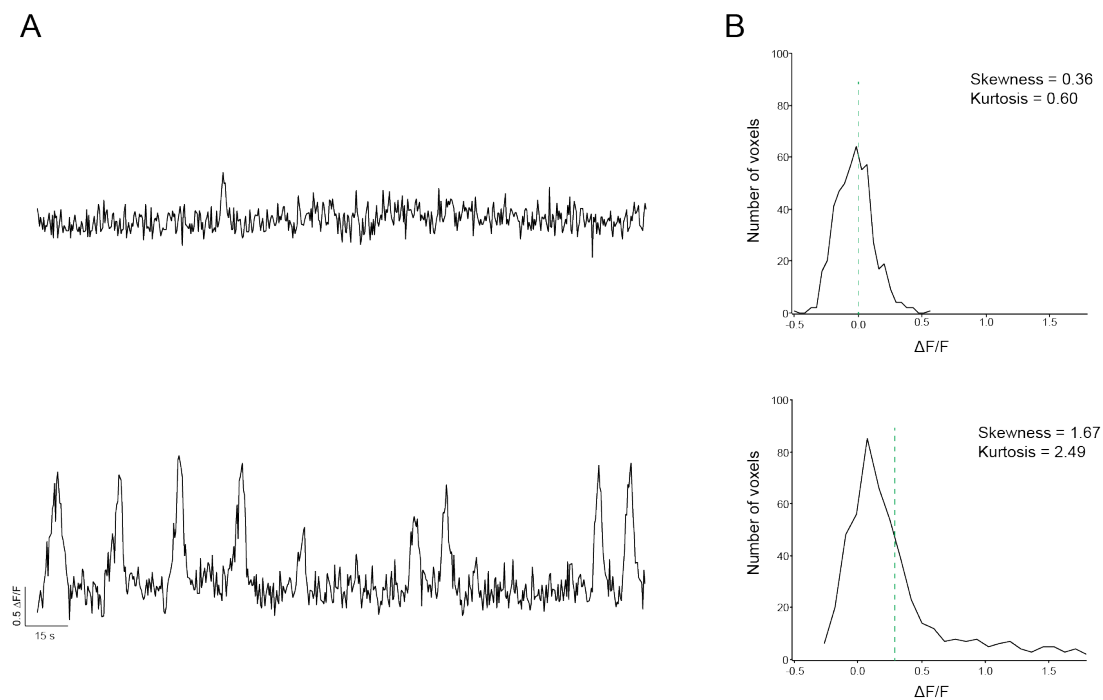


**Figure 2.8 Identification of responding traces.** (**A**) Example traces ($\Delta$F/F) of an unresponding (top) and responding (bottom) ROI (individual voxel). (**B**) Distribution of $\Delta$F/F values for the traces shown in A. Dashed green line indicates mean. Kurtosis is given as excess kurtosis. Mean values were $-0.003$ (top trace) and 0.326 (bottom trace).

### ROI position

The ROI position was determined by the relative x/y coordinates of the voxel or ROI in the time-series. Therefore, all positional information was relative and subject to a single field of view. Image series were rotated so that the rostro-caudal axis was parallel to the horizontal axis. In order to measure retinotopy, I compared the relative position of the voxel/ROI along the horizontal axis to the relative position of the RF centre (on a 10-by-10 grid).

### Measuring spatial receptive fields

Spatial receptive fields were measured by calculating the response to small, 4° diameter spots sweeping horizontally and vertically across the screen on a 10-by-10 grid (Figure 2.6). As the stimuli were presented in a pseudo-random order, the response traces were first automatically sorted. The spatial RF was then mapped as a 10-by-10 response map; responses $R$ to the horizontal and vertical sweeps through each location were multiplied based on the assumption that RFs are separable into x and y (Niell and Smith, 2005, Figure 2.9). To quantify RF size, the resulting 2D RF was fitted with a bivariate Gaussian function using least squares minimisation. The bivariate Gaussian function was described by:

$$f(x,y) = z_0 + A \exp\left[ \frac{-1}{2(1-cor^2)} \left( \left( \frac{x-x_0}{xwidth} \right)^2 + \left( \frac{y-y_0}{ywidth} \right)^2 \right) \right]$$

where $A$ is the amplitude of the Gaussian, *cor* is the cross-correlation term, $x$ and $y$ are independent spatial coordinates, $x_0$ and $y_0$ are the RF centre points and *xwidth* and *ywidth* are the standard deviations (SD) from the peak along the respective axes. For further analysis, RF width and height were defined as 4 x SD of the Gaussian, i.e., 4 x *xwidth* and 4 x *ywidth* respectively (Figure 2.9). Goodness of fit was tested using a chi squared statistic and an empirically derived threshold of $\chi^2 = 2$ was used to exclude RFs with a poor curve fit further analysis (neuropil data only).
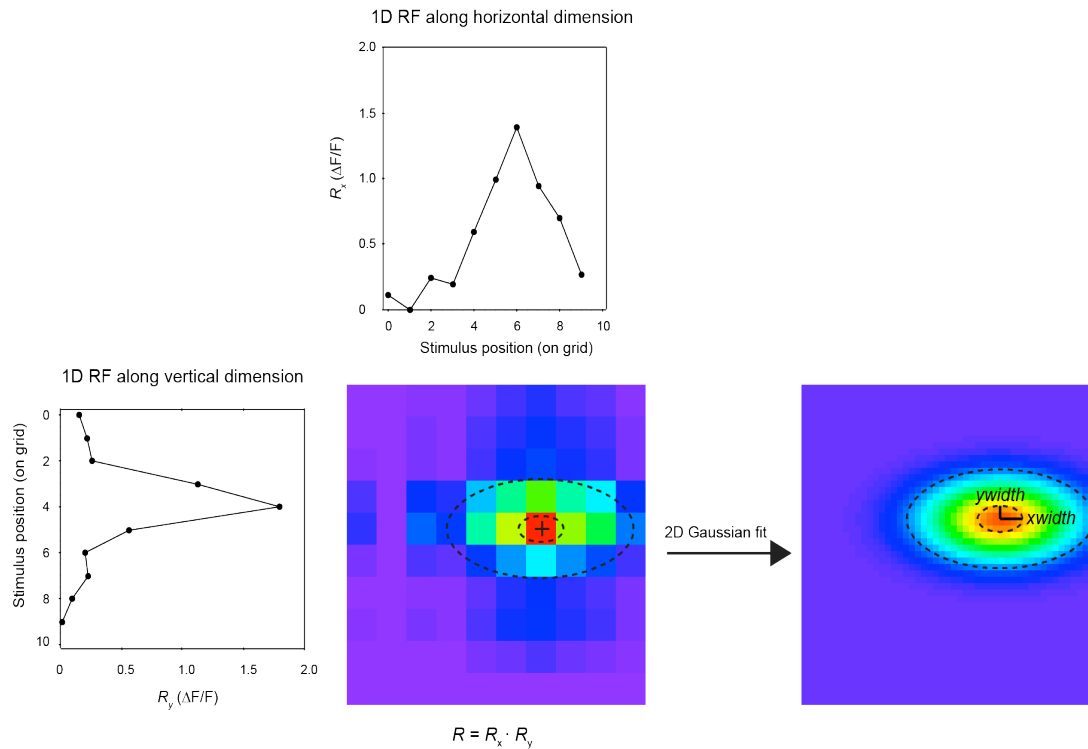
**Figure 2.9 Measurement of spatial receptive fields.** Receptive fields along the horizontal (top) and vertical dimension (left) for one voxel are shown as the maximum response during each stimulus presentation interval. The 1D RFs were multiplied to create a 10-by-10 map of the 2D RF (shown in centre). The 2D RF was fitted with a bivariate Gaussian function to determine the dimensions of the RF (right). RF height and width were defined as 4 x SD of the Gaussian (outer dashed line). *xwidth* and *ywidth* are the standard deviations from the peak of the Gaussian (inner dashed line). Cross indicates RF centre as determined by parametric fitting.

# Chapter 3

# Imaging neuronal activity in the optic tectum of older zebrafish larvae

The use of genetically encoded calcium indicators provides a non-invasive means of monitoring neuronal activity *in vivo*. The combination of calcium imaging and simultaneous visual stimulation offers a powerful solution to study how visual information is processed in the brain. Small, transparent and genetically amenable zebrafish larvae present an ideal model organism for this approach, as the whole visual pathway is accessible for imaging. In the past, this method has been applied to study the neuronal processes underlying prey detection and capture (Bianco and Engert, 2015) and escape responses (Temizer et al., 2015; Dunn et al., 2016). Similarly, this approach has been employed to study the visual response properties of tectal neurons (Del Bene et al., 2010; Gabriel et al., 2012; Grama and Engert, 2012; Hunter et al., 2013b; Kassing et al., 2013; Preuss et al., 2014; Hollmann et al., 2015). The optic tectum is of particular interest as it represents the central visual processing area in lower vertebrates. It is involved in a number of visual behaviours, in particular those that rely on a detailed map of visual space, such as phototaxis (Burgess et al., 2010), prey detection and capture (Bianco and Engert, 2015; Muto et al., 2013), and escape responses (Dunn et al., 2016; Temizer et al., 2015). Tectal neurons encode fundamental information about objects in visual space, such as orientation and size of the object as well as direction of motion (Del Bene et al., 2010; Gabriel et al., 2012; Grama and Engert, 2012; Hunter et al., 2013b; Kassing et al., 2013; Preuss et al., 2014; Hollmann et al., 2015).

The zebrafish visual system develops rapidly (Easter and Nicola, 1996) and many forms of visual behaviour emerge relatively early in development, e.g., phototaxis, early shoaling and independent feeding are present at 5 dpf (Burgess et al., 2010; Engeszer et al., 2007; Strähle et al., 2012). A number of other behaviours however, particularly those related to social interactions or learning arise later in development; shoaling and social preferences, as well as pattern learning, arise between the age of 2 to 4 weeks (Dreosti et al., 2015; Engeszer et al., 2007; Valente et al., 2012). In addition, visual acuity has also been shown to improve with age (Bilotta, 2000). These findings suggest that the visual system continues to adapt beyond the early larval stage. It remains unknown whether these changes are also reflected in the properties of tectal neurons. Unlike the commonly used *huc* promoter (Kim et al., 2014), the NBT promoter drives robust expression of GCaMP3 in the larval zebrafish brain up to 21 dpf (Figure 3.1); thus providing an exciting opportunity to study the functional properties of the visual system for an extended period of time, during which new visual behaviours arise.

As part of my Ph.D. training, I developed an experimental paradigm to study the visual response properties of tectal neurons in older larvae (up to 21 dpf). In brief, zebrafish larvae, which expressed GCaMP3 panneuronally under the NBT promoter, were immobilised in agarose and mounted on a raised stage within a custom-made imaging chamber. This chamber was then placed under a confocal microscope and filled with carboxygenated imaging solution. One side of the chamber was covered with opaque film, serving as a screen onto which a set of visual stimulations was projected. Simultaneously, neuronal activity in the optic tectum was recorded via confocal calcium imaging.

# 3.1 Expression of NBT:GCaMP3 in the retinotectal system of zebrafish

Genetically encoded calcium indicators (GECIs) such as GCaMP are widely used to monitor brain activity (Fetcho et al., 1998; reviewed in: Grienberger and Konnerth, 2012). Calcium ions ($Ca^{2+}$) act as second messengers and play an essential role in the excitability of neurons and the transduction of signals. During neuronal activity the concentration of intracellular $Ca^{2+}$ increases, thus providing a proxy for measuring activity. GCaMP was first engineered by Nakai et al. in 2001 and has since been continuously improved (Tallini et al., 2006; Tian et al., 2009; Akerboom et al., 2012; Ohkura et al., 2012; Chen et al., 2013; Muto et al., 2013; Sun et al., 2013; Badura et al., 2014). In the present study, I used the NBT:GCaMP3 transgenic zebrafish line, which was kindly provided by Dr. Vincent Cunliffe. These fish express the calcium reporter GCaMP3 (Tian et al., 2009) panneuronally under the control of the *Xenopus* neuronal beta-tubulin (NBT) promoter (Bronchain et al., 1999).

In the optic tectum, GCaMP3 expression was observed in both the neuropil and in the majority of PVN somata (Figure 3.1, right). GCaMP3 expression levels were robust in fish aged 10 to 21 dpf (Figure 3.1, left).
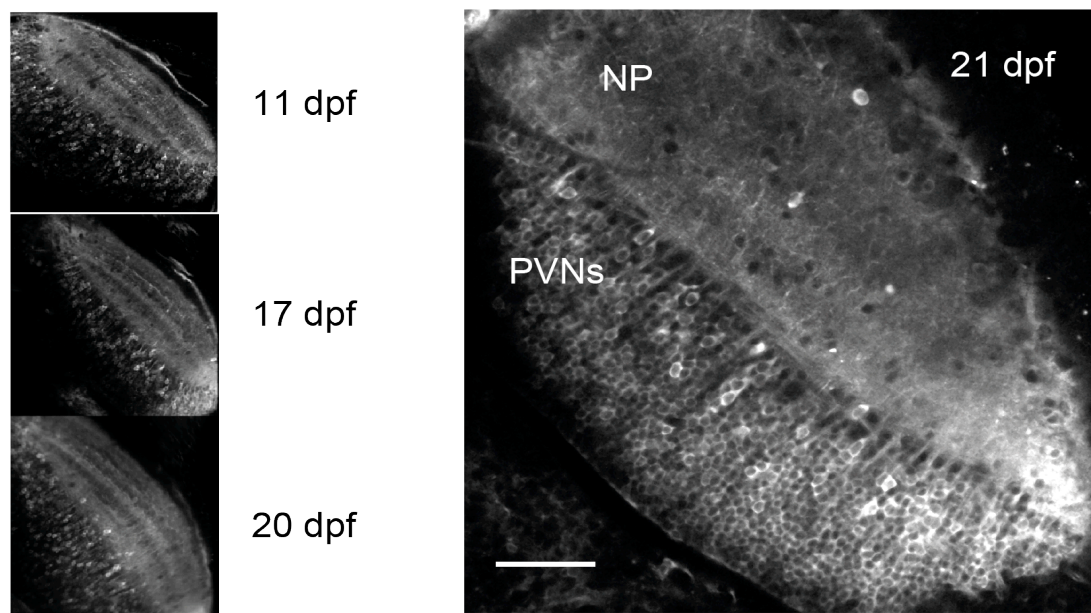


**Figure 3.1 NBT:GCaMP3 expression in the optic tectum in late stage larvae.** GCaMP3 expression was robust in fish aged 10 to 21 dpf. Shown here are representative confocal images of one tectal hemisphere at 11, 17 and 20 dpf (left panel). GCaMP3 was expressed in both the tectal neuropil (NP) and in the majority of PVN somata (PVNs). Scale bar: 50 μm.

To determine whether GCaMP3 labelling in the tectal neuropil also included presynaptic input from the retina i.e., axons of retinal ganglion cells (RGCs), I looked at GCaMP3 expression in the eye. In the eye, sparse GCaMP3 labelling was observed in the inner plexiform layer (IPL), which contains the dendrites of RGCs, and a small number of cells ($2.75 \pm 0.9$ per field of view, n = 10 randomly selected fields of view from 5 fish at 10 dpf) were labelled in the ganglion cell layer (Figure 3.2 A, B). Initially, these cells were thought to be misplaced amacrine cells as no labelling of the optic nerve was observed via confocal imaging (confocal z-stacks of the entire eye, n = 5 fish, 10 dpf; data not shown). To confirm this, Konstantinos Lygdas, a Ph.D. student in the lab, performed immunostaining on sections of the eye. These experiments revealed that a small number of NBT:GCaMP3 positive cells in the ganglion cell layer expressed the RGC marker zn5. In addition, a small number of RGC axons was labelled by NBT:GCaMP3 (Figure 3.2 B, C). Thus, a small number of NBT:GCaMP3 labelled neurites in the tectal neuropil is of presynaptic, retinal origin. However, labelling of RGCs was sparse compared to the dense labelling observed in the tectal neuropil. Moreover, large areas of the tectal neuropil were responsive to visual stimuli; only a small percentage of responding voxels could have been of retinal origin. Furthermore, responses from the neuropil were generally similar to those recorded from PVN cell bodies. We are therefore confident, that the recorded neuronal activity was mainly of postsynaptic origin and reflected the response properties of tectal neurons.

While the expression of GECIs often decreases with age (> 7 dpf) in commonly used *huc* driven lines (Kim et al., 2014), transgenic NBT:GCaMP3 fish offer the opportunity to study the role of the optic tectum for an extended period of time.
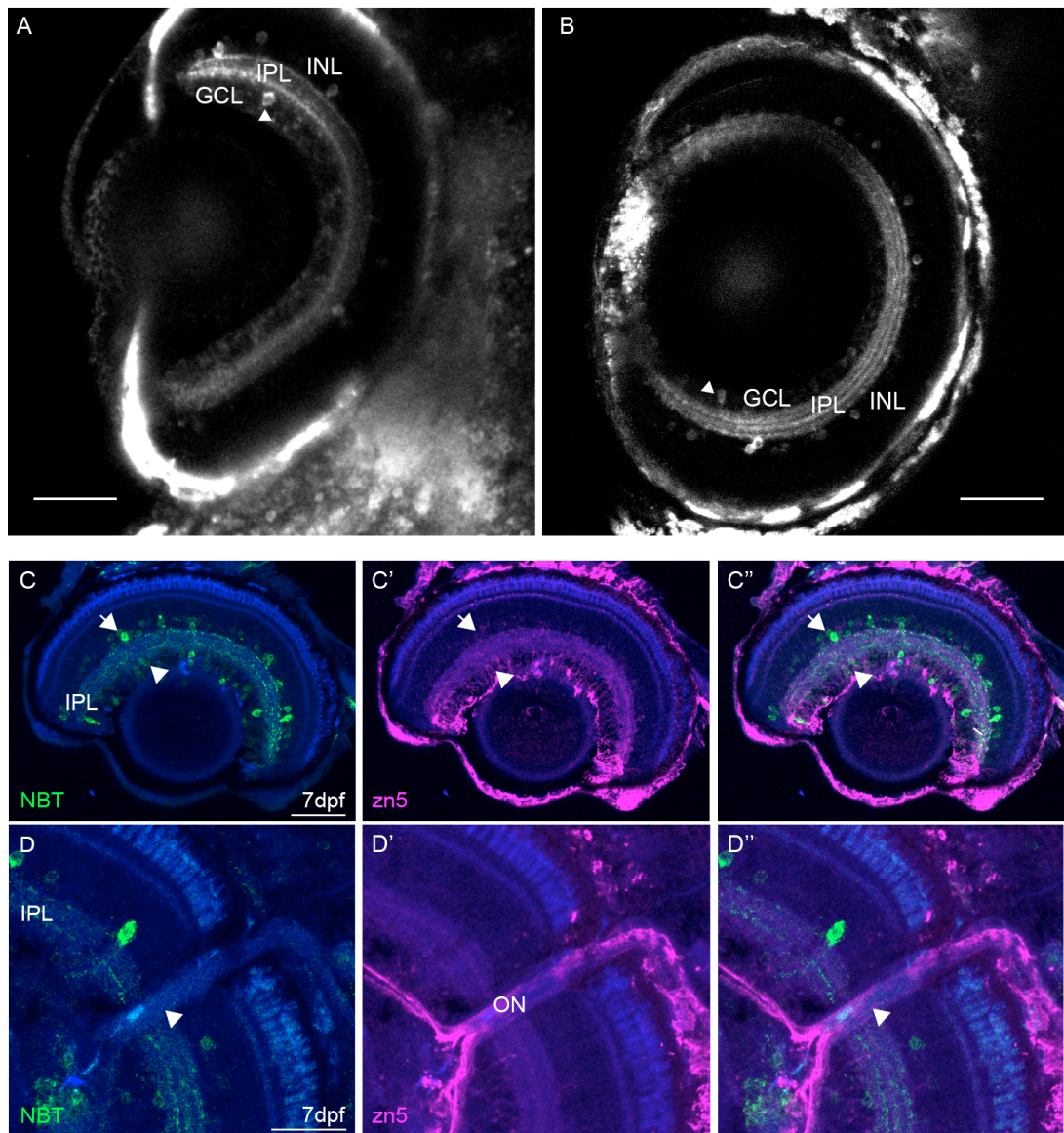
**Figure 3.2 NBT:GCaMP3 expression in the eye.** (**A**), (**B**) Optical sections of the eye in 10 dpf larvae, in dorsal (A) and lateral (B) view. GCaMP3 labelling was evident in the inner plexiform layer (IPL) and a small number of cells was labelled in the ganglion cell layer (GCL, arrowheads), as well as in the inner nuclear layer (INL) (**C**), (**D**) Sections of the eye of 7 dpf larvae. (**C**) NBT:GCaMP3 labelled amacrine cells in the inner nuclear layer (arrows) and a small number of cells in the GCL (arrowheads). The latter were positive for zn5, a marker for retinal ganglion cells. (**D**), NBT:GCaMP3 labelled a small number of  retinal ganglion cells in the optic nerve (ON). Scale bars: 50 µm (A, B, C), 25 µm (D). Panels (C) and (D) by Konstantinos Lygdas and Dr Ryan MacDonald.

## 3.2 Calcium imaging and simultaneous visual stimulation in zebrafish larvae up to 21 dpf

### 3.2.1 Design of the imaging chamber and projector stand

**Imaging chamber**

Several versions of the imaging chamber were used in the process of setting up this study. The first chamber (Figure 3.3A) was designed to fit a Leica SP1 confocal microscope (used early on in my Ph.D.) and was manufactured from polycarbonate sheets (Physics workshop, University of Sheffield). Magnetic tape was used to hold a raised glass stage in place. However, the choice of material and the design were not ideal; the walls scratched easily, the optical quality left much to be desired and the magnetic tape was not strong enough to hold the stage securely in place.

In order to improve the quality and speed of confocal imaging, I started using an Olympus FV1000 confocal microscope during the 2nd year of my Ph.D. training. I, therefore, designed a new chamber to fit this setup (Figure 3.3B): This time the chamber was manufactured from Perspex, which proved more resistant to scratches and offered better optical quality. In addition, the chamber was fitted with stainless steel inlays to securely fix the stage within the chamber.

The quality of the finished chamber, however, was unsatisfactory; the solvent used to join the parts clouded the material around the seams, leaving unwanted visual cues. I, therefore, designed the next chamber to be made from one piece; the chamber was made by CNC turning a block of Perspex and then polishing the walls to achieve the desired optical quality (Chemical & Biological Engineering workshop, University of Sheffield). This last imaging chamber (Figure 3.3C) and the Olympus FV1000 microscope were used for all experiments presented in Chapters 4 and 5.

**Projector stand**

A small tripod bought together with the projector, proved unsuitable, as it was not tall enough and was easily moved accidentally during the experiment. Therefore a small mount was designed onto which the projector could be fixed with a screw (Figure 3.3D). Additionally, the mount could be fitted onto a magnetic stand, providing a stable solution for holding the projector in place.
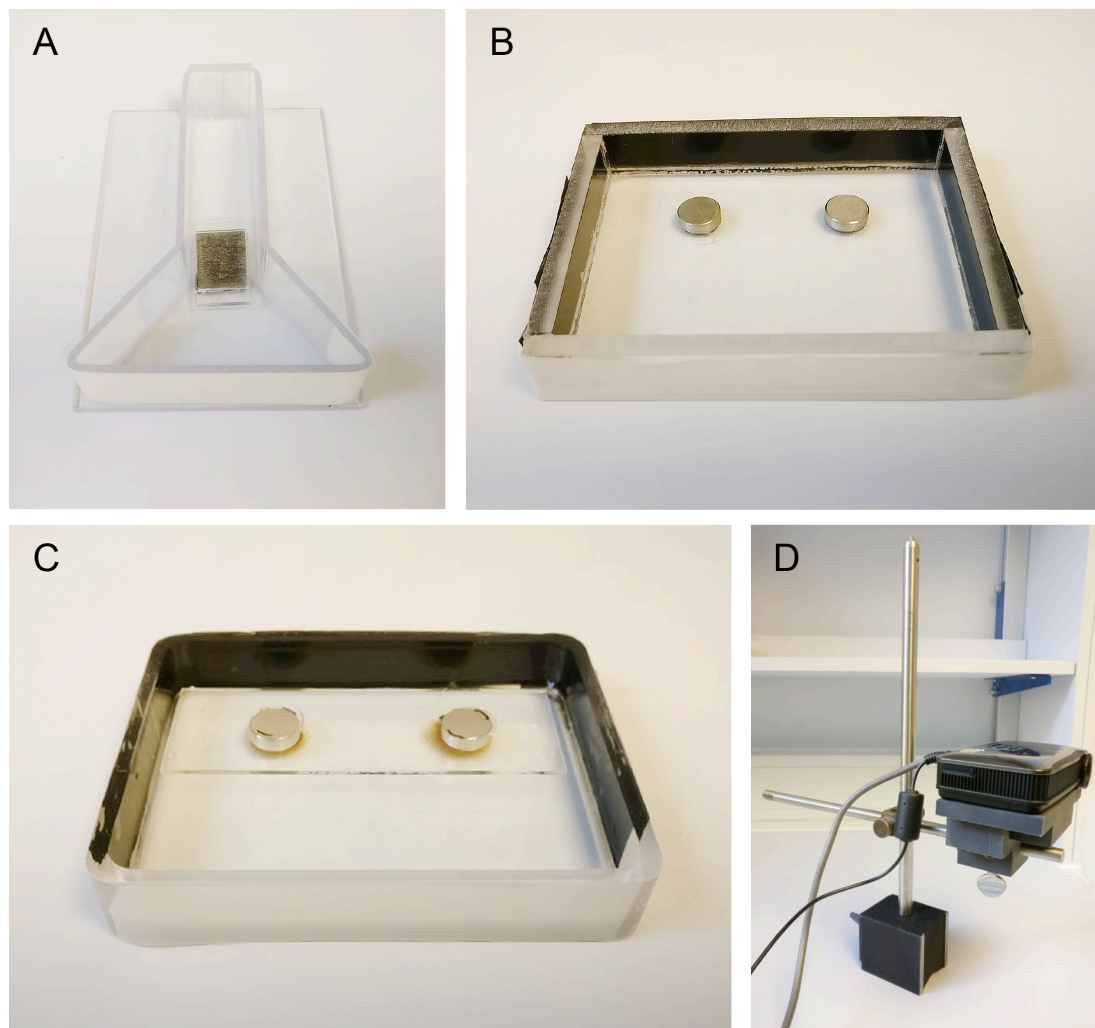
**Figure 3.3 Imaging chambers and projector stand.** (**A**) First chamber, manufactured from polycarbonate. Front wall was covered with opaque film. Raised glass stage was fixed with magnetic tape. (**B**) The second chamber was manufactured from Perspex and had two stainless steel inlays to hold a glass stage in place. The outside was covered in black tape (back, sides) and opaque film (front). (**C**) The final chamber was made from a single block of Perspex. It also had two stainless steel inlays to hold a glass stage in place. As with the previous chamber, the front was covered in opaque film (screen), whereas the sides were covered in black tape. Dimensions of the final chamber were 90 (L) x 70 (W) x 15 mm, wall thickness was 3 mm. (**D**) Custom-built projector mount, fitted on magnetic stage.

## 3.2.2 Imaging visually evoked activity in the optic tectum of older zebrafish larvae

In order to study the visual response properties of tectal neurons in older larvae, I developed an experimental paradigm for calcium imaging and simultaneous visual stimulation. The protocol was based on previous work in young (7 dpf) zebrafish larvae (Nikolaou et al., 2012), adapted for the use of zebrafish larvae up to the age of 21 dpf. Zebrafish larvae were immobilised in low melting point (LMP) agarose for the duration of the experiment. The concentration of LMP agarose was increased to 3.5% (from 2% in the original protocol, Nikolaou et al., 2012) and this was sufficient to restrain even relatively large 21 dpf larvae. However, from around 14 dpf onwards, fish rarely responded to the visual stimulations, which had reliably evoked strong tectal responses in younger larvae. As the ability of zebrafish larvae to take up oxygen by diffusion through their skin decreases with age (Rombough, 2002), this reduced responsiveness in older larvae may have been due to low oxygen supply to the brain. To facilitate oxygen uptake, I increased the amount of oxygen in the imaging solution by aerating the solution with a mix of 95% oxygen and 5% carbon dioxide for 30 minutes prior to the experiment. Aeration, however, reduced the pH of the imaging solution to approx. pH 4.6. To achieve an ideal pH of 7.5 (as used in the local aquarium facility), the solution was buffered in a mix of monosodium phosphate (1.2 mM) and sodium hydrogen carbonate (22.6 mM) prior to aeration. This increased the pH to the desired range of 7.3 - 7.6 after 30 minutes of aeration. These measures significantly improved the visual responsiveness in $14 - 18$ dpf larvae. By 21 dpf however, zebrafish largely depend on their gills to take up oxygen (Rombough, 2002). To decrease the risk of cerebral hypoxia during the up to three-hour-long imaging sessions, the agarose covering one gill was carefully removed for fish $\geq$ 18 dpf, so that ventilation of the gill was possible.

Initially, agarose covering the eye was removed prior to imaging to allow an unobstructed view of the screen. However, this often resulted in eye movements during the experiment, creating artificial variation in the data. As the project licence covering this study did not permit injection of neuromuscular blockers into the eye to prevent eye movements, we decided to not remove the agarose around the eye and cut the agarose close to the eye instead. This proved practicable and no deterioration or change in responses was observed.

Larvae were kept in E3 until 5 dpf, and E3 medium without methylene blue was used as imaging solution at first. During optimisation of the protocol, however, E3 was substituted with aquarium water, which seemed a more natural choice for use with older larvae, which were housed in tanks in the aquarium.

One problem frequently encountered during the early stages of this study, was that the agarose with the embedded fish would come loose and float off the glass stage during longer experiments. After some trial and error, fish were mounted on plastic coverslips, which provided better adhesion to agarose. The coverslip was then fixed on to the glass stage with Blu Tack. Combined, these modifications allowed me to monitor tectal activity in zebrafish larvae aged up to 21 dpf and for up to three hours.

### 3.2.3 Evoking visual responses in the optic tectum

The first step in setting up this study was to confirm whether light responses could be evoked in the tectum of NBT:GCaMP3 zebrafish larvae. Initially, an amber LED ($\lambda$ = 590 nm) was used to apply light pulses. The LED was mounted close to the imaging chamber and was controlled via a DAQ (data acquisition) device (LabJack). This temporary setup was later replaced by a mini projector presenting a full-field flashing stimulus (alternating black and white background) at different frequencies (2, 4, 6, 8 and 10 Hz). Generally, a 20 s period of darkness was followed by 20 s of flickering light; this was repeated five times, i.e., for each flicker frequency (Figure 3.4D, top).

Once tectal responses could be reliably evoked using full-field stimuli, I introduced stimulations with small moving shapes. Moving stimuli generally evoked strong responses in the optic tectum, with filled, black shapes usually causing the largest responses (Figure 3.4D, bottom). Further stimuli used in this study included small bars, combinations of bars and contours of simple shapes (squares, circles, triangles, and semicircles).

## Generation and presentation of visual stimuli

Visual stimulations were generated using the Psychophysics Toolbox Version 3 (PTB-3, Brainard, 1997; Kleiner et al., 2007; Pelli, 1997). PTB-3 is a free toolbox for Matlab or GNU Octave and allows the user to display and animate both visual and acoustic stimulations in a precise manner. All visual stimulation scripts used in this study were custom-written.

A pico projector was used to project stimulations onto the screen of the imaging chamber. The projector output was set to minimum brightness and to LED mode 'Economic' (<25 lumens); this reduced the risk of blinding the animal and also avoided the use of a Notch filter. To synchronise confocal imaging and the onset of visual stimulation, image acquisition was controlled by an external trigger. As the stimulation laptop did not have any serial or parallel ports, a DAQ device (LabJack) was used to send a 200 ms long TTL pulse to the microscope computer and trigger the start of the confocal time-series. The LabJack was controlled via the labJack.m script provided by Opticka (downloaded from github.com).
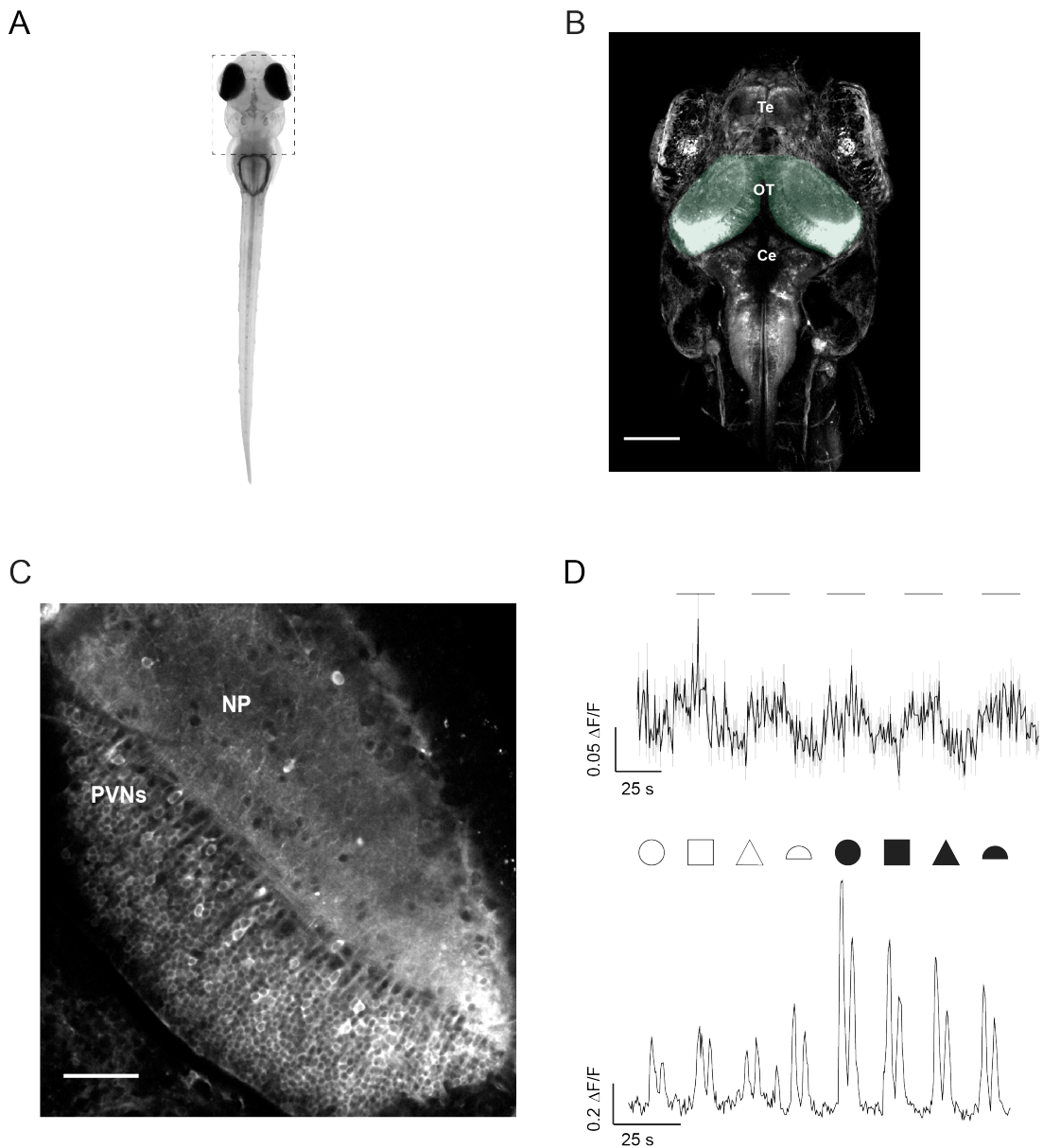
**Figure 3.4 Imaging neuronal activity in zebrafish larvae.** (**A**) Dorsal view of a zebrafish larva at 10 dpf, dashed box indicates the area shown in B. (**B**) NBT:GCaMP3 expression in the brain of a 12 dpf larva, maximum intensity projection of a confocal z-stack through the entire brain. Te, Telencephalon, OT, Optic tectum, Ce, Cerebellum. Tectal hemispheres are highlighted in green. (**C**) Optical section of the right tectal hemisphere in a 21 dpf larva. GCaMP3 is expressed in both the neuropil (NP) and somata of periventricular neurons (PVNs). (**D**) Visual responses in the optic tectum. *Top*: Average response ($\Delta F/F$) to flickering full-field stimulus (2, 4, 6, 8, 10 Hz, n = 72 ROIs in the NP in one field of view, 9 dpf). *Bottom*: Average response to moving objects (stimuli shown on top, n = 2187 voxels in NP, one field of view, 13 dpf). Scale bars: 200 μm (B), 50 μm (C). Error bars indicate SEM.

## 3.3 Conclusions

A central question in visual neuroscience is how the responses of individual neurons give rise to visual perception, and ultimately result in visually-guided behaviour. Calcium imaging with simultaneous visual stimulation presents a valuable tool to address this question. Zebrafish in particular provide an excellent model organism for this approach and have been used to study the visual response properties of neurons in the optic tectum, the main visual processing area of lower vertebrates (Del Bene et al., 2010; Gabriel et al., 2012; Grama and Engert, 2012; Hunter et al., 2013b; Kassing et al., 2013; Preuss et al., 2014; Hollmann et al., 2015).

The zebrafish visual system develops rapidly and many forms of visually guided behaviour are already present at 5 dpf (Burgess et al., 2010; Easter and Nicola, 1996; Engeszer et al., 2007; Strähle et al., 2012). However, behaviours related to visual learning and social preferences emerge later in development (Dreosti et al., 2015; Engeszer et al., 2007; Valente et al., 2012). To understand whether these behavioural developments are reflected on the functional level, it is important to study the visual response properties of neurons in older larvae.

Here, I have presented an experimental paradigm to record tectal activity in response to visual stimuli in zebrafish larvae aged $10 - 21$ dpf. The use of transgenic NBT:GCaMP3 fish, combined with a modified protocol for calcium imaging, provides the opportunity to study how the response properties of tectal neurons change during maturation of the visual system.

# 3.4 Future work

NBT:GCaMP3 expression levels were still high at 21 dpf and it would be interesting to extend the imaging period to juvenile fish. However, as described in section 3.2.2, the ability of zebrafish to take up oxygen through their skin decreases with age and by 21 dpf larvae largely depend on their gills. In order to extend the imaging period beyond 21 dpf, an alternative approach for supplying the fish with oxygen is needed. In adult fish, this has been achieved by intubation; a small tube is placed in the fish's mouth and provides a constant flow of fresh imaging solution to the gills. This approach has recently been successfully applied to juvenile fish (Olt et al., 2016) and offers a solution to image zebrafish larvae beyond the age of 21 dpf. In the future, imaging neuronal activity could also be improved by expressing brighter alternatives to GCaMP3 (e.g., GCaMP6) under the NBT promoter.

# Chapter 4

# Spatial receptive fields in the zebrafish optic tectum

## 4.1 Introduction

The concept of receptive fields (RFs) is of significant value in the study of visual processing in the nervous system. The process of mapping RFs generates an important readout of the visual tuning properties of individual neurons. The spatial receptive field of a neuron is defined as the area in visual space where a light stimulus can elicit a response, i.e., trigger the firing of action potentials or changes in the membrane potential of the cell (Hartline, 1938). Classically, spatial RFs have been mapped using moving or flashing simple stimuli, such as bars or small spots (reviewed in: Ringach, 2004). Spatial RFs provide valuable information about the following parameters:

1) **RF size**: Comparing RF sizes at different levels of the visual pathway provides insight into how visual information is processed. For example, in mammals, RFs gradually increase in size and complexity along the visual pathway; this observation originated the concept of hierarchical processing (Hubel and Wiesel, 1962). In fish, the neocortex is absent; a hierarchical visual pathway similar to the mammalian one has not been described. Instead, the optic tectum (OT), which receives major direct input from the retina, is considered as the main site of visual processing. It has yet to be determined whether RF size and complexity change with increasing OT depth, as it has been observed in birds (Schmidt and Bischof, 2001; Verhaal and Luksch, 2013). 2) **RF sharpness**: Receptive fields undergo dynamic refinement during development (Gaze et al., 1974; Holt and Harris, 1983). Measuring the size of a RF and the sharpness of its tuning profile (usually calculated as the ratio of the half-

maximum amplitude of the tuning curve over the geometric mean of the half-widths at half-maximum; Zhang et al., 2011) at different developmental stages can shed light on the processes involved in the maturation of sensory systems (Binns and Salt, 1997; Tao and Poo, 2005; Zhang et al., 2011). 3) **RF shape and orientation**: Hubel and Wiesel's (1962) seminal work on the visual cortex of cats, demonstrated how the elongated, oriented RFs of simple cortical cells can be generated by the hierarchical convergence of round RFs in the lateral geniculate nucleus (LGN). RFs in the optic tectum of fishes often have complex, non-homogenous shapes (e.g., chevron) and accessory fields (Schellart and Spekreijse, 1976; Guthrie and Banks, 1978; Sajovic and Levinthal, 1982a). How exactly these RFs are generated and what their role may be, remains fairly unexplored. 4) **Visuotopic organisation**: The OT is involved in orienting behaviours, which require a map of visual space; similarly to the function of its mammalian counterpart, the superior colliculus (SC). Positional information is conserved in a retinotopic map, i.e., neighbouring cells in the OT receive input from neighbouring retinal ganglion cells (RGCs) and therefore from points close to each other in the visual environment. Niell and Smith (2005) observed a strong correlation between cell body position and position of RF centre in relation to visual space for tectal PVN neurons. Bollmann and Engert (2009) suggested that a similar arrangement is likely to be found in the neuropil; however, this has yet to be confirmed in zebrafish.

Zebrafish are highly visual animals and provide a popular model for studying the visual system. In recent years, research has focused on understanding the functional mechanisms and underlying circuitry of visual processing in the optic tectum (reviewed in Chapter 1). Despite the fact that mapping the RFs of neurons can provide valuable information about how visual input is processed, surprisingly little is known about the visual receptive fields of tectal neurons. So far, only a handful of studies have characterised RF properties in zebrafish. More than 30 years ago, Sajovic and Levinthal (1982a, 1982b) provided the first description of RFs in the adult zebrafish tectum. Using small flashing and sweeping spots and single-unit recordings from the periventricular layer, they mapped RFs in adult zebrafish. Four types of tectal neurons were identified according to their principal response types: 1) The majority of tectal cells were classed as *Type I*. These cells show no firing in the dark and exhibit brief bursts of spikes in response to a small spot turning ON or OFF. However, they respond better to moving stimuli and often have compound

RFs. 2) *Type T* cells are the second most commonly observed type. These cells are similar to *Type I* cells, however, they are spontaneously active and show phasic ON and OFF responses, which are longer than those of *Type I* cells. 3) *Type S* cells are less frequent and show no firing in darkness, but exhibit sustained responses to light stimulation, and when a small spot is turned ON. 4) *Type B* cells fire regular bursts in darkness but are completely insensitive to moving stimuli. Turning stationary spots ON or OFF either increases or decreases the burst rate.

This classification, however, is not always definite and mixed types of responses were observed. In general, Sajovic and Levinthal (1982a) observed that tectal cells had relatively large RF sizes (mean width: 34°, 38.6°, and 35.6°; mean height: 24.9°, 28.2°, and 25.4° for *I, T* and *S* cells, respectively), were organised retinotopically and mostly had overlapping ON and OFF areas.

In the early 2000's zebrafish became increasingly popular as a model system in neuroscience. Niell and Smith (2005) building on the original work of Sajovic and Levinthal focused on the development of tectal response properties in zebrafish larvae (up to 9 dpf). Using cluster analysis, Niell and Smith (2005) confirmed that the four broad response types described by Sajovic and Levinthal (1982a) were already present at 78 hpf. They observed that other properties, such as RF appearance, size and the retinotopic organisation of RF centres also developed rapidly and did not change much after 84 hpf. Overall, Niell and Smith (2005) demonstrated that many response properties of tectal neurons emerge relatively early in the development and undergo little refinement after 78 hpf. More recently, however, Zhang and colleagues (2011) found that similarly to *Xenopus* (Tao and Poo, 2005; Akerman and Cline, 2006), RFs in the zebrafish tectum undergo spatial refinement between 4 dpf and 9 dpf. This refinement period is characterised by an initial expansion in RF size (both excitatory and inhibitory) from 4 dpf to 6 dpf, followed by a decrease in RF size from 6 dpf to 9 dpf. During this period, excitatory and inhibitory RFs become well matched and spatial tuning profiles are sharpened. Zhang et al. (2001) attributed this functional refinement, to changes in the convergence of the excitatory retinal input, i.e., the strengthening of synaptic connections in the RF centre, and weakening of connections in the periphery. Interestingly, this elimination of synapses is not reflected in the morphology of axonal or dendritic arbours.

While Zhang et al., (2001) described an initial period of RF refinement, it remains unknown whether the RFs of tectal neurons undergo any further changes in late-

stage larvae or juvenile zebrafish. This is of particular interest because behavioural experiments have shown that between 2 and 4 weeks post-fertilisation, zebrafish start to exhibit complex social behaviours (Dreosti et al., 2015; Hinz and de Polavieja, 2017) as well as the ability to learn (Valente et al., 2012). Using NBT:GCaMP3 fish, I have investigated the RF properties of tectal cells in late stage larvae, aged $14 - 18$ dpf. In particular, I have studied RF size, shape, orientation and the topographic organisation of RF centres. While previous studies solely focused on the cell bodies of periventricular neurons, the largest group of cells in the OT (Nevin et al., 2010), I have also studied the RF properties of the tectal neuropil. As described in section 1.1.5 of the introduction, the neuropil is a highly organised structure, containing the dendrites and axons of tectal neurons, afferent axons, as well as a small number of interneurons, where the majority of tectal processing is thought to be taking place.

## 4.2 Estimation of spatial RF size with flashing bars

As described in the previous section, spatial RF sizes of tectal cells have been reported for young larvae (9 dpf) and adult zebrafish. In my initial set of experiments, I used flashing bars to rapidly define the borders of receptive fields in the optic tectum of late-stage larvae (14-18 dpf).

Large flashing bars (2 Hz, vertical bars: 6° (W) × 35° (H), horizontal bars: 124° (W) × 6° (H)) were presented at different positions on the screen. Vertical bars were presented along the horizontal axis of the screen to estimate the horizontal dimension of the RF, and vice versa to obtain the vertical dimension of the RF (Figure 4.1A). Responding traces were fitted with a Gaussian function and RF widths were defined as $2 \times \sigma$ (Figure 4.1C, D). Figure 4.1E indicates that RF sizes in the tectal neuropil differ widely, but are generally relatively large as the majority of RFs are between 15° and 60° in width. The mean RF size along the horizontal dimension was 36.7° ± 22.6 (n = 147 ROIs from 4 fish, ± SD, Figure 4.1 E). RF sizes along the vertical dimension were considerably smaller; the mean RF size was 21.2° ± 25.8 (n = 158 ROIs from 4 fish, ± SD, Figure 4.1 E). However, the size of the screen in the vertical dimension was relatively small, only subtending a visual angle of 35°. On manual inspection, many ROIs showed high responses to bars located at the upper border of the screen, suggesting that a considerable proportion of RFs were located (partly) outside the area covered by the screen. Therefore, the calculated RF height may well underestimate the actual size of the RFs. RF sizes were also calculated for the PVN cell bodies, however, the flashing bar stimulus was not very effective and only very few cells in all four fish responded well to this stimulus.

A
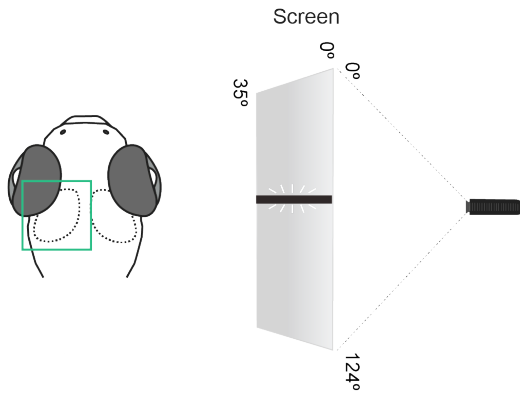


B
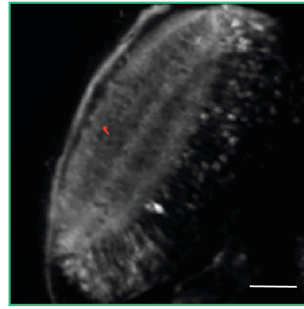


C
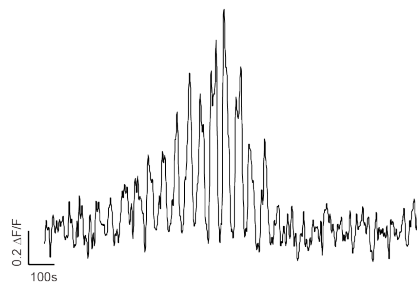


D
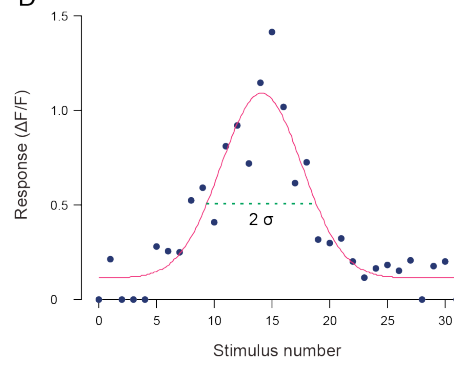


E(i)
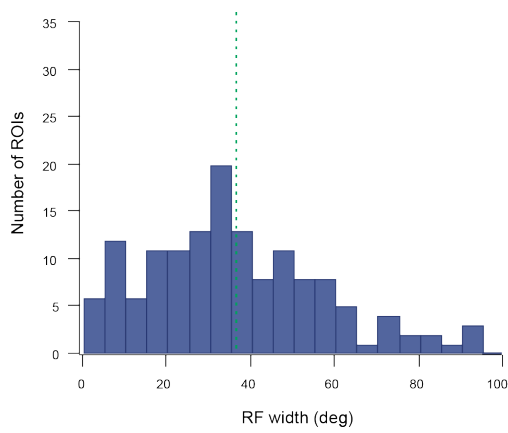


E(ii)
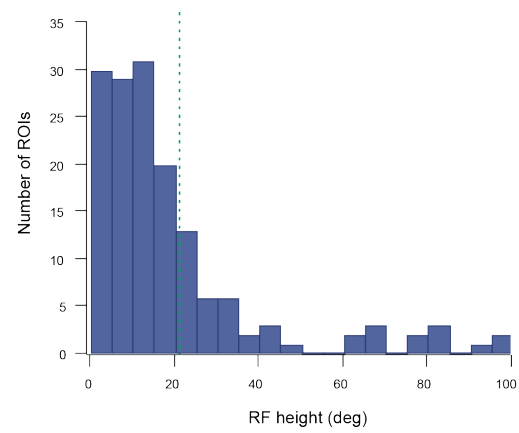


F
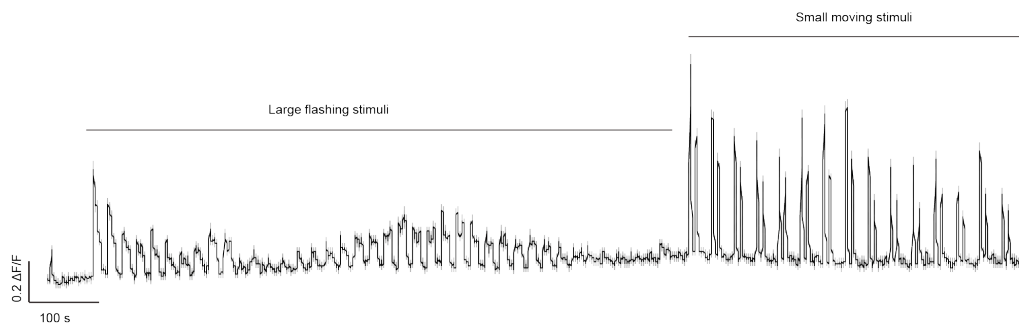
**Figure 4.1 Estimating RF size with flashing bars.** (**A**) Schematic diagram of visual stimulation: a flashing bar (2 Hz) was presented at different positions along the horizontal axis. Green box indicates contralateral tectum imaged in (B). (**B**) Dorsal view of one tectal hemisphere of a NBT:GCaMP3 zebrafish larvae (12 dpf). Example ROI presented in (C) and (D) is highlighted in red. (**C**) Fluorescence changes of example ROI in response flashing bar at different positions. (**D**) Response trace shown in (C) fitted with a Gaussian distribution. RF width was defined as $2 \times \sigma$. (**E**) E(i) Distribution of RF widths (n = 147 ROIs) and E(ii) RF heights (n = 158 ROIs) in the tectal neuropil. Green dashed line indicates mean. (**F**) Average responses to flashing (bars) and moving stimuli (angles), (n = 184 ROIs). Data from 4 fish. Scale bar: 50 μm

# 4.3 RF mapping with small moving spots

While flashing bars provided a fast stimulation to estimate RF sizes in the tectal neuropil there are a number of caveats to consider when employing this method: i) The bars were relatively large and therefore did not provide detailed information about the shape of the RF. ii) The majority of PVN cell bodies did not respond to flashing bars, and iii) The responses to large flashing bars were much lower than those evoked by small moving stimuli (Figure 4.1 F). In order to attain a more detailed characterisation of spatial RFs in the optic tectum, I employed a stimulation routine, which had successfully been used in the past to map the RFs of tectal cells in young larvae (Niell and Smith, 2005) and adult zebrafish (Sajovic and Levinthal, 1982a): A small spot moved across the screen in two cardinal directions (top-to-bottom and posterior-to-anterior, as shown in Figure 4.2A. For a detailed description of the stimulus see Materials and Methods, section 2.2.2). The resulting vertical and horizontal tuning curves (i.e., responses to horizontally and vertically moving spots, respectively) were multiplied for each ROI, creating a 2D spatial RF (Figure 4.2C). In order to analyse and compare RF parameters, such as width, height and RF centre, the 2D RFs were then fitted with a bivariate Gaussian distribution; RF width and height were defined as $4\sigma$ along the respective axis. A total of 48 PVN cell bodies and 7790 voxels (neuropil) from 6 fish were analysed.

A



B



C

Response to horizontal sweeps   Response to vertical sweeps

$R(x,y) = R(x) \cdot R(y)$

$R(x,y) = R(x) \cdot R(y)$

0, 0

10, 10

0.5 ΔF/F

15 s

D

Neuropil (voxels)                                    PVN cell bodies

Response amplitude
$R(x) \cdot R(y)$

2

1

0
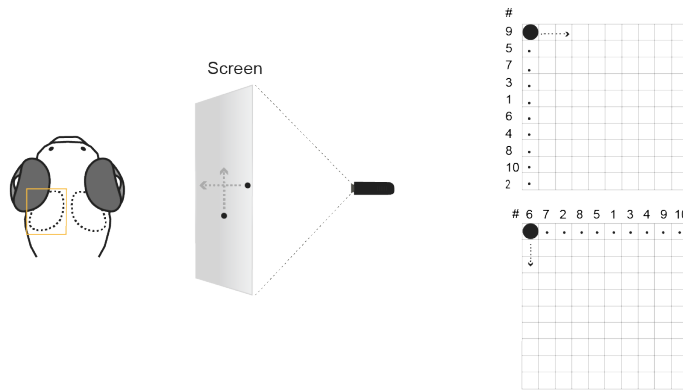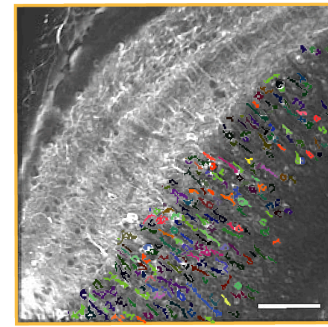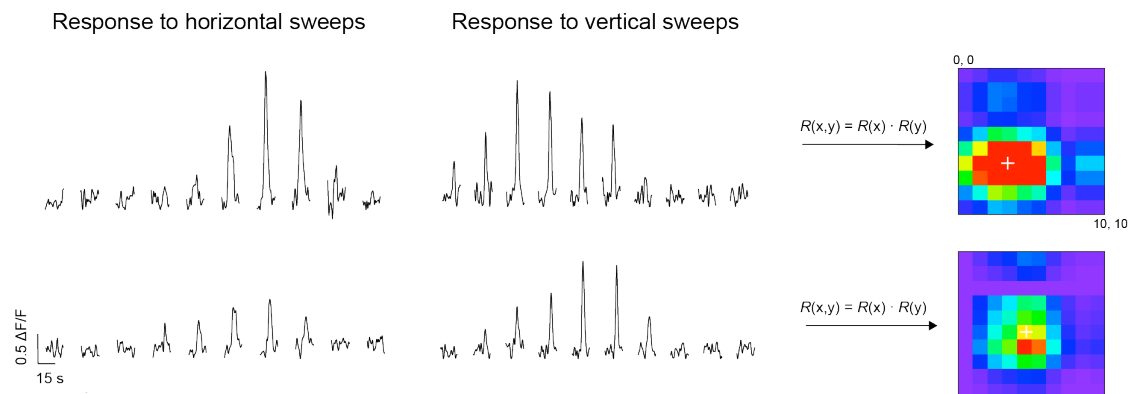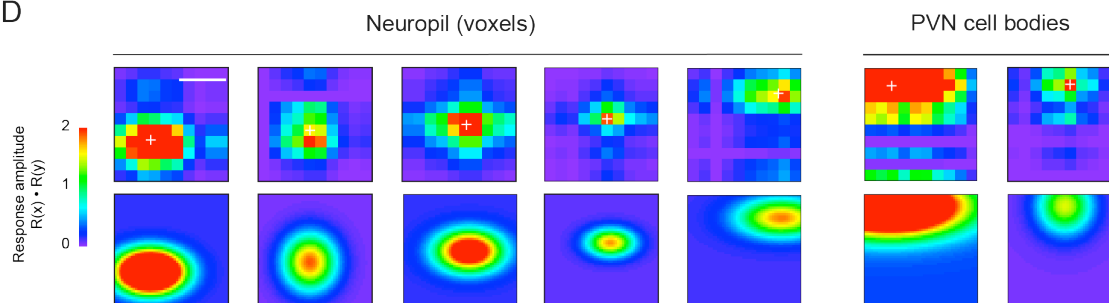
**Figure 4.2 Mapping receptive fields in the optic tectum with small spots.** (**A**) Schematic diagram of the experimental setup (left) and small spot visual stimulation (right). Yellow box indicates region imaged in (B). (**B**) Dorsal view of one tectal hemisphere of a transgenic zebrafish larvae (18 dpf) expressing GCaMP3 in both the tectal neuropil and cell bodies of PVN neurons. Confocal time-series were analysed either on a voxel-wise basis (neuropil) or on a region of interest (ROI) basis (cell bodies). Cell bodies were randomly colour-coded for better visualisation. (**C**) Representative ΔF/F traces for two voxels in the neuropil, in the response to a small spot moving horizontally or vertically across a 10-by-10 grid on the screen. The stimuli were presented in a pseudo-random order; the response traces shown here were manually sorted for presentation purposes. Responses to vertical and horizontal sweeps were multiplied for each location, resulting in the 2D RFs shown on the right. (**D**) Top: Examples of spatial RFs in the tectal neuropil and cell bodies of PVN neurons, colour-coded to show response amplitudes for each point on a 10-by-10 grid. Bottom: 2D RFs fitted with a bivariate Gaussian distribution. White cross indicates RF centre as determined by parametric fitting with a Gaussian distribution. Scale bars: 50 µm for fluorescence image, 20 degrees for RFs (white bar in first image).

## 4.3.1 Receptive fields in the optic tectum are relatively large

About 5-20% of cells per field of view exhibited robust responses to the spots at different positions. Manual inspection revealed a variety of RFs, differing in size, shape, and position of the centre, both in the neuropil (NP, Figure 4.2D, left) and the cell bodies of the periventricular neurons (CB, Figure 4.2D, right). Most RFs could be described as having a round or elliptical shape, and a clearly defined centre. The majority of elliptical RFs were elongated in the horizontal direction (average width/height ratio was 1.9 for neuropil (7790 voxels from 6 fish) and 3.1 for cell bodies (48 cells, 5 fish)).

In general, the sizes of RFs in the neuropil were similar to those in the cell bodies. The majority of RFs were between 10° and 90° in width and 10° and 50° in height. Mean RF sizes were 44.9° ± 20.8° (width) and 28.4° ± 13.8° (height) for the neuropil (± SD, Figure 4.3A,B, magenta bars) and 53° ± 30.9° (width) and 28.7° ± 24.9° (height) for cell bodies (± SD, Figure 4.3A,B, blue bars). The overall size was described as the area covered by the RF ($\pi \times$ width $\times$ height, Figure 4.3C). As the stimuli were only presented in a small portion of the visual field (48.9 x 48.9 degrees), many of the RFs were located at the borders of the grid, and only a portion of the RF was mapped. To test, whether fitting these RFs with a bivariate Gaussian function still resulted in a correct estimate of RF size, I compared the size distribution of all RFs with the distribution of a subset of RFs, whose centre was located in the middle of the grid. RF size distribution, as well as mean RF size values for both groups, were similar and I, therefore, assumed that the result of the

Gaussian fit correctly predicted RF size even for RFs which were partly located outside the grid (NP, mean RF width: 44.9° ± 20.8° (all), 42.4° ± 14.1° (centre-only); mean RF height: 28.4° ± 13.8° (all), 25° ± 9.3° (centre-only). CB, mean RF width: 53° ± 30.9° (all), 48.2° ± 22.8° (centre-only); mean RF height: 28.7° ± 24.9° (all), 37.2° ± 13.7° (centre-only)).

The size of RFs was independent of the position of the RFs in the neuropil. However, response maps of RF size, where individual voxels were colour-coded according to RF size, revealed a 'hot spot' pattern where large-size RFs appear to be arranged in clusters and RF size gradually decreases with distance from these 'hot spots' (Figure 4.3E).

**Figure 4.3 Spatial receptive field sizes in the optic tectum.** (**A, B**) Blue bars: Distributions of RF width (left) and height (right) in the neuropil (A) and PVN cell bodies (B) Green bars show subset of voxels or cell bodies, which are located in the centre of the grid. (**C**) Distribution of overall RF area in the neuropil (magenta) and PVN cell bodies (blue). (**D**) RF shape displayed as ratio of RF width/RF height. (E) RF sizes in the neuropil form 'hot spots'. (NP: n = 7790 voxels from 6 fish; CB: n = 48 cells from 5 fish; Age: 14, 16 and 18dpf) Scale bars: 50 μm

A



B



C



D



E
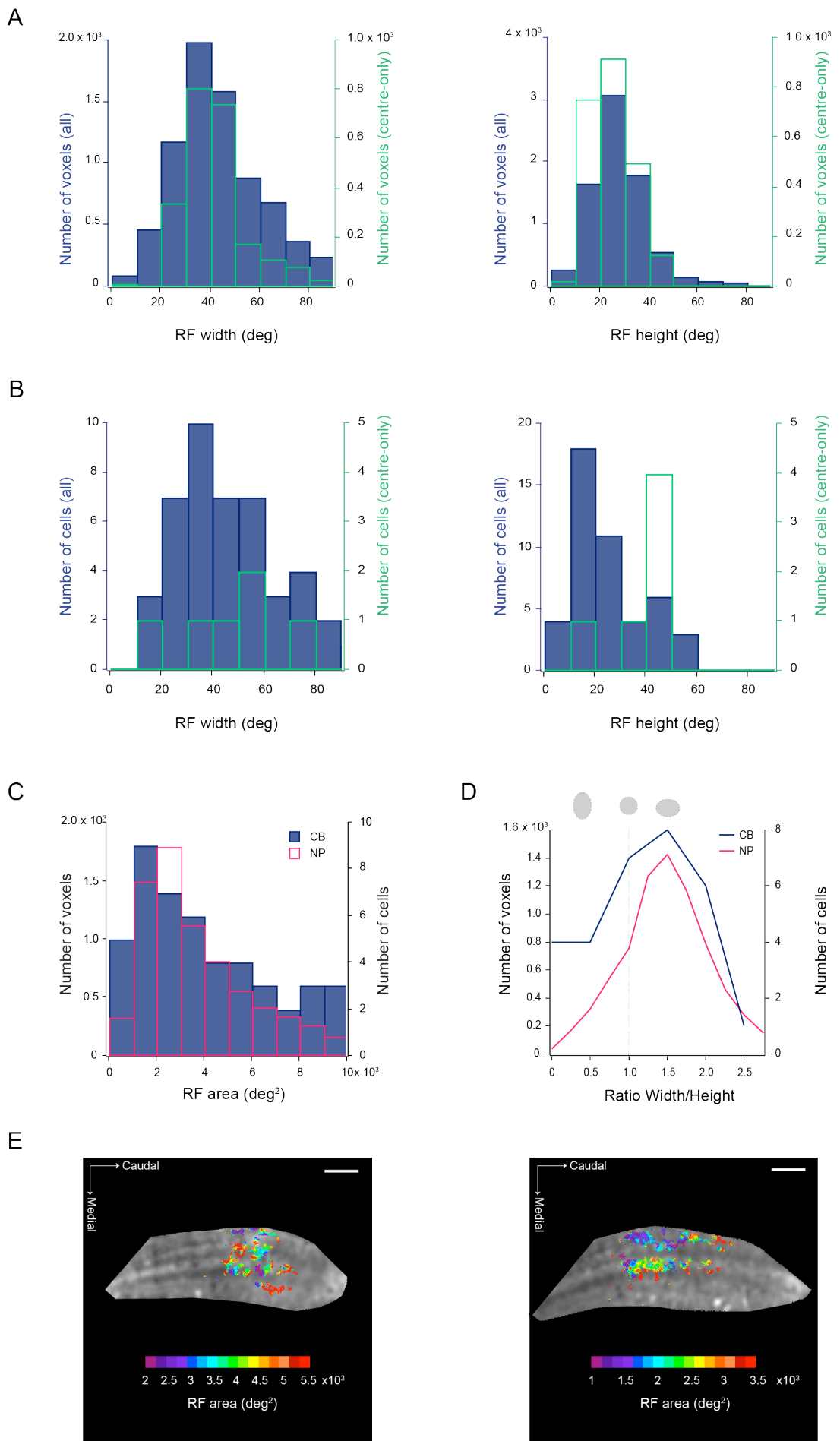
## 4.3.2 Receptive field size decreases with age

It was observed that the RF sizes were markedly different in the different age groups; RF size significantly decreased from 14 to 18 dpf. Figure 4.4 illustrates the average spatial RF size from 6 (5 fish for cell body data) individual fish aged 14 (n = 2), 16 (n = 2) and 18 dpf (NP: n = 2; CB, n = 1). Both width and height of the RFs gradually decreased with age. In the neuropil, the average RF width was 62.6° ± 21.7° at 14 dpf, 53.3° ± 17.2° at 16 dpf, and 32.2° ± 12.4° at 18 dpf. Similarly, the average RF height decreased from 37.3° ± 13.7 at 14 dpf to 30.4° ± 11.7 at 16 dpf, to 23.3° ± 12.8° at 18 dpf. For cell bodies the average RF width changed from 60.3° ± 32.4° at 14 dpf, to 51.3° ± 28.4° at 16 dpf to 28.3° ± 14.2° at 18 dpf. Likewise, RF height decreased from 36.4° ± 29.3° at 14 dpf to 22.6° ± 13.8° at 16 dpf and 11.6° ± 4.6° at 18 dpf. All RF sizes are stated as ± SD. The differences between age groups were significant ($p < 0.05$, two-sample $t$-test) for all comparisons but one; in cell bodies, the average RF width did not change significantly between 14 and 16 dpf (p = 0.4).
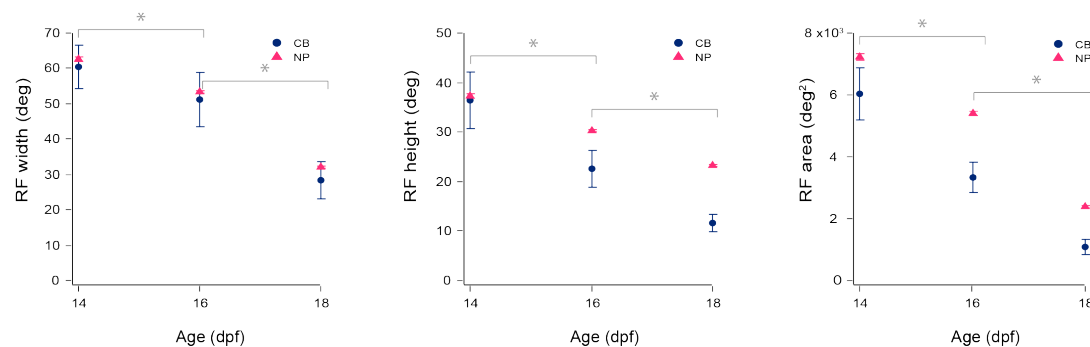


**Figure 4.4 Spatial RFs decrease in size from 14 dpf to 18dpf.** RF width (left), RF height (middle) and RF area (right) at 14 dpf, 16 dpf and 18dpf in neuropil (magenta triangle) and cell bodies (blue circle). Error bars indicate SEM. (NP: n = 7790 voxels from 6 fish; CB: n = 48 cells from 5 fish)

### 4.3.3 Retinopic organisation of receptive fields

Both the cell bodies and the neuropil exhibited a highly retinotopic organisation; the position of the RF centre correlated with the relative location of the cell or ROI within the optic tectum. Cells and ROIs located at the rostral end of the tectum responded to stimuli in the anterior portion of the visual field, whereas cells and ROIs at the caudal end, responded to stimuli in the posterior part (Figure 4.5). This correlation was strong for both cell bodies (Figures 5B, D) and ROIs in the neuropil (Figures 5A, C) in all fish (NP: mean correlation coefficient (Pearson's correlation coefficient, PCC) for all fish = $0.83 \pm 0.023$, n = 7790 voxels in 6 fish; CB: mean correlation coefficient (PCCs) for all fish = $0.85 \pm 0.033$, n = 48 cells from 5 fish). A corresponding relationship between the top-to-bottom visual axis and the dorso-ventral position within the OT was observed when imaging at different depths but was not detected in a single image plane. The ROI position in relation to the neuropil layer (superficial to deep) had no effect on the position of the RF centre (Figure 5A).

A



B

Neuropil

PVN cell bodies



RF centre position

Anterior                                Posterior
              0          10

RF centre position

Anterior                                Posterior
              0          10

C



c = 0.94
slope = 0.074 ± 0.00058

Relative RF centre position

Relative voxel position (px)

c = 0.845097
slope =0.11 ± 0.016

Relative RF centre position

Relative position of cell body (px)
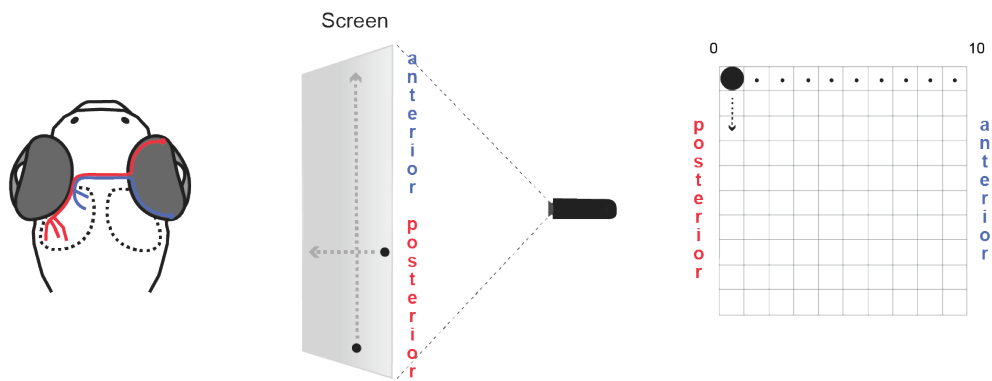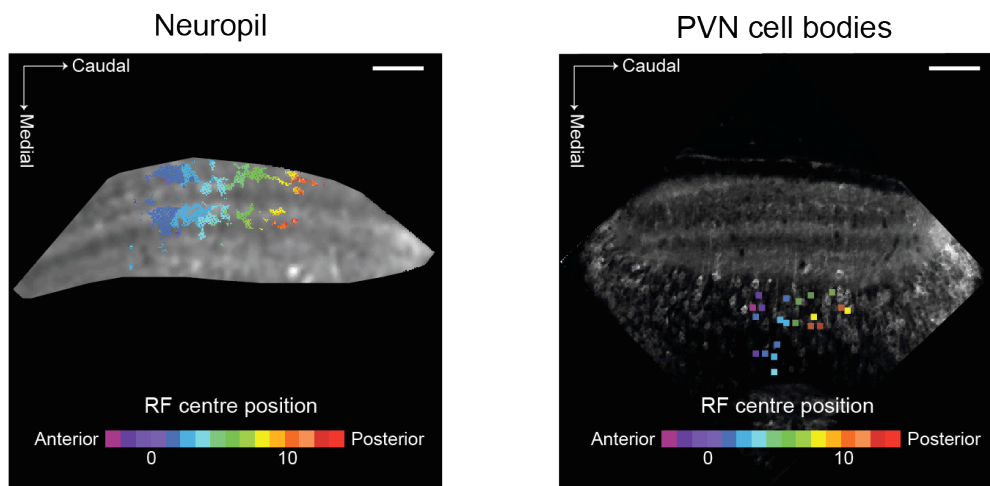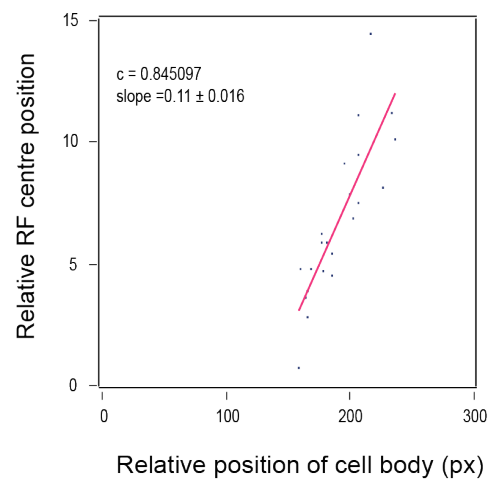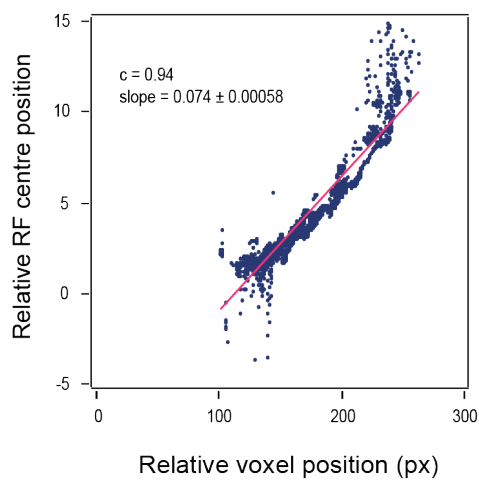
**Figure 4.5 Visuotopic organisation of RF centres in the optic tectum**. (**A**) Schematic diagram of the experimental setup for visual stimulation, also illustrating the retinotopic organisation of visual input to the optic tectum: retinal ganglion cells located in the anterior part (red) of the retina, convey information about the posterior part of the visual field and project to the posterior part of the optic tectum and vice versa. (**B**) Position of RF centre, as determined by parametric fitting of a bivariate Gaussian distribution, along the anterior − posterior axis shows visuotopic organisation in the neuropil (left) and PVN cell bodies (right). Representative examples of one field of view. (**C, D**) Visuotopic correlation illustrated as regression fit to RF centre versus relative position of voxel (**C**) or cell body (**D**) within the optic tectum (in pixels). Data corresponds to fields of view shown in B. c calculated as Pearsons's correlation coefficient. Scale bar: 50 µm

## 4.4 Discussion and future work

In the research study presented in this thesis, I have mapped spatial RFs in the OT with large flashing bars and small moving spots in zebrafish aged 12 − 18 dpf. Despite the fact that zebrafish is a popular model organism in the field of visual neuroscience, relatively little is known about the response properties of neurons in their primary visual processing area, the optic tectum, and only a handful of studies have focused on the RF properties of these cells. Sajovic and Levinthal (1982a, 1982b) were the first to provide a detailed description of RF shapes and sizes in adult zebrafish and defined four different principal response types in tectal neurons. This research was followed up by Niell and Smith (2005), who used a similar approach to study RF properties and the development of tectal response properties in young larvae. Despite the difference in age, the average RF size and principal response types were similar in both studies. Niell and Smith (2005) concluded that many response properties, including RF size, develop relatively early and do not change drastically after 84 hpf. More recently, however, Zhang and colleagues (2011) found that tectal neurons in zebrafish, similar to those in frogs (Tao and Poo, 2005), do indeed undergo a period of RF refinement between 4 and 9 dpf.

### 4.4.1 Estimating spatial RF sizes with flashing bars

Large flashing bars proved to be an effective stimulus to estimate RF sizes in the tectal neuropil. On the other hand, PVN cell bodies rarely responded to this stimulus. The reason for this non-response is not obvious, considering that large bars had been used previously to estimate orientation and direction selectivity of tectal neurons in zebrafish (Hunter et al., 2013b) and small flashing spots had been

successfully employed to map tectal RFs (Sajovic and Levinthal, 1982b, 1982a). However, the experiments presented in this thesis confirmed that RF sizes in the neuropil are similar to those reported for PVN cell bodies; the average RF size, 36.7° was very similar to RF sizes reported in tectal neurons in young larvae, 40° (Niell and Smith, 2005), and adult zebrafish, 36.1° (Sajovic and Levinthal, 1982a).

## 4.4.2 Mapping spatial receptive fields with small moving spots

To describe the spatial RFs in the OT in more detail, I also employed a second approach. Mapping with small moving spots evoked reliable responses in the tectal neuropil, however, only $5 - 20$ % of the PVN cell bodies responded reliably to this stimulus. This proportion is similar to what has been reported by Niell and Smith (2005) and can be explained by the fact that only two (type I and T), out of four tectal response types, respond to moving stimuli (Sajovic and Levinthal, 1982b). While another type (type B) only responds to overall changes in illumination, a third large group (type S) of tectal cells has been shown to respond best to flashing spots (Sajovic and Levinthal, 1982b). Unfortunately, due to the time restrictions of this Ph.D. study, it was not possible to do experiments using a combination of both flashing and moving stimuli to enhance the representation of tectal cell types. This is something that future research on tectal receptive fields in older zebrafish larvae should aim to address. The observed RFs differed in size and shape, but always displayed a clearly defined contour and centre; they appeared largely similar to the RFs observed by Niell and Smith (2005, Figure S1). The vast majority of RFs could be described as circular or elliptical. This is consistent with the findings of a recent study on the archerfish optic tectum (Reichenthal et al., 2018). Complex, multi-centre RFs or RFs with accessory fields, which have been previously observed in adult zebrafish (Sajovic and Levinthal, 1982a) and other teleosts, such as perch (Guthrie and Banks, 1978) and goldfish (Schellart and Spekreijse, 1976), were not observed in the present Ph.D. study. This may be explained by a phenomenon described by Sajovic and Levinthal (1982a), that is, compound RFs could be observed when the stimulus consisted of a white spot on a dark background; however, when a black spot on a white background was used instead (as was the case in the present Ph.D. study) the accessory fields disappeared. This phenomenon has not been described for other fish (Guthrie, 1990) and its exact mechanisms remain

unexplored. It is of note that the two-dimensional RFs presented in this thesis were calculated as the outer product of two one-dimensional RF vectors. This approach results in RFs, which are either round or elongated along one direction (horizontally or vertically). Diagonally-oriented, curved or chevron RFs previously described in adult zebrafish (Sajovic and Levinthal, 1982a) and perch (Guthrie and Banks, 1978) could therefore not be detected. Rather than calculating the 2D RF from two 1D RF vectors, future experiments should be adapted to take the actual response to the stimulus at each position on the 10-by-10 grid. For example, instead of moving the spot along the whole grid, a smaller spot could be used, which only moves within each individual square of the grid. This way the 2D RF could be constructed from the individual responses to each stimulus position, which would result in a more detailed and realistic representation of the RF.

## 4.4.3 Receptive field orientation

The vast majority of tectal RFs reported in this thesis were elongated along the horizontal dimension. A larger horizontal component has also been described by Sajovic and Levinthal (1982a, by a factor of 1.4 vs. 1.6 in the present study) in adult zebrafish. In contrast, in the archerfish tectum, the majority of elongated RFs are oriented along the vertical axis (Reichenthal et al., 2018). Interestingly, tectal cells in archerfish are also predominantly tuned to vertical orientations (Ben-Tov et al., 2013), whereas in zebrafish the majority of tectal cells prefer horizontal orientations (Hunter et al., 2013b), as presented in Chapter 5. It is, therefore, possible that the preferred stimulus orientation of a tectal neuron is a direct consequence of the shape of its RF. This is the case in amacrine cells (reviewed in: Antinucci and Hindges, 2018); however, further experiments with direct comparisons of RF shape and preferred orientation, are needed to test this. The difference in RF shape and orientation tuning between archerfish and zebrafish is unlikely to be caused by the natural scene statistics of their visual environment, as both species live in an aquatic habitat and frequently swim close to the water surface (Ben-Tov et al., 2013; McClure et al., 2006). Therefore, the vertical tuning in archerfish may present a special case and be a result of the unusual hunting technique employed by these fish. Archerfish are highly specialised visual predators that shoot down their prey (usually insects located above the waterline) with a jet of water from their mouth.

## 4.4.4 Receptive field size

RF sizes in the optic tectum of fishes are relatively large: often ranging from 30° - 160° (Guthrie, 1990, p. 309). This is also the case in zebrafish: Niell and Smith (2005) reported a mean RF width of 40° in 9 dpf larvae and Sajovic and Levinthal (1982a) measured a mean width of 36.1° and mean height of 26.2° (average value of I, T and S cell types). In contrast, RF sizes in the superior colliculus of mammals tend to be much smaller, with RF diameters ranging from 3° to 15° in rats (Sauvé et al., 2002) and mean values of approx. 12° in mice (Wang et al., 2010), and 21° in hamsters (Carrasco et al., 2005). Why tectal RFs in fish are larger than in other vertebrates has yet to be decisively determined. However, it has been suggested that large RF sizes might present an adaption to the underwater environment (Balboa and Grzywacz, 2003).

At first glance, the average values for tectal cell RF width and height reported in this thesis, 55° and 28.7° respectively, seem to be somewhat larger than what has previously been reported for zebrafish. Because of the different method used here, compared to methods previously employed by other researchers, to calculate the extent of the RF, the RF sizes reported here cannot be directly compared with those in the existing literature. Notably, the RF sizes reported in this study were noticeably different in the three age groups. In fact, RF width decreased by more than 50 % from 14 dpf (60.3°) to 18 dpf (28.3°). This reduction in size was evident in both PVN cell bodies and the neuropil and had a similar effect on RF width and height. While RF reduction in the zebrafish optic tectum does not seem to have a morphological component, the initial expansion of RF size between 4 and 6 dpf, reported by Zhang and colleagues (2011), appears to be the result of an increase in branch number and length of retino-tectal projections (Meyer, 2006), and a similar development in the dendritic trees of tectal neurons (Niell et al., 2004). This developmental process is thought to be completed by 6 - 7 dpf (Niell et al., 2004; Meyer and Smith, 2006). Therefore, it seems unlikely that RF size would increase again from 9 dpf to 14 dpf and the discrepancy between the values reported here and those found by Niell and Smith (2005) may be due to differences in calculating RF size.

There is little mention in the literature in relation to whether RF size continues to decrease during the juvenile period, i.e., after the initial phase of visual development. Carrasco et al., (2005) reported a gradual decrease in RF size during late juvenile

stages in the SC of the hamster until $46 - 51$ days postnatal, when RFs have reached maturity. While Zhang and colleagues reported that the RFs of retina ganglion cells do not change significantly between 4 and 6 dpf, development in the retina continues beyond 14 dpf (Mumm et al., 2006; Schroeter et al., 2006). The data presented here suggests that RFs in the optic tectum undergo further refinement beyond the age of 9 dpf. In order to conclusively determine how RF size changes during maturation, future experiments should ideally include fish from 9 dpf onwards and well into juvenile stages, or even adulthood. While we are confident that GCaMP expression remains high in juvenile NBT:GCaMP3 fish (described in Chapter 3), additional measures must be taken to ensure sufficient provision of oxygen in fish aged > 21 dpf, such as intubation (Kassing et al., 2013; Olt et al., 2016). In addition, it would be interesting to test whether the continued reduction of RF size is accompanied by an increase in RF sharpness.

When neuropil voxels are colour-coded according to RF size in a response map, a pattern emerges; rather than a random distribution of RF sizes, it seems that there are 'hot spots' of very large RFs, which gradually become smaller as distance increases. While it has been reported that in non-foveate fish, such as zebrafish (Maurer et al., 2011), the RFs of retinal terminals in the tectum are mostly of a similar size (Guthrie, 1990, p. 302), little is known on how RF size is organised on the postsynaptic level. An equivalent pattern has not been observed in the PVN cell bodies; however, this may be due to the low numbers of responding somata per field of view. The finding presented here would need to be backed up by further experiments. It is particularly important to exclude the possibility that this pattern is an artefact created by convolution during the pre-processing filter step (Gaussian filter, $3 \times 3$ kernel). Possible alternatives would be, for example, to restrict Gaussian filtering to the temporal dimension or use a non-convolutive filter, such as the Kalman filter. In addition, it would be beneficial to increase the number of responsive voxels in the neuropil to obtain a more complete response map; this could be achieved by using a 2-photon microscope or confocal microscope with a more sensitive GaAsP detector, or by switching to a brighter version of GCaMP.

## 4.4.5 Retinotopic organisation of RFs

Similar to the SC in mammals, the OT in fish is involved in orienting behaviours (Nevin et al., 2010), implying, that position in visual space needs to be conserved. It has long been known that retinal input to the optic tectum is organised topographically (Sperry, 1963). Axons from the nasal retina terminate in the posterior portion of the OT and axons from temporal retina end in the anterior OT. Similarly, afferents originating in the dorsal retina project to the ventral OT and vice versa (Stuermer, 1988). This retinotopic organisation is also reflected in the RFs of tectal cells (Niell and Smith, 2005). A study by Bollmann and Engert (2009) in *Xenopus* has shown that visually-drive calcium signals are topographically organised within the dendritic tree of individual tectal neurons, suggesting that retinotopy is also evident in the tectal neuropil. In the present study I confirmed that, in zebrafish, visually evoked responses in the neuropil are also organised in a highly retinotopic manner. Exactly how spatial information is conserved in a structure with large RFs, such as the OT however, has not been shown yet. Sajovic and Levinthal (1982a), proposed that this information may be conserved in the temporal component of the response.

## 4.4.6 Stimulus limitations

The findings presented here may have provided a simplistic description of the tectal RFs because of the basic and artificial nature of the stimulus (i.e., small spot moving in two directions), the results described here provide a simplistic description of the tectal RFs. While white noise stimuli or simply spots moving in several directions (including diagonal) could, in theory, provide a more detailed RF structure, the resulting description of RFs would also be far from complete. Ideally, one would choose stimuli that the animal will encounter in their natural environment to study visual neurons and their functions. For zebrafish, underwater movies could be used to probe the RFs of tectal neurons. On the downside, controlling all stimulus parameters when using natural movies is almost impossible. Computer animated movies of kin fish or predators, on the other hand, may provide a more viable alternative. In fact, animated images of a relevant predator have successfully been used in behavioural experiments with zebrafish (Gerlai et al., 2009).

It also remains unclear why RF sizes differed between the two different stimuli i.e., flashing bars and moving spots. RF sizes measured with flashing bars are almost two-fold larger than those mapped with small spots. It may be that this discrepancy is due to comparing RFs of ROIs with those of individual voxels. However, inspection of RF size maps in the neuropil (Figure 4.3E) suggested that RF size gradually changes between neighbouring pixels. Therefore, a two-fold increase of RF size due to grouping neighbouring pixels seems unlikely. It is possible that large bars and small moving spots recruit different processing pathways in the optic tectum, which may differ in their response properties. Small moving spots, for example, have been shown to evoke appetitive behaviour in zebrafish (Bianco et al., 2011; Filosa et al., 2016; Semmelhack et al., 2014).

### 4.4.7 Concluding remarks

In the present study, I mapped the spatial receptive fields in the OT of zebrafish, using small moving spots. I focused on several RF properties, including RF size, shape, and orientation, as well as the location of their centres. The results presented here largely confirm previous findings by Sajovic and Levinthal (1982b, 1982a) and Niell and Smith (2005), although a direct comparison of RF sizes proved unfeasible due to the different methods used for calculating the border of the RFs. Notably, new evidence emerged that RFs in the OT are likely to undergo further refinement after 9 dpf. This new evidence highlighted the importance of older larvae for studying visual processing in the optic tectum.

The optic tectum is the main visual processing area in fish and is involved in a variety of different visual behaviours. RFs in this structure have been described to be relatively large; in fact here it was demonstrated that 50% of tectal neurons were larger than 40° in width. A consequence of the large RF size is that during natural visual behaviour, multiple object features of an object will fall within one RF. Behavioural experiments in the lab have shown that when exploring an object (2D black triangle) zebrafish keep a certain distance so that the apparent size of the object (triangle base) ranges between 20° and 36° (unpublished manuscript presented in Chapter 5). This result suggests that the apparent size of objects during exploration is smaller than the average RF. Further evidence for this line of thought comes from the distance zebrafish keep from kin fish during natural behaviour. At 16 dpf, for example, zebrafish keep a mean inter-individual distance of

approximately 5 body lengths (Hinz and Polavieja, 2017); for an average body length of 5 mm, the apparent size of a kin fish is 11.4°. Therefore, multiple objects or multiple features of a large object may simultaneously fall within the RF of an individual. This hypothesis is further explored in Chapter 5, which addresses the question of how local features, i.e., features that are smaller than the RF, are processed in the OT.

# Chapter 5

# Processing and nonlinear integration of local features by zebrafish optic tectum

The present thesis follows an alternative thesis format and the findings of this chapter are presented in form of a manuscript titled: "Processing and nonlinear integration of local features by zebrafish optic tectum". This manuscript is intended for submission for publication.

Author contributions:

I designed, set-up and performed the experiments (calcium imaging), analysed the data and generated the stimulation scripts. I revised the first draft of the manuscript and subsequently prepared a substantially reworked version of the manuscript and prepared the figures.

Yulia Nikolaeva carried out the behavioural experiments.

Anton Nikolaev designed and supervised the experiments. He performed and analysed the behavioural experiments and helped with the analysis of the imaging data. He wrote the first draft of the manuscript and commented on the final reworked version.

# 5.1 Processing and nonlinear integration of local features by zebrafish optic tectum

Abbreviated title: Processing of local features by the tectum

Katharina Bergmann, Yulia Nikolaeva, and Anton Nikolaev[$]

Department of Biomedical Science

The University of Sheffield

Western Bank,

Sheffield, S10 2TN, UK

Corresponding author:

Anton Nikolaev ([a.nikolaev@sheffield.ac.uk](a.nikolaev@sheffield.ac.uk))

Number of pages: 29

Number of figures: 5

Abstract: 218 words

Introduction: 966 words

Discussion: 1292

## 5.2 Abstract

The optic tectum is the main visual processing area in zebrafish and thus is important for a number of visually-driven behaviours. A key question is how information about the visual environment is processed and integrated in the optic tectum, in order to generate visually-guided behaviour. To understand this, it is important to study the response properties of tectal neurons, i.e., their preference for certain features of the visual input. The optic tectum receives orientation-, direction- and size-selective input from the retina, which is used to compute feature selectivity in tectal neurons. We hypothesise that due to their large receptive fields, neurons in the optic tectum receive information about multiple, local object features, i.e., features that are smaller than the receptive field, at the same time. Using a behavioural novel object paradigm, we observed that when zebrafish explore an object, the apparent size of the object was comparably smaller than the average receptive field of a tectal neuron, which was supportive of our hypothesis. We then performed calcium imaging in the optic tectum of larval zebrafish, while simultaneously presenting them with a set of local orientations, i.e., differently oriented small bars and combinations thereof. The results indicated that the optic tectum exhibits tuning to local orientations and their combinations and that these features are integrated in a sublinear manner.

## 5.3 Introduction

Zebrafish rely on vision for fundamental aspects of survival, e.g., hunting prey (Gahtan, 2005), avoidance of predators (Gerlai et al., 2009; Temizer et al., 2015) and kin recognition (Hinz et al., 2013). In lower vertebrates, the optic tectum is widely considered as the main visual processing centre. In zebrafish, the optic tectum is involved in key visually-guided behaviours, in particular those that rely on a detailed map of visual space, such as phototaxis (Burgess et al., 2010), prey detection and capture (Gahtan, 2005; Muto et al., 2013; Semmelhack et al., 2014; Bianco and Engert, 2015; Filosa et al., 2016) and escape responses (Temizer et al., 2015; Dunn et al., 2016). Evidence from studies on birds and archerfish suggest that the optic tectum might also perform other complex visual computations, such as object recognition (Rogers and Miles, 1972; Soto and Wasserman, 2014) and saliency detection (Ben-Tov et al., 2015), both of which have been traditionally thought to take place in the visual cortex. To understand how the optic tectum contributes to such a variety of neural computations, it is essential to study the visual tuning properties of tectal neurons in detail.

Feature selective neurons, and the underlying neural circuits have been well studied in recent years. These studies have identified tectal neurons selective for stimulus size (Niell and Smith, 2005; Del Bene et al., 2010; Preuss et al., 2014), orientation (Hollmann et al., 2015; Hunter et al., 2013a; Kassing et al., 2013; Thompson and Scott, 2016) and direction of motion (Niell and Smith, 2005; Ramdya and Engert, 2008; Gabriel et al., 2012; Grama and Engert, 2012; Hunter et al., 2013a; Kassing et al., 2013; Hollmann et al., 2015; Abbas et al., 2017). On the other hand, only a handful of studies have focused on the receptive field (RF) properties of these cells (Niell and Smith, 2005; Sajovic and Levinthal, 1982b, 1982a; Zhang et al., 2011; Bergmann et al., 2018). Interestingly, similar to other fish, tectal neurons in zebrafish have relatively large receptive fields, i.e., they integrate information from a large area of visual space. For example, the average RF width is 36° in adult zebrafish (Sajovic and Levinthal, 1982b), 40° in young zebrafish larvae (Niell and Smith, 2005), and 53° in older zebrafish larvae (Bergmann et al., 2018)., In their environment, zebrafish are likely to encounter multiple objects (which may enter and pass through its visual field at the same time), e.g., multiple fish in a shoal (Saverino and Gerlai, 2008; Buske and Gerlai, 2011) or predators in the distance (Bass and Gerlai, 2008).

Thus, due to their large RF size, individual tectal neurons might receive information about multiple features (of one or several objects) at the same time. This raises the question of how local features, i.e., features that are smaller than the receptive field of a cell, are processed in the optic tectum and how information from multiple features is integrated within individual neurons. Here, we examined this by imaging tectal activity in response to small, oriented bars and combinations thereof. Orientation-selectivity has been well studied in the retino-tectal system (Nikolaou et al., 2012; Kassing et al., 2013; Lowe et al., 2013; Thompson and Scott, 2016; Johnston et al., 2014; Hollmann et al., 2015; Antinucci et al., 2016). Four orientation-selective (OS) subtypes have been identified in the retinotectal input (Lowe et al., 2013) and existing evidence suggests that these are inherited by tectal neurons (Hunter et al., 2013a). While small, local features have been used to study size selectivity in the optic tectum, orientation selectivity has often been studied in the past using large, oriented bars (Nikolaou et al., 2012; Hunter et al., 2013a; Lowe et al., 2013). These bars were often larger than the average receptive field size. In this paper, we will, therefore, refer to these stimuli as global orientations (Figure 1). Whether the optic tectum also encodes information about local orientations remains fairly unexplored. Bars of different orientations can be easily combined to generate more complex, composite features, such as angles or intersections; thus, providing the opportunity to study how information about local features is integrated within
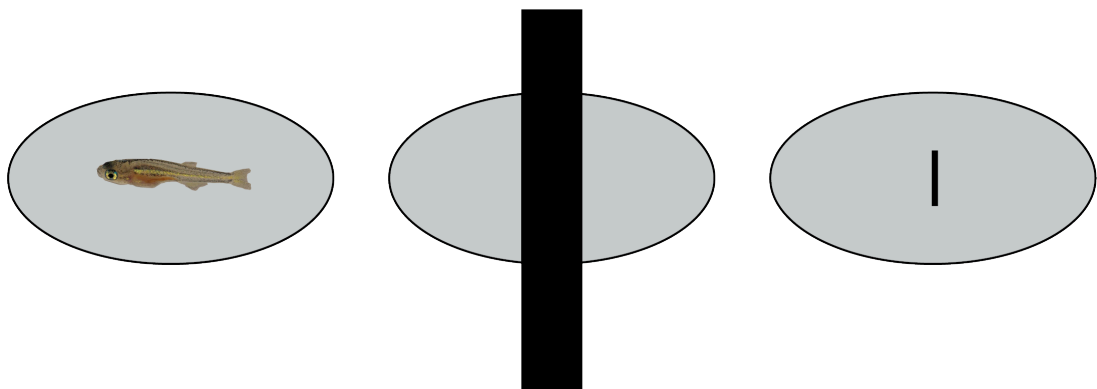


**Figure 5.1 Tectal receptive fields and visual stimuli.** The average receptive field size of a tectal neuron in $14 - 18$ dpf zebrafish larvae is 53° in width and 29° in height. Left, the average apparent length of a kin fish at 24 dpf is approximately 28°. Middle, large bars (10°×63°) to test global orientation selectivity. Right, small bars (0.7°×8.9°) used here to test tuning to local features

tectal neurons. At the same time, combinations of bars, i.e., angles, intersections or simple shapes, offer the opportunity to test whether the optic tectum may extract information about shape, beyond orientation and size selectivity. This has not yet been tested in zebrafish; however, considering (i) the complex nature of visual computations performed by the optic tectum, (ii) the complex non-homogenous receptive field shapes of tectal neurons (Sajovic and Levinthal, 1982a), and (iii) the fact that orientation selectivity is already computed at the level of the retina (Nikolaou et al., 2012; Lowe et al., 2013; Johnston et al., 2014), it seems likely that neurons in the optic tectum may encode information about complex features.

Here, we study how tectal neurons process and integrate information about the orientation of individual and multiple local features, i.e., features smaller than the average RF. First, we used a behavioural paradigm to demonstrate that when zebrafish inspect a novel object, the apparent size of the object is smaller than the average RF size of a tectal neuron. This supports our hypothesis that the RF of a single neuron may receive information about multiple local features belonging to the same object. Second, we imaged neural activity in the optic tectum and showed that tectal neurons preferentially respond to small bars in horizontal orientation and also exhibit tuning to various combinations of orientations. Finally, we provide evidence for sublinear summation of local features by tectal neurons. Our findings provide a first description of how local orientations are processed within the optic tectum.

# 5.4 Materials and methods

All experimental procedures were performed according to UK Home Office regulations (Animals (Scientific Procedures) Act 1986) and approved by the Ethical Review Committee at the University of Sheffield.

## 5.4.1 Animals and husbandry

Zebrafish were maintained at 28°C on a 14/10 light/dark cycle and fed twice a day, including the day of the experiment (Filosa et al., 2016). For calcium imaging, the previously described transgenic NBT:GCaMP3 line was used, which expresses GCaMP3 panneuronally (Bergmann et al., 2018). All experiments were performed in the pigmentation mutant *nacre* (Lister et al., 1999).

## 5.4.2 Imaging and visual stimulation

Imaging was performed as previously described in Bergmann et al., (2018). In brief, zebrafish larvae 14-21 days post-fertilisation (dpf) were immobilised in 3.5 % low-melting-point agarose and mounted dorsal side up, onto a removable stage, which was then placed in a custom-made imaging chamber. To increase oxygen absorption during the experiment, agarose around the gills was carefully removed and the imaging solution (filtered aquarium water buffered in 1.2mM $NaH_2PO_4$ and 23 mM $NaHCO_3$) was aerated with a 95% $O_2$ and 5% $CO_2$ mix for 30 minutes. No oxygenation was applied during the experiment. One wall of the imaging chamber was covered with opaque film (Cinegel #3026, Rosco EMEA, London, UK) and served as projection screen. Because of the short working distance of the microscope, the screen size was 90 mm (W) x 15 mm (H) (124 x 35 degrees). Fish watched the screen either with the left or the right eye, with an eye-to-screen-distance of 2.7 cm. Visual stimuli were generated using custom-written code for Matlab (MathWorks, Natick, MA) with the Psychophysics Toolbox (Brainard, 1997; Pelli, 1997; Kleiner et al., 2007). The stimuli consisted of black bars and combinations of bars, which had a size of 0.7° x 8.9° (Figures 3,4) or 0.7° x 11.8° (Figure 5). Three sets of visual stimuli were used: (i) a set of 12 bars, at six different orientations (0°, 30°, 90°, 120°, 150°) and two different positions; (ii) a set of 15 angles with five different angular sizes (30°, 60°, 90°, 120°, 150°) presented at three different orientations (0°, 120°, 240°);

(iii) a set of composite and single stimuli, consisting of a square, the four individual bars of the square, and the four corners of the square. Visual stimuli moved along the horizontal axis at 35 °/s. This reduced positional bias caused by some stimuli being closer to the RF centre (along the horizontal axis) than others. Each stimulus set was presented three times. Stimuli were always centred at half the height of the screen; the imaging plane was always in the middle third of the optic tectum. RF sizes were not mapped routinely prior to the experiments. However, the stimuli were much smaller than the average RF size in tectal neurons (Figure 5.1).

Imaging of neural activity was performed using an FV1000 confocal microscope (Olympus, Tokyo, Japan) at the Wolfson imaging facility at the University of Sheffield, fitted with a 40x (NA 0.8) LUMPlan objective (Olympus). Confocal time-series were acquired at a rate of 2.3 Hz, at a resolution of 1.24×1.24µm (256×256 pixels).

## 5.4.3 Image analysis

Confocal time-series were analysed using SARFIA, (Dorostkar et al., 2010) and custom-written scripts for Igor Pro (WaveMetrics, Lake Oswego, OR). Images were registered (TurboReg for ImageJ; Thevenaz et al., 1998) and filtered (average filter, kernel size 3×3) prior to further analysis. Individual regions of interest (ROIs) were defined by thresholding the average image using the Laplace operator. Normalised signal intensity changes ($\Delta F/F0$) were calculated for each ROI and averaged for three repetitions of the same stimulus set. To define responding ROIs in an unbiased manner the distribution of $\Delta F/F0$ was calculated for each individual ROI and only traces with excess kurtosis > 1 were considered as visually responsive. This approach effectively separated non-responding, noisy traces from traces, which exhibited transient fluorescence changes in response to visual stimulation. A single response metric, $R$, was defined as the maximum signal amplitude during each stimulus interval.

The orientation selectivity index (OSI) was calculated as previously described (Niell and Stryker, 2008) after averaging the responses to the same orientation at two different positions. ROIs were regarded as orientation-selective when OSI > 0.5 (Hunter et al., 2013a).

ROI position within the neuropil was defined using SARFIA for Igor Pro (Dorostkar et al., 2010b). The borders of the neuropil were defined manually and the position of the centre of mass of each ROI was automatically detected by defining the superficial border as 0% and the lower border (towards the somata of periventricular neurons) as 100%. Based on size and position, each ROI in the neuropil was likely to represent a fragment of one or several dendrites.

## 5.4.4 Novel object paradigm

Single zebrafish larvae (14-22 dpf) were placed in a novel chamber (110 x 75 x 45 mm). The chamber walls were covered with an opaque film (Rosco EMEA, London, UK) and a black 2D object (isosceles triangle with a base length of 17 mm or 9 mm) was positioned on one of the walls. The object did not change in size, position or brightness and therefore the behaviour observed in these experiments cannot be explained by avoidance of a looming stimulus (Temizer et al., 2015; Dunn et al., 2016). Fish were monitored for 20-30 minutes using the ViewPoint behavioural analysis system (ViewPoint, Lyon, France). Data analysis was performed using the ViewPoint software and custom-written scripts for IgorPro.

To analyse the fish-to-object distance during exploratory behaviour, the position of the fish (i.e., the x-y-coordinates) was calculated for each frame using the ViewPoint software. The distance of the fish to the wall containing the object was binned (10 bins) and averaged for the moments of time when the fish was in the half of the chamber containing the object. The average fish-to-object distance was defined as the average y-coordinate at x = 58 mm (horizontal position of the object centre). Analysis was performed on the first 2 minutes of the experiment; the time fish larvae take to explore an object (Andersson et al., 2015).

## 5.4.5 Experimental design and statistical analysis

All experiments were performed at stages preceding sex differentiation. All fish showing a robust response to moving stimuli were included in the analysis. Data analysis was automated or semi-automated (see Image analysis section). Statistical analysis was performed using Igor Pro. Statistical significance of the differences in response to various stimuli was defined using a one-way ANOVA test with Bonferroni correction or a *t*-test (paired and unpaired). All data are shown as mean ± SEM When IgorPro reported p = 0, the p-value was reported as p<< 0.001.

# 5.5 Results

## 5.5.1 Individual tectal neurons presumably process multiple local features simultaneously

Each neuron in the optic tectum receives input from a restricted region in the visual field of the animal. The size and position of this region are defined by the spatial receptive field (RF) of each neuron. Comparing the RF sizes of tectal neurons with the apparent size (angular size) of objects zebrafish encounter in their environment sheds light onto how tectal neurons process object information: (i) by selecting individual features or (ii) by integrating information about multiple local features. If the object spans an area substantially larger than a single RF, the object is likely represented by the concerted activity of multiple neurons. If, however, the object 'fits' within a single RF, an individual neuron might simultaneously process information about multiple object features. Considering the large size and complex structure of RFs in the zebrafish optic tectum (Sajovic and Levinthal, 1982; Niell and Smith, 2005) the latter may be true. Here, we used an experimental paradigm in which individual fish inspected a novel static object, to compare the average apparent size of the object with the average RF size of tectal neurons. Zebrafish larvae were placed in a chamber with a 2D object on one wall (Figure 5.2A), and their exploratory behaviour was recorded.

On approaching the object (i.e., when swimming towards the wall containing the object), the fish typically turned, keeping a certain distance from the object (Figure 2*B*). When the fish was directly in front of the object (see Materials and Methods), the average distance was 2.6 ± 0.2 cm (n = 22 fish) for the large object and 2.6 ± 0.4 cm (n = 8 fish) for the small object (Figure 5.2C). Judging from the mean distance that the fish kept to the object, the average apparent size (triangle base) of the object was 36.2° (2 × arctan (1.7 / 5.2)) for the large object and 19.6° for the small object.
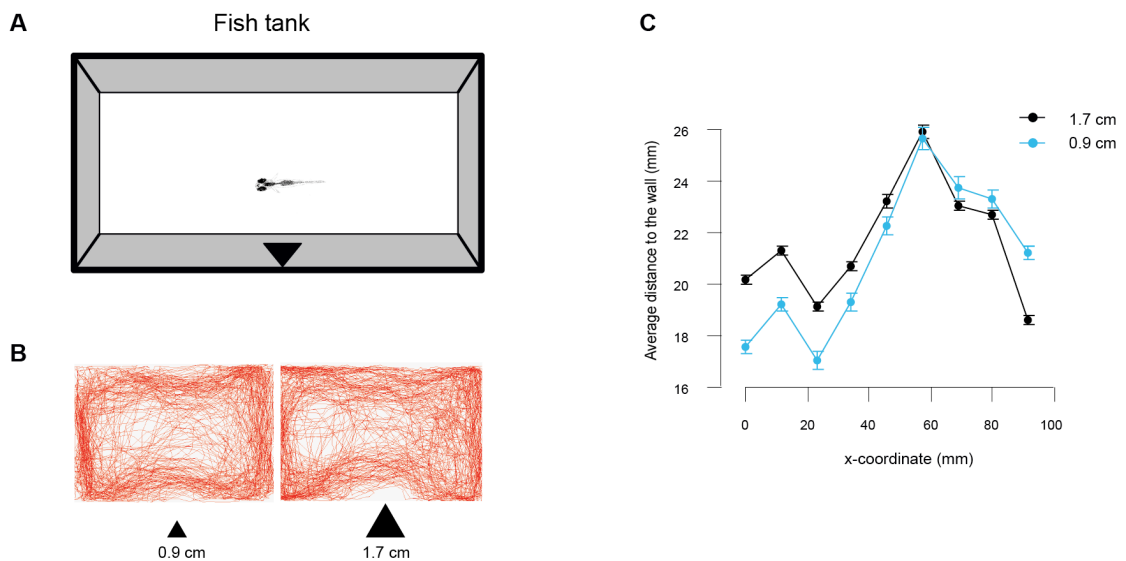


**Figure 5.2 Novel object paradigm indicates that tectal neurons are likely to process multiple features.** (**A**) Schematic of the behavioural chamber. Fish were placed for 30 minutes in an unfamiliar chamber, with a black triangle shown on one wall. (**B**) Example trajectories of two individual fish inspecting a small (left) and a large (right) novel object. Triangle marks x-axis position of the object. (**C**) Average fish-to-object distance, shown as a function of the average x-coordinate for small (n = 8 fish, blue) and large (n = 22 fish, black) objects. Origin of the x-coordinate is the left bottom corner of the behavioural chamber as shown in A, B. Error bars indicate SEM.

For moving objects, the apparent object size can be inferred e.g., from the average fish-to-fish distance in a shoal: in 24 dpf zebrafish larvae, this distance was reported to be 2 body lengths (Hinz and de Polavieja, 2017). Therefore, the apparent size of an average fish neighbour is approx. 28° (2 × arctan (8 / (2 × 16)). This implies that the typical apparent size of a conspecific is smaller than the average RF size of a tectal neuron, which is 53° in 14-18 dpf larvae (Bergmann et al., 2018) and 36° in adult zebrafish (Sajovic and Levinthal, 1982a). Similarly, the average distance to a 7 cm big predator (Indian Leaf Fish) has been reported to be around 20 cm (Bass and Gerlai, 2008), making the apparent size of the predator approx. 20° (2 × arctan (7 /

2 × 20). Thus, during natural behaviour zebrafish are often presented with multiple moving objects (or multiple features belonging to the same object) that are smaller than the average RF size in the optic tectum.

Thus, for both moving and static objects the entire object, containing multiple local object features (e.g., the objects in Figure 5.2 contain a set of three lines in different orientations) typically 'fits' within the average tectal RF. This poses two important questions regarding the processing of visual information by the optic tectum. First, how does the optic tectum process orientation of local features? Second, how are multiple local features being processed by an individual neuron? To address these questions we performed calcium imaging in the optic tectum while presenting the fish with different sets of local stimuli.

## 5.5.2 Optic tectum encodes local orientations and their combinations

To start unravelling how local features are processed by the optic tectum, we used two sets of local features, which were considerably smaller than the average tectal RF: (i) local orientations and (ii) combinations of orientations.

### Preference for horizontal local orientations in tectal neuropil and PVN cell bodies

We investigated the preference for orientation of local features in the tectal neuropil and the somata of PVN cell bodies, using a set of 12 small bars in 6 different orientations (0°-150°) at two different positions (Figure 5.3A). Figure 5.3B shows example responses of three individual ROIs in the neuropil (left) and somata of periventricular neurons (PVNs, right), which were either tuned to horizontal orientations (top), vertical orientations (middle) or showed no orientation tuning (bottom). Average responses to local orientations of all visually-responsive traces from ROIs in the neuropil (left) and PVN cell bodies are presented in Figure 3C. Orientation had a significant effect on the responses to small bars in the neuropil ($p \ll 0.001$, $F_{(5,3474)} = 17.3$, $Fc = 3.9$; $n = 580$ ROIs from 6 fish; one-way ANOVA test with Bonferroni correction (30 comparisons)), but not on the responses of PVN cell bodies ($p = 0.07$, $F_{(5,1158)} = 2.0$, $Fc = 3.9$; $n = 194$ cells from 6 fish; one-way ANOVA with Bonferroni correction for (30 comparisons)). However, in

both, neuropil and cell bodies, horizontally oriented bars evoked significantly stronger responses than vertically oriented ones (neuropil: paired t (579) = 10.2, p << 0.001; cell bodies: paired t (193) = 2.2, p = 0.03). Next, OS ROIs and cell bodies were identified by applying a stringent inclusion criterion: 10.0 % of ROIs (58 out of 580 ROIs) in the neuropil and 23.2 % of cell bodies (45 out of 194) had an orientation selectivity index (OSI) > 0.5 (Hunter et al., 2013a). The distribution of preferred orientations in OS ROIs and cell bodies is shown in Figure 5.3D.

Overall, tectal neurons responded particularly well to horizontal bars, which evoked significantly higher responses than vertical bars. Notably, orientation tuning was more pronounced in the tectal neuropil, whereas in the PVN cell bodies local orientations appeared to be more evenly represented.

It is possible that the different responses to bars are caused by differences in position rather than orientation, e.g., the horizontal bar was closer to the cell's RF centre (along the vertical axis) than the vertical bar. To test whether this was the case, we compared the responses to horizontal bars at two different positions. Figure 5.3E (left) shows that position did indeed affect the response to horizontal bars. Next, we manually selected traces with near-equal responses to horizontal bars at the two positions, indicating that both bars were located within the receptive field. Notably, on average horizontal bars still evoked stronger responses than vertical bars, indicating that different responses to oriented bars are not caused simply by differences in bar position.

**A**



**B(i)**  Neuropil



**C(i)**



**D(i)**



**B(ii)**  Cell bodies
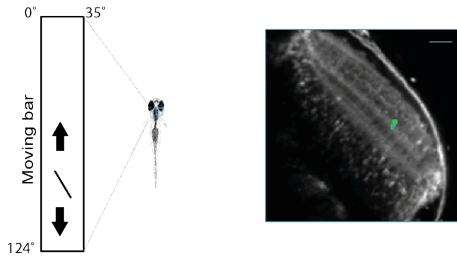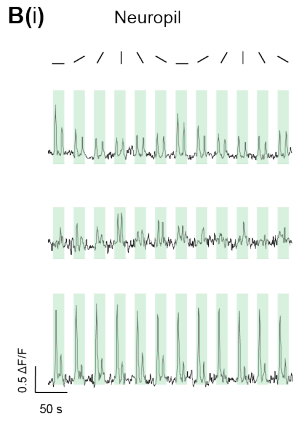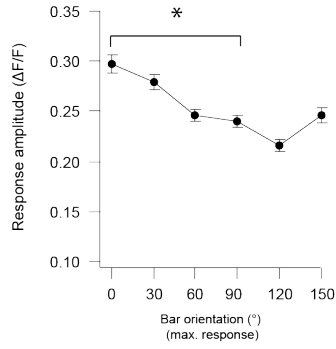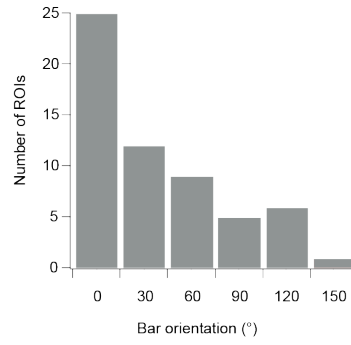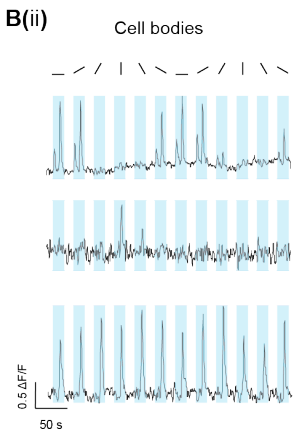


**C(ii)**
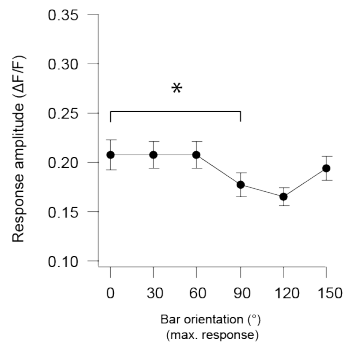


**D(ii)**
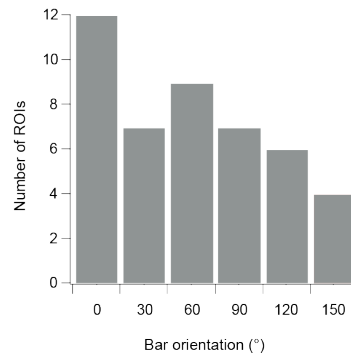


**E(i)**
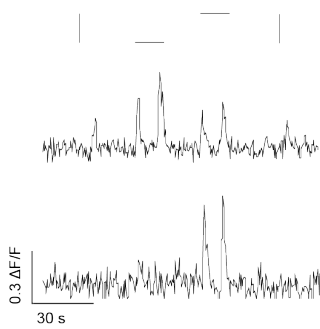


**E(ii)**
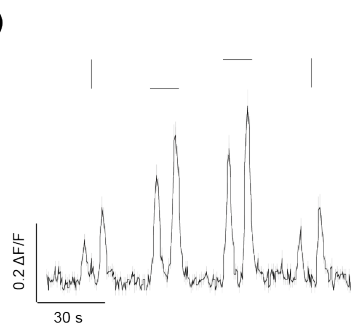
**Figure 5.3 Optic tectum encodes local orientations.** (**A**) Schematic of visual stimulation (left) and dorsal view of one tectal hemisphere of NBT:GCaMP3 zebrafish larvae. Example ROI highlighted in green. (**B**) Example fluorescence traces in response to small oriented bars (stimulus shown above first trace) in the tectal neuropil **B**(i) and the cell bodies of PVN neurons **B**(ii). Top traces show tuning to horizontal orientations, middle traces to vertical orientations and bottom traces show no tuning. (**C**), Average response amplitudes evoked by small bars in the neuropil (**C**(i)), and cell bodies (**C**(ii)). Horizontal bars (0°) evoked significantly higher responses than vertical bars (90°), paired t-test, n = 580 neuropil ROIs, n = 194 cell bodies, 6 fish. (**D**) Distribution of OS selective (OSI>0.5) responses in the neuropil (**D**(i)) and cell bodies (**D**(ii)). (**E**) **E**(i), Stimulus position may affect response to small bars in individual ROIs. **E**(ii) Average responses to small bars of 53 ROIs with similar responses to horizontal bars at both positions. Preference for horizontal orientations was still evident in this subpopulation. Scale bar: 50µm. Error bars indicate SEM

## Tectal neuropil shows preference for combinations of similarly oriented bars

We next tested how tectal neurons respond to combinations of local orientations. The stimulus set consisted of a set of 5 different angles (30°, 60°, 90°, 120°, 150°) at 3 different orientations (rotated by 0°, 120°, 240°, Figure 5.4A); like with single bars, the stimuli moved horizontally across the screen. In Figure 5.4B, three example traces illustrate the variety of responses evoked by moving angles in the neuropil (left) and the cell bodies (right). Some ROIs and cell bodies responded selectively to acute angles (top) or a specific subset of angles (middle), whereas others responded independently of angular size and orientations (bottom). On average, angular size and orientation had a significant effect on the responses to small angles in both the neuropil and PVN cell bodies (Figure 5.4C; neuropil: n = 725 ROIs from 6 fish; $F_{(14,10860)}$ = 103.9, Fc = 2.9, p << 0.001; cell bodies: n = 314 from 6 fish; $F_{(14,4695)}$ = 22.2, Fc = 2.9, p << 0.001; one-way ANOVA test with Bonferroni correction (210 comparisons)). Several general characteristics of the response evoked by moving angles were observed reliably over time, i.e., over three repetitions of the stimulus set and across all tested fish (n = 6). Acute angles, i.e., combinations of bars with similar orientations (stimulus #2, #7 and #12) often caused the highest responses, whereas vertically-oriented obtuse angles (stimulus #13 and #15) evoked the weakest responses. Their corresponding average responses (Figure 5.4C,D; neuropil: n = 725 ROIs from 6 fish) were 0.28 ± 0.01, 0.26 ± 0.01 and 0.29 ± 0.01 (acute angles) vs. 0.11 ± 0.01 and 0.12 ± 0.003 (obtuse). In addition, angle #8 often evoked the highest response (average response: 0.29 ± 0.01). Selectivity for acute angles was particularly evident in the most superficial neuropil layers (70-100%),

where responses to acute angles were significantly larger than in the deeper (0 to 30%) layers of the neuropil (Figure 5.4F, n = 243 ROIs (superficial) and 164 ROIs (deep); *t*-test: angles #2: $t$ (163, 242) = -10.2, p<<0.001; #7: $t$ (163,242) = -9.5, p<<0.001; #12: $t$ (163, 242) = -13.5, p<<0.001). In the neuropil, responses to angles decreased with increasing angular size (Figure 5.4D). This trend was not observed in the response of PVN cell bodies (Figure 5.4D).

In line with the observed preference for single horizontal bars (Figure 3), angles, which contained a horizontal bar, evoked larger responses in the neuropil than angles without (Figure 5.4E, average values 0.23 ± 0.01 and 0.18 ± 0.01, n = 715, respectively; Paired *t*-test: paired $t$ (714) = 18.3, p<<0.001). However, the preference for acute angles cannot be explained by the length of the horizontal projection of individual bars. If this was the case, acute angle #2 cause a much higher response than the vertically or nearly-vertically oriented acute angles #7 and #12. This is not the case in the superficial neuropil (Paired *t*-test (angles #2 and #7): $t$ (242) = 1.6, p = 0.1).

**Figure 5.4 Optic tectum encodes combinations of local orientations**. (**A**) Schematic of visual stimulation (left) and dorsal view of one tectal hemisphere of NBT:GCaMP3 zebrafish larvae. Example ROI highlighted in green. (**B**) Example fluorescence traces in response to small angles (stimulus shown above first trace) in the tectal neuropil **B**(i) and the cell bodies of PVN neurons **B**(ii). Top and middle traces show selective responses to particular angles, whereas bottom traces show no tuning. (**C**) Average responses to angles in the neuropil (**C**(i))and cell bodies(**C**(ii)). Angular size and orientation had a significant effect in both the neuropil and PVN cell bodies (one-way ANOVA p << 0.001, n = 725 neuropil ROIs, n = 314 cell bodies, 6 fish). (**D)**, Response amplitude decreased with increasing angular size in the neuropil (**D**(i)), but not in the cell bodies (**D**(ii)). (**E)**, Angles which contained a horizontal bar evoked significantly higher responses than those without (paired *t*-test, p<0.001, n = 715, 6 fish). (**F**) Preference for acute angles was more pronounced in the superficial neuropil (*t*-test p<<0.001, $n_{superficial}$ = 243 ROIs $n_{deep}$ = 164 ROI, 6 fish). Scale bar: 50μm. Error bars indicate SEM.

**A**



**Neuropil**

**Cell bodies**

**B(i)**

**B(ii)**

**C(i)**

Neuropil



**C(ii)**

Cell bodies

0.2 ΔF/F

25 s

0.2 ΔF/F

25 s

**D(i)**

**D(ii)**

**E**



Response amplitude (ΔF/F)

Angular size

Response amplitude (ΔF/F)

Angular size

Average response amplitude (neuropil)

Horizontal bar

deep neuropil
superficial neuropil

**F**



0.2 ΔF/F

20 s
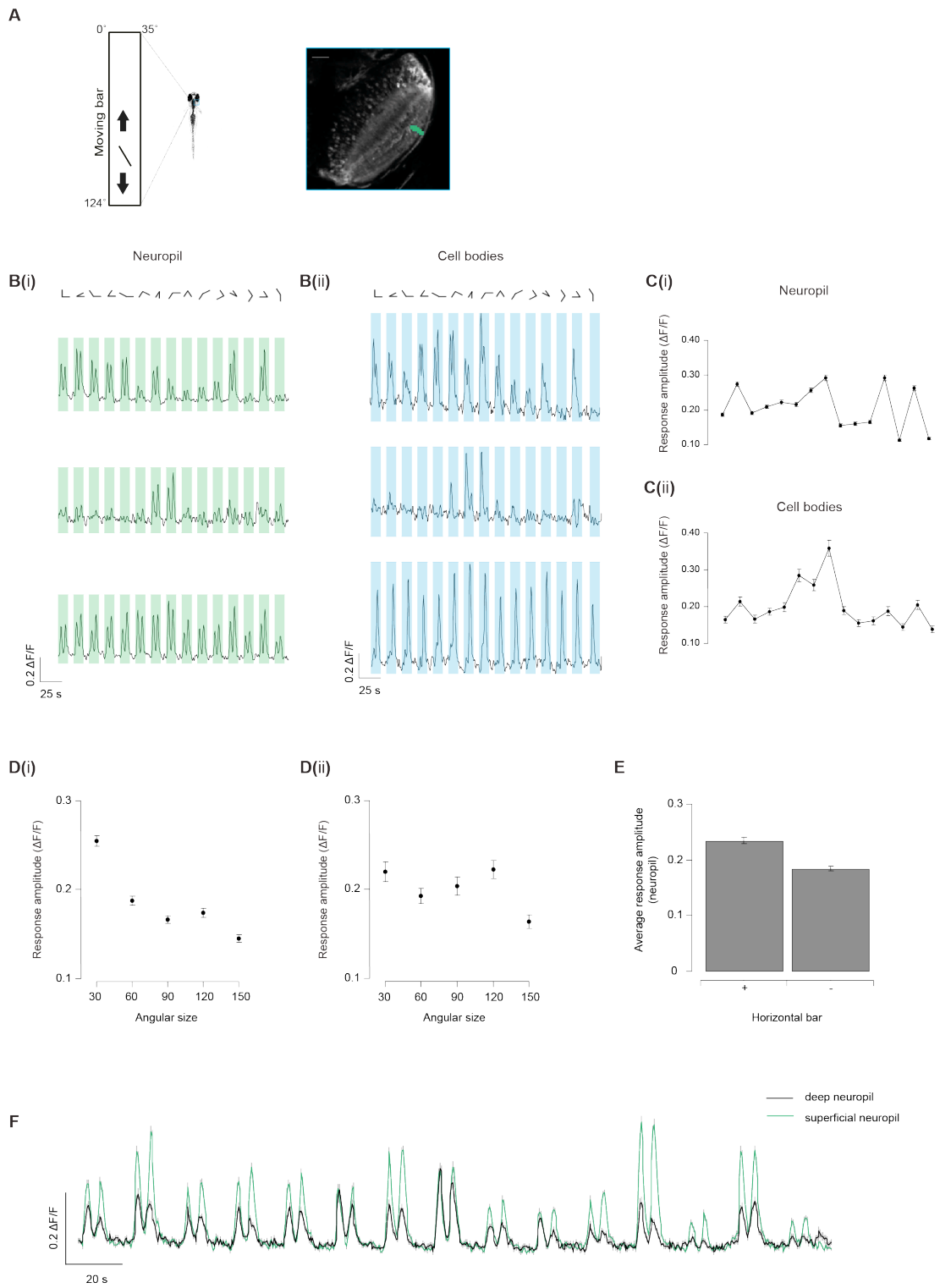
### 5.5.3 Local orientations are integrated in a sublinear fashion within the tectal neuropil

We hypothesised that due to their large receptive field sizes, tectal neurons may process multiple local object features simultaneously. Our finding that the optic tectum encodes both local orientations and their combinations supports this hypothesis. However, this raises the question of how spatial information on individual features is integrated within tectal neurons. To uncover the mechanism by which spatial information is integrated in tectal neurons, we stimulated visually responsive neurons in the optic tectum with a set of moving stimuli consisting of simple features (i.e., lines and angles) and a composite feature (i.e. square) (Figure 5.5B, top). We then compared the responses evoked by individual and composite features. Analysis of the average responses to the composite feature (i.e., square) and two sets of simple features (i.e., lines and angles in different orientations and positions, Figure 5.5B) suggested that object features are integrated in a sublinear manner: average responses to the composite feature were smaller than the sum of responses to the simple features (Figure 5.5B-E). The average linearity coefficient, the ratio between the response to the composite feature and the summed response to simple features, was $0.39 \pm 0.01$ for lines and $0.37 \pm 0.01$ for angles (n = 567 ROIs in the neuropil, 5 fish) with virtually no ROIs showing linear summation (Figure 5.5C). This result cannot be attributed to saturation of the calcium-indicator, because higher response amplitudes could be observed when increasing the stimulus contrast (i.e., using filled shapes instead of contours, Figure 5.5F).

The average response of an ROI to the composite feature was very similar to the response evoked by its preferred individual feature. Figure 5*D* illustrates the distribution of the ratio of the response amplitude evoked by the composite feature and the maximum response amplitude to the preferred individual feature. The average ratio was 0.92 ± 0.02 (n = 567 ROIs, 5 fish).

This observation is similar to the result of a MAX operation, where the neuronal response is determined only by the strongest stimulus (Lampl et al., 2004). In 1999, Riesenhuber and Poggio proposed a hierarchical model for visual object recognition in the cortex. According to this model, neurons in the cortex perform one of two pooling mechanisms, either the linear weighted sum or MAX pooling.

To determine whether spatial summation in the optic tectum could be approximated by either the linear weighted sum or by MAX pooling, we calculated an informative index-value of the predicted response to the composite feature (as a function of the power from which each response to a simple feature is taken):

$$R(p) = \sqrt[p]{\sum_i r_i^p}$$

where $R$ is the response to the composite feature, and $r_i$ is the response to an individual feature. When p = 1, the summation is linear, and p >> 1 indicates MAX pooling. Figure 5*E* illustrates the predicted response to the composite feature, calculated from responses to simple features as a function of their summation power (n = 567 ROIs, 5 fish). Comparing the predicted (filled line) and actual (dotted line) responses to the composite feature gave p > 2 (Figure 5*E*). Similarly, when individual ROIs were analysed separately, more than 90% of ROIs showed p > 2.

These observations indicate that in the tectal neuropil, responses evoked by a composite feature are explained by the linear sum of its components. Rather, information about individual components is integrated in a highly sublinear fashion. In Figure 5*E*, the predicted response approximates the actual response value for large values of p. This suggests that spatial summation in the tectal neuropil may be approximated by MAX pooling.

**A**



**B(i)**

Composite feature

Simple feature set 1          Simple feature set 2

0.1 ΔF/F

40 s

**Neuropil**

**B(ii)**

Composite feature

Simple feature set 1          Simple feature set 2

0.1 ΔF/F

40 s

**Cell bodies**

**C**



**D**



**E**

$$R(p) = \sqrt[p]{\sum r_i^p}$$
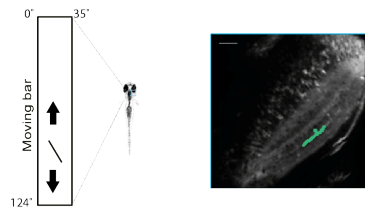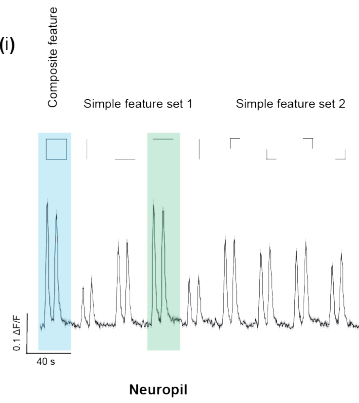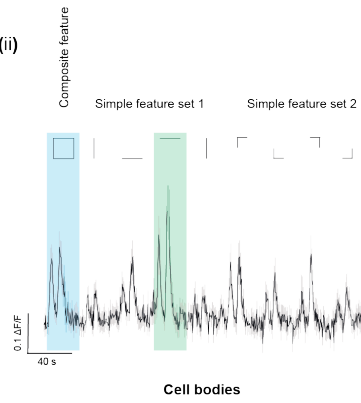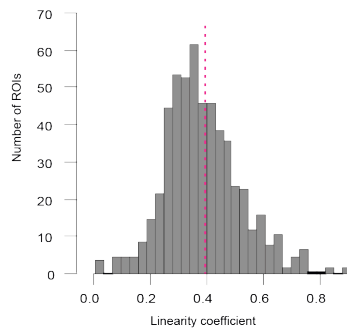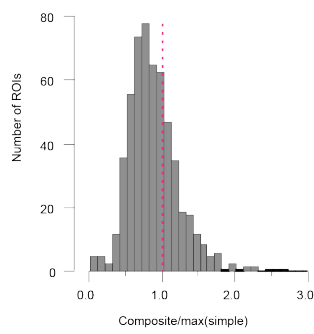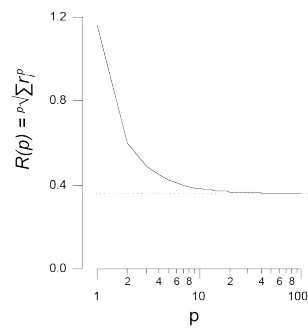
**F**
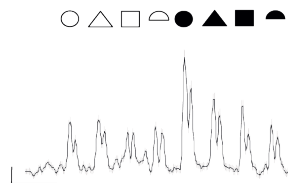
**Figure 5.5 Optic tectum exhibits sublinear spatial integration**. (**A**) Schematic of visual stimulation (left) and dorsal view of one tectal hemisphere of NBT:GCaMP3 zebrafish larvae. Example ROI highlighted in green. (**B**) Example fluorescence traces in response to composite and individual features (stimulus shown above trace) in the tectal neuropil **B**(i) and the cell bodies of PVN neurons **B**(ii). Response amplitude to the composite feature (blue) is similar to the response evoked by preferred simple feature (green). (**C**) Distribution of linearity coefficient (ratio between response amplitude evoked by composite feature and the sum of response amplitudes to simple features). (**D**) Distribution of the ratio between composite feature response and response to the preferred simple feature, n = 567 ROIs from 5 fish. (**E**) Spatial integration of features can be approximated by max pooling. Solid line: Predicted response to the composite feature, calculated from individual responses to simple features as a function of their summation power. Pink dotted lines in (C,D) denotes average value. (**F**) Contour stimuli do not saturate the calcium response, n = 252 ROIs, from 1 fish. Error bars indicate SEM. Scale bar: 50µm

# 5.6 Discussion

Here, we have studied how neurons in the optic tectum of larval zebrafish process and integrate information about local features. Based on the large receptive field sizes of tectal neurons (Sajovic and Levinthal, 1982a; Niell and Smith, 2005; Bergmann et al., 2018), we hypothesized that individual neurons may need to process multiple local features simultaneously. Using a novel object paradigm, we gathered behavioural evidence supportive of this idea. When inspecting a new object, zebrafish keep a certain distance, resulting in the apparent object size being smaller than the average size of a tectal receptive field. Next, we used calcium imaging to study the responses to local orientations in the optic tectum. Our data demonstrated that the optic tectum encodes local orientations and combinations thereof. In particular, we showed that horizontal orientations and acute angles evoked the highest responses in the tectal neuropil, whereas local orientations and angular size are more evenly represented in the activity of PVN the cell bodies. Furthermore, our data indicated that local features are integrated in a highly sublinear manner within the tectal neuropil.

## 5.6.1 Tuning to horizontal orientations in the optic tectum

Orientation selectivity in the optic tectum is inherited from orientation-selective (OS) retinal input (Hunter et al., 2013a). Four subtypes of OS responses in the ganglion cell projections have been reported in the optic tectum (Lowe et al., 2013). It has also been found that tectal neurons exhibit OS responses, and their tuning profiles match those reported in the OS ganglion cell projections (Hunter et al., 2013a). Two of the tectal OS populations responded best to near-horizontal orientations (16°and 174°, respectively) (Hunter et al., 2013). We found that ROIs in the neuropil and PVN cell bodies showed a preference towards certain local orientations. Firstly, horizontal-oriented local features evoked significant responses in both the tectal neuropil and the cell bodies of PVN neurons. Secondly, horizontal bars evoked the most frequent OS responses. These findings suggest that tectal neurons exhibit a clear preference for horizontal orientations. In combination with the findings of Hunter et al., (2013), we propose that the horizontal feature subset is selectively enhanced in the zebrafish retino-tectal system. This preference to horizontal orientations is also reflected in the shape of tectal receptive fields, which have been reported to be elongated along the horizontal dimension (Bergmann et al., 2018; Sajovic and Levinthal, 1982a).

It is widely accepted that the response properties of visual neurons are shaped by the visual input they receive (Simoncelli and Olshausen, 2001). Thus, it is possible that the preference towards horizontal orientations in the optic tectum of zebrafish is the result of their visual environment; where horizontal-oriented features may either occur more frequently than others or convey behaviourally relevant information. Many moving horizontal-oriented objects that zebrafish encounter in their natural environment are mostly likely to be other fish, either predators or kin fish. In addition, horizontal stripes are reportedly important for shoaling and mate choice (Turnell et al., 2003; Rosenthal and Ryan, 2005). Interestingly, neurons in the archerfish optic tectum, unlike in zebrafish, are predominantly tuned to vertical orientations (Ben-Tov et al., 2013) and their receptive fields are also elongated along the vertical dimension (Reichenthal et al., 2018). This might be related to the fact that archerfish are highly specialised visual predators using a jet of water to shoot down insects located above the waterline. Thus, positional information along the vertical dimension plays an important role for these fish.

Receptive field properties and tuning preferences of tectal neurons may, therefore, be shaped by behaviourally relevant visual input.

## 5.6.2 Tuning to complex local features in the optic tectum

In addition to individual local orientations, we used combinations of orientations, i.e., a set of different angles, to study the response properties of tectal neurons. Our findings suggest that the optic tectum in zebrafish extracts information about complex shapes beyond simple orientation or size selectivity. Although tuning to simple composite shapes has been observed in the visual cortex area 2 (V2) of mammals (Hegdé and Essen, 2003), to our knowledge, it has not been reported in the optic tectum of zebrafish. Shape tuning in V2 is thought to be the result of hierarchical processing along the ventral stream and presumably arises from the selective convergence of OS input from V1 and a corresponding increase in RF size by a factor of roughly 3 (Wilson and Wilkinson, 2015). In the absence of a neocortex, hierarchical processing of visual information is not thought to occur in fish as it does in the mammalian visual system. However, the retinal input received by the optic tectum is already orientation selective, and RFs in the optic tectum of zebrafish are on average approximately three times larger than those of retinal ganglion cells (Sajovic and Levinthal, 1982a). Thus, shape tuning in the optic tectum may be generated through convergence of differently tuned OS inputs. Taking into account recent research in archerfish, demonstrating that the spatiotemporal RF characteristics of tectal neurons resemble those of simple and complex cells described in V1 (Reichenthal et al., 2018), our findings suggest that in the absence of a neocortex, the OT may implement visual processing computations similar to those previously described in mammals.

### 5.6.3 Local features appear to be processed differently by the neuropil and PVN cell bodies

In our results, individual local orientations and combinations of local orientation evoked selective responses in both the tectal neuropil and the cell bodies. However, tuning to these local features appeared to be more pronounced in ROIs of the neuropil, whereas local orientations and angular sizes were more evenly represented in the cell bodies. This observation suggests that the activity measured in the somata of tectal neurons does not necessarily reflect the extent of local processing and integration of visual information in the dendrites. A similar effect has been reported in the retina, where local computations in the dendritic trees of amacrine cells were not reflected in the activity in the soma (Grimes et al., 2010). Visual processing in the optic tectum is generally thought to predominantly take place within the neuropil (Nevin et al., 2010). Our findings suggest that in order to understand how visual information is processed by the optic tectum, it is important to study how information about visual features is represented in the neuropil.

## 5.6.4 Nonlinear integration in the optic tectum

Here, we demonstrated that tectal neurons can process multiple local object features. To determine how information about these features is integrated in the optic tectum we calculated an informative index value. Our results indicate that spatial integration in the optic tectum is highly sublinear and might be approximated by MAX pooling (Figure 5). Other mechanisms, however, e.g., average pooling, also need to be considered in order to conclusively determine how spatial information is integrated within the optic tectum. Moreover, additional factors, such as the temporal components of the stimulus may influence the response to the composite feature. It is also possible, that different cell types may perform different types of pooling. These factors have not been taken into account here; however, future research should be aimed at addressing these questions. This is particularly important in light of the observation that on average, acute angles evoked stronger responses: Assuming that all stimuli are positioned within the RF centre, this preference is at odds with MAX pooling.

Nonlinear integration has been proposed to occur at various stages of the visual pathway in mammals. In the primate retina, a population of retinal ganglion cells exhibits nonlinear integration of spatial information (Schwartz et al., 2012; Turner and Rieke, 2016). In addition, extreme forms of nonlinear summation such as MAX pooling have been observed in V1 complex cells (Lampl et al., 2004). Theoretical studies suggest that MAX pooling might be (i) optimal for sparsely distributed features in the visual input; (ii) good for compact representations of the visual input; (iii) used to decrease the number of sequential neural computations, and (iv) used to increase the robustness to withstand noise (Boureau et al., 2010).

The zebrafish optic tectum performs many neural computations, such as object localisation, motion direction and speed estimation. However, these computations require precise object position information in the retinotopic map (Johnston and Lagnado, 2015) and the massively overlapping and large RFs of tectal neurons might limit such precision. In addition, multiple objects (or multiple object features) typically enter and exit the RFs of tectal neurons at the same time. MAX pooling could potentially provide a strategy to overcome these constraints.

## Author contributions

**KB**, Conception and design, Acquisition of data, Analysis and interpretation of data, drafting or revising the manuscript;

**YN**, Acquisition of data;

**AN**, Conception and design, Acquisition of data, Analysis and interpretation of data, drafting or revising the manuscript.

# References

Abbas, F., Triplett, M.A., Goodhill, G.J., Meyer, M.P., 2017. A Three-Layer Network Model of Direction Selective Circuits in the Optic Tectum. Front. Neural Circuits 11.

Andersson, M.Å., Ek, F., Olsson, R., 2015. Using visual lateralization to model learning and memory in zebrafish larvae. Sci. Rep. 5, 8667.

Antinucci, P., Suleyman, O., Monfries, C., Hindges, R., 2016. Neural Mechanisms Generating Orientation Selectivity in the Retina. Curr. Biol. 26, 1802–1815.

Anzai, A., Peng, X., Van Essen, D.C., 2007. Neurons in monkey visual area V2 encode combinations of orientations. Nat. Neurosci. 10, 1313–1321.

Bass, S.L.S., Gerlai, R., 2008. Zebrafish (Danio rerio) responds differentially to stimulus fish: The effects of sympatric and allopatric predators and harmless fish. Behav. Brain Res. 186, 107–117.

Ben-Tov, M., Donchin, O., Ben-Shahar, O., Segev, R., 2015. Pop-out in visual search of moving targets in the archer fish. Nat. Commun. 6, 6476.

Ben-Tov, M., Kopilevich, I., Donchin, O., Ben-Shahar, O., Giladi, C., Segev, R., 2013. Visual receptive field properties of cells in the optic tectum of the archer fish. J. Neurophysiol. 110, 748–759.

Bergmann, K., Meza Santoscoy, P., Lygdas, K., Nikolaeva, Y., MacDonald, R.B., Cunliffe, V.T., Nikolaev, A., 2018. Imaging Neuronal Activity in the Optic Tectum of Late Stage Larval Zebrafish. J. Dev. Biol. 6, 6.

Bianco, I.H., Engert, F., 2015. Visuomotor Transformations Underlying Hunting Behavior in Zebrafish. Curr. Biol. 25, 831–846.

Boureau, Y.L., Ponce, J., Lecun, Y., 2010. A theoretical analysis of feature pooling in visual recognition. Presented at the 27th International Conference on Machine Learning, ICML 2010.

Burgess, H.A., Schoch, H., Granato, M., 2010. Distinct Retinal Pathways Drive Spatial Orientation Behaviors in Zebrafish Navigation. Curr. Biol. 20, 381–386.

Buske, C., Gerlai, R., 2011. Shoaling develops with age in Zebrafish (Danio rerio). Prog. Neuropsychopharmacol. Biol. Psychiatry 35, 1409–1415.

Del Bene, F., Wyart, C., Robles, E., Tran, A., Looger, L., Scott, E.K., Isacoff, E.Y., Baier, H., 2010. Filtering of Visual Information in the Tectum by an Identified Neural Circuit. Science 330, 669–673.

Dunn, T.W., Gebhardt, C., Naumann, E.A., Riegler, C., Ahrens, M.B., Engert, F., Del Bene, F., 2016. Neural circuits underlying visually evoked escapes in larval zebrafish. Neuron 89, 613–628.

Filosa, A., Barker, A.J., Dal Maschio, M., Baier, H., 2016. Feeding State Modulates Behavioral Choice and Processing of Prey Stimuli in the Zebrafish Tectum. Neuron 90, 596–608.

Gabriel, J.P., Trivedi, C.A., Maurer, C.M., Ryu, S., Bollmann, J.H., 2012. Layer-Specific Targeting of Direction-Selective Neurons in the Zebrafish Optic Tectum. Neuron 76, 1147–1160.

Gahtan, E., 2005. Visual Prey Capture in Larval Zebrafish Is Controlled by Identified Reticulospinal Neurons Downstream of the Tectum. J. Neurosci. 25, 9294–9303.

Gerlai, R., Fernandes, Y., Pereira, T., 2009. Zebrafish (Danio rerio) responds to the animated image of a predator: Towards the development of an automated aversive task. Behav. Brain Res. 201, 318–324.

Grama, A., Engert, F., 2012. Direction selectivity in the larval zebrafish tectum is mediated by asymmetric inhibition. Front. Neural Circuits 6.

Grimes, W.N., Zhang, J., Graydon, C.W., Kachar, B., Diamond, J.S., 2010. Retinal Parallel Processors: More than 100 Independent Microcircuits Operate within a Single Interneuron. Neuron 65, 873–885.

Haug, M.F., Biehlmaier, O., Mueller, K.P., Neuhauss, S.C., 2010. Visual acuity in larval zebrafish: behavior and histology. Front. Zool. 7, 8.

Hegdé, J., Essen, D.C.V., 2003. Strategies of shape representation in macaque visual area V2. Vis. Neurosci. 20, 313–328.

Hinz, C., Kobbenbring, S., Kress, S., Sigman, L., Müller, A., Gerlach, G., 2013. Kin recognition in zebrafish, Danio rerio, is based on imprinting on olfactory and visual stimuli. Anim. Behav., Including Special Section: Behavioural Plasticity and Evolution 85, 925–930.

Hinz, R.C., de Polavieja, G.G., 2017. Ontogeny of collective behavior reveals a simple attraction rule. Proc. Natl. Acad. Sci. U. S. A. 114, 2295–2300.

Hollmann, V., Lucks, V., Kurtz, R., Engelmann, J., 2015. Adaptation-induced modification of motion selectivity tuning in visual tectal neurons of adult zebrafish. J. Neurophysiol. jn.00568.2015.

Hunter, P.R., Lowe, A.S., Thompson, I.D., Meyer, M.P., 2013. Emergent Properties of the Optic Tectum Revealed by Population Analysis of Direction and Orientation Selectivity. J. Neurosci. 33, 13940–13945.

Johnston, J., Ding, H., Seibel, S.H., Esposti, F., Lagnado, L., 2014. Rapid mapping of visual receptive fields by filtered back projection: application to multi-neuronal electrophysiology and imaging. J. Physiol. 592, 4839–4854.

Johnston, J., Lagnado, L., 2015. General features of the retinal connectome determine the computation of motion anticipation. eLife 4.

Kassing, V., Engelmann, J., Kurtz, R., 2013. Monitoring of Single-Cell Responses in the Optic Tectum of Adult Zebrafish with Dextran-Coupled Calcium Dyes Delivered via Local Electroporation. PLoS ONE 8, e62846.

Lampl, I., Ferster, D., Poggio, T., Riesenhuber, M., Ferster, D., Poggio, T., 2004. Intracellular measurements of spatial integration and the MAX operation in complex cells of the cat primary visual cortex. J Neurophys 92, 2704–2713.

Lister, J.A., Robertson, C.P., Lepage, T., Johnson, S.L., Raible, D.W., 1999. nacre encodes a zebrafish microphthalmia-related protein that regulates neural-crest-derived pigment cell fate. Dev. Camb. Engl. 126, 3757–3767.

Lowe, A.S., Nikolaou, N., Hunter, P.R., Thompson, I.D., Meyer, M.P., 2013. A Systems-Based Dissection of Retinal Inputs to the Zebrafish Tectum Reveals Different Rules for Different Functional Classes during Development. J. Neurosci. 33, 13946–13956.

Muto, A., Ohkura, M., Abe, G., Nakai, J., Kawakami, K., 2013. Real-Time Visualization of Neuronal Activity during Perception. Curr. Biol. 23, 307–311.

Nevin, L.M., Robles, E., Baier, H., Scott, E.K., 2010. Focusing on optic tectum circuitry through the lens of genetics. BMC Biol. 8, 126.

Niell, C.M., Smith, S.J., 2005. Functional Imaging Reveals Rapid Development of Visual Response Properties in the Zebrafish Tectum. Neuron 45, 941–951. Nikolaou, N., Lowe, A.S., Walker, A.S., Abbas, F., Hunter, P.R., Thompson, I.D., Meyer, M.P., 2012. Parametric Functional Maps of Visual Inputs to the Tectum. Neuron 76, 317–324.

Preuss, S.J., Trivedi, C.A., vom Berg-Maurer, C.M., Ryu, S., Bollmann, J.H., 2014. Classification of Object Size in Retinotectal Microcircuits. Curr. Biol. 24, 2376–2385.

Ramdya, P., Engert, F., 2008. Emergence of binocular functional properties in a monocular neural circuit. Nat. Neurosci. 11, 1083–1090.

Reichenthal, A., Ben-Tov, M., Segev, R., 2018. Coding Schemes in the Archerfish Optic Tectum. Front. Neural Circuits 12.

Riesenhuber, M., Poggio, T., 1999. Hierarchical models of object recognition in cortex. Nat. Neurosci. 2, 1019–1025. https://doi.org/10.1038/14819

Rogers, L.J., Miles, F.A., 1972. Centrifugal control of the avian retina. V. Effects of lesions of the isthmo-optic nucleus on visual behaviour. Brain Res. 48, 147–156.

Rosenthal, G.G., Ryan, M.J., 2005. Assortative preferences for stripes in danios. Anim. Behav. 70, 1063–1066.

Sajovic, P., Levinthal, C., 1982a. Visual response properties of zebrafish tectal cells. Neuroscience 7, 2427–2440.

Sajovic, P., Levinthal, C., 1982b. Visual cells of zebrafish optic tectum: mapping with small spots. Neuroscience 7, 2407–2426.

Saverino, C., Gerlai, R., 2008. The social zebrafish: behavioral responses to conspecific, heterospecific, and computer animated fish. Behav. Brain Res. 191, 77–87.

Schwartz, G.W., Okawa, H., Dunn, F.A., Morgan, J.L., Kerschensteiner, D., Wong, R.O., Rieke, F., 2012. The spatial structure of a nonlinear receptive field. Nat. Neurosci. 15, 1572–1580.

Semmelhack, J.L., Donovan, J.C., Thiele, T.R., Kuehn, E., Laurell, E., Baier, H., 2014. A dedicated visual pathway for prey detection in larval zebrafish. eLife 3.

Simoncelli, E.P., Olshausen, B.A., 2001. Natural image statistics and neural representation. Annu. Rev. Neurosci. 24, 1193–1216.

Soto, F.A., Wasserman, E.A., 2014. Mechanisms of object recognition: what we have learned from pigeons. Front. Neural Circuits 8.

Temizer, I., Donovan, J.C., Baier, H., Semmelhack, J.L., 2015. A Visual Pathway for Looming-Evoked Escape in Larval Zebrafish. Curr. Biol. 25, 1823–1834.

Thompson, A.W., Scott, E.K., 2016. Characterisation of sensitivity and orientation tuning for visually responsive ensembles in the zebrafish tectum. Sci. Rep. 6, srep34887.

Turnell, E.R., Mann, K.D., Rosenthal, G.G., Gerlach, G., 2003. Mate Choice in Zebrafish (Danio rerio) Analyzed With Video-Stimulus Techniques. Biol. Bull. 205, 225–226.

Turner, M.H., Rieke, F., 2016. Synaptic Rectification Controls Nonlinear Spatial Integration of Natural Visual Inputs. Neuron 90, 1257–1271.

Wilson, H.R., Wilkinson, F., 2015. From orientations to objects: Configural processing in the ventral stream. J. Vis. 15, 4–4.

Zhang, M., Liu, Y., Wang, S. -z., Zhong, W., Liu, B. -h., Tao, H.W., 2011. Functional Elimination of Excitatory Feedforward Inputs Underlies Developmental Refinement of Visual Receptive Fields in Zebrafish. J. Neurosci. 31, 5460–5469.

# 6 Conclusions and perspectives

This PhD study investigated the visual response properties of neurons in the optic tectum, which is the main visual processing centre in zebrafish. Exploring these properties is central to better understanding the mechanisms of visual processing in the optic tectum of lower vertebrates. It employed a mixed approach of synchronised visual simulation and calcium imaging to explore the activity of tectal neurons in response to simple, moving stimuli. It was decided to conduct experiments on older larvae (14-21 dpf) because complex social and learning behaviours have been reported to emerge between two and four weeks of age. This was made possible by using a new transgenic zebrafish line (i.e., NBT:GCaMP3) in which the expression of the genetically encoded calcium indicator remained stable over time.

A custom set-up (protocol) was developed to conduct experiments in older zebrafish larvae aged 14-21 dpf. In the first part of this thesis, this set-up was employed to measure the spatial receptive fields of tectal neurons with small moving spots. Firstly, the results demonstrated that receptive fields sizes in the optic tectum of older larvae were relatively large and predominantly elongated along the horizontal dimension, which is consistent with previously reported findings in young larvae (9 dpf) and adult zebrafish. Secondly, it was confirmed that receptive field centres are organised retinotopically, both in the cell bodies, and in the neuropil. Thirdly, it was observed that receptive field sizes decrease drastically between 14 and 18 dpf. This suggested that receptive field development is not completed by 9 dpf as previously believed; instead, receptive field refinement continues beyond this age.

Based on the finding that receptive field sizes in the optic tectum of older larvae are relatively large, in the second part of this thesis, a new hypothesis was formulated that tectal neurons might process multiple local features (i.e., features smaller than their receptive field) simultaneously. To test how the optic tectum encodes local features, a set of small, moving oriented bars was used as stimuli. The results suggested that not only does the optic tectum encode local features but is also tuned to horizontal-oriented local stimuli. In addition, the same small bars were combined (in pairs of two) to create a set of different moving angles. This stimulus set was used to test whether the optic tectum exhibits tuning beyond local orientation selectivity. Indeed, the results demonstrated that tectal neurons exhibit preferential responses to certain combinations of orientations, i.e., angles. This suggests that the optic tectum

may extract information about complex shapes. Notably, the tectal neuropil displayed a preference for acute angles, which was particularly evident in its superficial layers. Next, it was tested how information about these multiple local features was integrated by tectal neurons. To do this a set of moving stimuli, consisting of simple features (i.e., lines and angles) and a composite feature (i.e. square) was used. The results demonstrated that the response to the composite feature was similar to the response evoked by the preferred simple feature, suggesting that local features are spatially integrated in a sublinear fashion.

The outcomes of the work presented in this thesis, add to our understanding of how visual information provided by the retina is processed within the optic tectum. Furthermore, observations made in this study also have implications for future research. In particular, the present study emphasises the importance of studying vision in older animals. While it was previously known that complex visual behaviours related to social interactions and learning emerge relatively late during zebrafish development, the findings presented here, suggest that further changes also occur on the functional level.

On another note, the work presented here illustrated the significance of studying how visual information is processed in the tectal neuropil. When comparing the responses of neuropil and cell bodies, some differences were observed, e.g., flashing bars and moving spots evoked robust responses in the tectal neuropil, but much less so in the cell bodies. Moreover, while cell bodies also showed preference for horizontal-oriented bars, local orientations overall appeared to be more evenly represented in the cell bodies and the preference for acute angles was not as pronounced. This finding suggested that the extent of visual processing in the optic tectum might not entirely be reflected in the activity of cell bodies. This can be explained by the strictly defined architecture of the optic tectum, where cell bodies are located outside the area where the majority of processing is thought to take place.

# 6.1 Future work

## 6.1.1 Tuning to local features

The results presented in Chapter 5 suggest that tectal neurons encode local features. The stimuli used to study local orientation tuning were smaller than the majority of tectal receptive fields. Although unlikely, positional effects might have caused the selectivity for certain orientations and angles, i.e., some stimuli might have been closer to the receptive field centre than others and, therefore, evoked stronger responses. Future experiments may include quick receptive field measurements to provide a direct comparison of RF size and shape with OS tuning properties.

The results presented in Chapter 5 also indicated that local features are integrated in a sublinear fashion. In this study, this has been tested only with one set of stimuli, which contained horizontal and vertical bars. However, evidence presented here suggested that horizontal bars evoke significantly higher responses than vertical bars. Therefore, one could assume that the observed effect does not represent sublinear tuning, but rather a simple orientation preference of tectal neurons towards horizontal bars. To exclude this possibility, future work may employ various sets of single and composite features, such as a circle, and individual arc segments of the circle, in different orientations.

It would also be of interest to compare angles, intersections and non-joint bars with the same orientation and lengths to test whether tuning to angles can be explained by the position and orientation of the vertex. Finally, it would be interesting to further explore if other features of visual input, such as contrast, spatial frequency or colour are also encoded locally.

# 7 Bibliography

Abbas, F., Triplett, M.A., Goodhill, G.J., Meyer, M.P., 2017. A Three-Layer Network Model of Direction Selective Circuits in the Optic Tectum. Front. Neural Circuits 11.

Ackman, J.B., Burbridge, T.J., Crair, M.C., 2012. Retinal waves coordinate patterned activity throughout the developing visual system. Nature 490, 219–225.

Adrian, E.D., Matthews, R., 1927. The action of light on the eye. J. Physiol. 63, 378–414.

Ahrens, M.B., Orger, M.B., Robson, D.N., Li, J.M., Keller, P.J., 2013. Whole-brain functional imaging at cellular resolution using light-sheet microscopy. Nat. Methods 10, 413–420.

Aizenberg, M., Schuman, E.M., 2011. Cerebellar-dependent learning in larval zebrafish. J. Neurosci. Off. J. Soc. Neurosci. 31, 8708–8712.

Akerboom, J., Chen, T.-W., Wardill, T.J., Tian, L., Marvin, J.S., Mutlu, S., Calderón, N.C., Esposti, F., Borghuis, B.G., Sun, X.R., Gordus, A., Orger, M.B., Portugues, R., Engert, F., Macklin, J.J., Filosa, A., Aggarwal, A., Kerr, R.A., Takagi, R., Kracun, S., Shigetomi, E., Khakh, B.S., Baier, H., Lagnado, L., Wang, S.S.-H., Bargmann, C.I., Kimmel, B.E., Jayaraman, V., Svoboda, K., Kim, D.S., Schreiter, E.R., Looger, L.L., 2012. Optimization of a GCaMP Calcium Indicator for Neural Activity Imaging. J. Neurosci. 32, 13819–13840.

Akerman, C.J., Cline, H.T., 2006. Depolarizing GABAergic conductances regulate the balance of excitation to inhibition in the developing retinotectal circuit in vivo. J. Neurosci. Off. J. Soc. Neurosci. 26, 5117–5130.

Andersson, M.Å., Ek, F., Olsson, R., 2015. Using visual lateralization to model learning and memory in zebrafish larvae. Sci. Rep. 5, 8667.

Antinucci, P., Suleyman, O., Monfries, C., Hindges, R., 2016. Neural Mechanisms Generating Orientation Selectivity in the Retina. Curr. Biol. 26, 1802–1815.

Antonini, A., Stryker, M.P., 1993. Development of individual geniculocortical arbors in cat striate cortex and effects of binocular impulse blockade. J. Neurosci. 13, 3549–3573.

Anzai, A., Peng, X., Van Essen, D.C., 2007. Neurons in monkey visual area V2 encode combinations of orientations. Nat. Neurosci. 10, 1313–1321.

Arenzana, F.J., Clemente, D., Sánchez-González, R., Porteros, Á., Aijón, J., Arévalo, R., 2005. Development of the cholinergic system in the brain and retina of the zebrafish. Brain Res. Bull., Evolution and Development of Nervous Systems 66, 421–425.

Baden, T., Berens, P., Franke, K., Román Rosón, M., Bethge, M., Euler, T., 2016. The functional diversity of retinal ganglion cells in the mouse. Nature, 529, pp. 345-350.

Badura, A., Sun, X.R., Giovannucci, A., Lynch, L.A., Wang, S.S.H., 2014. Fast calcium sensor proteins for monitoring neural activity. Neurophotonics 1,

Baier, H., 2013. Synaptic Laminae in the Visual System: Molecular Mechanisms Forming Layers of Perception. Annu. Rev. Cell Dev. Biol. 29, 385–416.

Balboa, R.M., Grzywacz, N.M., 2003. Power spectra and distribution of contrasts of natural images from different habitats. Vision Res. 43, 2527–2537.

Barlow, H.B., 2001. Feature detectors, in: The MIT Encyclopedia of the Cognitive Sciences. MIT Press, pp. 311–414.

Barlow, H.B., 1953. Summation and inhibition in the frog's retina. J. Physiol. 119, 69–88.

Barlow, H.B., Hill, R.M., Levick, W.R., 1964. Retinal ganglion cells responding selectively to direction and speed of image motion in the rabbit. J. Physiol. 173, 377–407.

Bass, S.L.S., Gerlai, R., 2008. Zebrafish (Danio rerio) responds differentially to stimulus fish: The effects of sympatric and allopatric predators and harmless fish. Behav. Brain Res. 186, 107–117.

Behrens, U., Wagner, H.-J., 2004. Terminal nerve and vision. Microsc. Res. Tech. 65, 25–32.

Ben Fredj, N., Hammond, S., Otsuna, H., Chien, C.-B., Burrone, J., Meyer, M.P., 2010. Synaptic activity and activity-dependent competition regulates axon arbor maturation, growth arrest, and territory in the retinotectal projection. J. Neurosci. Off. J. Soc. Neurosci. 30, 10939–10951.

Ben-Tov, M., Donchin, O., Ben-Shahar, O., Segev, R., 2015. Pop-out in visual search of moving targets in the archer fish. Nat. Commun. 6, 6476.

Ben-Tov, M., Kopilevich, I., Donchin, O., Ben-Shahar, O., Giladi, C., Segev, R., 2013. Visual receptive field properties of cells in the optic tectum of the archer fish. J. Neurophysiol. 110, 748–759.

Bergmann, K., Meza Santoscoy, P., Lygdas, K., Nikolaeva, Y., MacDonald, R.B., Cunliffe, V.T., Nikolaev, A., 2018. Imaging Neuronal Activity in the Optic Tectum of Late Stage Larval Zebrafish. J. Dev. Biol. 6, 6.

Bianco, I.H., Engert, F., 2015. Visuomotor Transformations Underlying Hunting Behavior in Zebrafish. Curr. Biol. 25, 831–846.

Bianco, I.H., Kampff, A.R., Engert, F., 2011. Prey capture behavior evoked by simple visual stimuli in larval zebrafish. Front. Syst. Neurosci. 5, 101.

Bilotta, J., 2000. Effects of abnormal lighting on the development of zebrafish visual behavior. Behav. Brain Res. 116, 81–87.

Binns, K., Salt, T.., 1997. Post eye-opening maturation of visual receptive field diameters in the superior colliculus of normal- and dark-reared rats. Dev. Brain Res. 99, 263–266.

Bjartmar, L., Huberman, A.D., Ullian, E.M., Rentería, R.C., Liu, X., Xu, W., Prezioso, J., Susman, M.W., Stellwagen, D., Stokes, C.C., Cho, R., Worley, P., Malenka, R.C., Ball, S., Peachey, N.S., Copenhagen, D., Chapman, B., Nakamoto, M., Barres, B.A., Perin, M.S., 2006. Neuronal Pentraxins Mediate Synaptic Refinement in the Developing Visual System. J. Neurosci. 26, 6269–6281.

Blakemore, C., Cooper, G.F., 1970. Development of the Brain depends on the Visual Environment. Nature 228, 477–478.

Bloomfield, S.A., Völgyi, B., 2009. The diverse functional roles and regulation of neuronal gap junctions in the retina. Nat. Rev. Neurosci. 10, 495–506.

Bollmann, J.H., Engert, F., 2009. Subcellular Topography of Visually Driven Dendritic Activity in the Vertebrate Visual System. Neuron 61, 895–905.

Boureau, Y.L., Ponce, J., Lecun, Y., 2010. A theoretical analysis of feature pooling in visual recognition. Presented at the 27th International Conference on Machine Learning, ICML 2010.

Braastad, B.O., Heggelund, P., 1985. Development of spatial receptive-field organization and orientation selectivity in kitten striate cortex. J. Neurophysiol. 53, 1158–1178.

Brainard, D.H., 1997. The Psychophysics Toolbox. Spat. Vis. 10, 433–436.

Branchek, T., Bremiller, R., 1984. The development of photoreceptors in the zebrafish, Brachydanio rerio. I. Structure. J. Comp. Neurol. 224, 107–115.

Briggman, K.L., Helmstaedter, M., Denk, W., 2011. Wiring specificity in the direction-selectivity circuit of the retina. Nature 471, 183–188.

Bronchain, O.J., Hartley, K.O., Amaya, E., 1999. A gene trap approach in Xenopus. Curr. Biol. 9, 1195-S1. h

Burgess, H.A., Schoch, H., Granato, M., 2010. Distinct Retinal Pathways Drive Spatial Orientation Behaviors in Zebrafish Navigation. Curr. Biol. 20, 381–386.

Burrill, J.D., Easter, S.S., 1994. Development of the retinofugal projections in the embryonic and larval zebrafish (Brachydanio rerio). J. Comp. Neurol. 346, 583–600.

Buske, C., Gerlai, R., 2011. Shoaling develops with age in Zebrafish (Danio rerio). Prog. Neuropsychopharmacol. Biol. Psychiatry 35, 1409–1415.

Carandini, M., 2005. Do We Know What the Early Visual System Does? J. Neurosci. 25, 10577–10597.

Carrasco, M.M., Razak, K.A., Pallas, S.L., 2005. Visual Experience Is Necessary for Maintenance But Not Development of Receptive Fields in Superior Colliculus. J. Neurophysiol. 94, 1962–1970.

Chen, T.-W., Wardill, T.J., Sun, Y., Pulver, S.R., Renninger, S.L., Baohan, A., Schreiter, E.R., Kerr, R.A., Orger, M.B., Jayaraman, V., Looger, L.L., Svoboda, K., Kim, D.S., 2013. Ultrasensitive fluorescent proteins for imaging neuronal activity. Nature 499, 295–300.

Clark, D.T., 1981. Visual responses in the developing zebrafish (Brachydanio rerio). Univeristy of Oregon, Eugene, OR.

Cleland, B.G., Levick, W.R., Wässle, H., 1975. Physiological identification of a morphological class of cat retinal ganglion cells. J. Physiol. 248, 151–171.

Connaughton, V.P., Behar, T.N., Liu, W.-L.S., Massey, S.C., 1999. Immunocytochemical localization of excitatory and inhibitory neurotransmitters in the zebrafish retina. Vis. Neurosci. 16, 483–490.

Connaughton, V.P., Graham, D., Nelson, R., 2004. Identification and morphological classification of horizontal, bipolar, and amacrine cells within the zebrafish retina. J. Comp. Neurol. 477, 371–385.

Del Bene, F., Wyart, C., 2011. Optogenetics: A new enlightenment age for zebrafish neurobiology. Dev. Neurobiol. 72, 404–414.

Del Bene, F., Wyart, C., Robles, E., Tran, A., Looger, L., Scott, E.K., Isacoff, E.Y., Baier, H., 2010. Filtering of Visual Information in the Tectum by an Identified Neural Circuit. Science 330, 669–673.

Demski, L.S., Northcutt, R.G., 1983. The terminal nerve: a new chemosensory system in vertebrates? Science 220, 435–437.

Derrington, A.M., Fuchs, A.F., 1981. The development of spatial-frequency selectivity in kitten striate cortex. J. Physiol. 316, 1–10.

Desimone, R., Albright, T.D., Gross, C.G., Bruce, C., 1984. Stimulus-selective properties of inferior temporal neurons in the macaque. J. Neurosci. 4, 2051–2062.

Desimone, R., Schein, S.J., 1987. Visual properties of neurons in area V4 of the macaque: sensitivity to stimulus form. J. Neurophysiol. 57, 835–868.

Dhande, O.S., Huberman, A.D., 2014. Retinal ganglion cell maps in the brain: implications for visual processing. Curr. Opin. Neurobiol. 24, 133–142.

Dhande, O.S., Stafford, B.K., Lim, J.-H.A., Huberman, A.D., 2015. Contributions of Retinal Ganglion Cells to Subcortical Visual Processing and Behaviors. Annu. Rev. Vis. Sci. 1, 291–328.

Diamond, J.S., 2017. Inhibitory Interneurons in the Retina: Types, Circuitry, and Function. Annu. Rev. Vis. Sci. 3, 1–24.

Dorostkar, M.M., Dreosti, E., Odermatt, B., Lagnado, L., 2010a. Computational processing of optical measurements of neuronal and synaptic activity in networks. J. Neurosci. Methods 188, 141–150.

Dorostkar, M.M., Dreosti, E., Odermatt, B., Lagnado, L., 2010. Computational processing of optical measurements of neuronal and synaptic activity in networks. J. Neurosci. Methods 188, 141–150.

Dreosti, E., Lopes, G., Kampff, A.R., Wilson, S.W., 2015. Development of social behavior in young zebrafish. Front. Neural Circuits 9.

Dunn, T.W., Gebhardt, C., Naumann, E.A., Riegler, C., Ahrens, M.B., Engert, F., Del Bene, F., 2016. Neural circuits underlying visually evoked escapes in larval zebrafish. Neuron 89, 613–628.

Durán, E., Ocaña, F.M., Broglio, C., Rodríguez, F., Salas, C., 2010. Lateral but not medial telencephalic pallium ablation impairs the use of goldfish spatial allocentric strategies in a "hole-board" task. Behav. Brain Res. 214, 480–487.

Durán, E., Ocaña, F.M., Martín-Monzón, I., Rodríguez, F., Salas, C., 2014. Cerebellum and spatial cognition in goldfish. Behav. Brain Res. 259, 1–8.

Easter, J., Stephen S., Nicola, G.N., 1996. The Development of Vision in the Zebrafish (Danio rerio). Dev. Biol. 180, 646–663.

Emran, F., Rihel, J., Dowling, J.E., 2008. A behavioral assay to measure responsiveness of zebrafish to changes in light intensities. J. Vis. Exp. JoVE.

Engeszer, R.E., Barbiano, L.A.D., Ryan, M.J., Parichy, D.M., 2007. Timing and plasticity of shoaling behaviour in the zebrafish, Danio rerio. Anim. Behav. 74, 1269–1275.

Engström, K., 1960. Cone Types and Cone Arrangement in the Retina of Some Cyprinids. Acta Zool. 41, 277–295.

Enroth-Cugell, C., Robson, J.G., 1966. The contrast sensitivity of retinal ganglion cells of the cat. J. Physiol. 187, 517–552.

Enroth-Cugell, C., Robson, J.G., Schweitzer-Tong, D.E., Watson, A.B., 1983. Spatio-temporal interactions in cat retinal ganglion cells showing linear spatial summation. J. Physiol. 341, 279–307.

Esposti, F., Johnston, J., Rosa, J.M., Leung, K.-M., Lagnado, L., 2013. Olfactory Stimulation Selectively Modulates the OFF Pathway in the Retina of Zebrafish. Neuron 79, 97–110.

Euler, T., Haverkamp, S., Schubert, T., Baden, T., 2014. Retinal bipolar cells: elementary building blocks of vision. Nat. Rev. Neurosci. 15, 507–519.

Fadool, J.M., 2003. Development of a rod photoreceptor mosaic revealed in transgenic zebrafish. Dev. Biol. 258, 277–290.

Fagiolini, M., Pizzorusso, T., Berardi, N., Domenici, L., Maffei, L., 1994. Functional postnatal development of the rat primary visual cortex and the role of visual experience: dark rearing and monocular deprivation. Vision Res. 34, 709–720.

Famiglietti, E.V.J., Kaneko, A., Tachibana, M., 1977. Neuronal Architecture of On and Off Pathways to Ganglion Cells in Carp Retina. Sci. New Ser. 198, 1267–1269.

Feierstein, C.E., Portugues, R., Orger, M.B., 2015. Seeing the whole picture: A comprehensive imaging approach to functional mapping of circuits in behaving zebrafish. Neuroscience 296, 26–38.

Fetcho, J.R., Cox, K.J., O'Malley, D.M., 1998. Monitoring activity in neuronal populations with single-cell resolution in a behaving vertebrate. Histochem. J. 30, 153–167.

Filosa, A., Barker, A.J., Dal Maschio, M., Baier, H., 2016. Feeding State Modulates Behavioral Choice and Processing of Prey Stimuli in the Zebrafish Tectum. Neuron 90, 596–608.

Friedrich, R.W., Jacobson, G.A., Zhu, P., 2010. Circuit neuroscience in zebrafish. Curr. Biol. CB 20, R371-381.

Gabriel, J.P., Trivedi, C.A., Maurer, C.M., Ryu, S., Bollmann, J.H., 2012. Layer-Specific Targeting of Direction-Selective Neurons in the Zebrafish Optic Tectum. Neuron 76, 1147–1160.

Gahtan, E., 2005. Visual Prey Capture in Larval Zebrafish Is Controlled by Identified Reticulospinal Neurons Downstream of the Tectum. J. Neurosci. 25, 9294–9303.

Gallant, J.L., Connor, C.E., Rakshit, S., Lewis, J.W., Van Essen, D.C., 1996. Neural responses to polar, hyperbolic, and Cartesian gratings in area V4 of the macaque monkey. J. Neurophysiol. 76, 2718–2739.

Galli, L., Maffei, L., 1988. Spontaneous impulse activity of rat retinal ganglion cells in prenatal life. Science 242, 90–91.

Gaze, R.M., Keating, M.J., Chung, S.H., 1974. The Evolution of the Retinotectal Map during Development in Xenopus. Proc. R. Soc. B Biol. Sci. 185, 301–330.

Gerlai, R., 2014. Social behavior of zebrafish: From synthetic images to biological mechanisms of shoaling. J. Neurosci. Methods 234, 59–65.

Gerlai, R., Fernandes, Y., Pereira, T., 2009. Zebrafish (Danio rerio) responds to the animated image of a predator: Towards the development of an automated aversive task. Behav. Brain Res. 201, 318–324.

Gnuegge, L., Schmid, S., Neuhauss, S.C., 2001. Analysis of the activity-deprived zebrafish mutant macho reveals an essential requirement of neuronal activity for the development of a fine-grained visuotopic map. J. Neurosci. Off. J. Soc. Neurosci. 21, 3542–3548.

Godement, P., Salaün, J., Imbert, M., 1984. Prenatal and postnatal development of retinogeniculate and retinocollicular projections in the mouse. J. Comp. Neurol. 230, 552–575.

Gollisch, T., Meister, M., 2010. Eye Smarter than Scientists Believed: Neural Computations in Circuits of the Retina. Neuron 65, 150–164.

Goodale, M.A., Milner, A.D., 1992. Separate visual pathways for perception and action. Trends Neurosci. 15, 20–25.

Grama, A., Engert, F., 2012. Direction selectivity in the larval zebrafish tectum is mediated by asymmetric inhibition. Front. Neural Circuits 6.

Grienberger, C., Konnerth, A., 2012. Imaging Calcium in Neurons. Neuron 73, 862–885.

Grimes, W.N., Zhang, J., Graydon, C.W., Kachar, B., Diamond, J.S., 2010. Retinal Parallel Processors: More than 100 Independent Microcircuits Operate within a Single Interneuron. Neuron 65, 873–885.

Gross, C.G., Rocha-Miranda, C.E., Bender, D.B., 1972. Visual properties of neurons in inferotemporal cortex of the Macaque. J. Neurophysiol. 35, 96–111.

Guthrie, D.M., Banks, J.R., 1978. The receptive field structure of visual cells from the optic tectum of the freshwater perch (Perca fluviatilis). Brain Res. 141, 211–225.

Hartline, H.K., 1938. The response of single optic nerve fibers of the vertebrate eye to illumination of the retina. Am. J. Physiol.-Leg. Content 121, 400–415.

Hartline, H.K., 1940. The effects of spatial summation in the retina on the excitation of the fibers of the optic nerve. Am. J. Physiol.-Leg. Content 130, 700-711.

Hartline, H.K., Ratliff, F., 1958. Spatial summation of inhibitory influences in the eye of limulus, and the mutual interaction of receptor units. J. Gen. Physiol. 41, 1049–1066.

Haug, M.F., Biehlmaier, O., Mueller, K.P., Neuhauss, S.C., 2010. Visual acuity in larval zebrafish: behavior and histology. Front. Zool. 7, 8.

Hegdé, J., Essen, D.C.V., 2003. Strategies of shape representation in macaque visual area V2. Vis. Neurosci. 20, 313–328.

Hegdé, J., Felleman, D.J., 2007. Reappraising the Functional Implications of the Primate Visual Anatomical Hierarchy. The Neuroscientist 13, 416–421.

Helmstaedter, M., Briggman, K.L., Turaga, S.C., Jain, V., Seung, H.S., Denk, W., 2013. Connectomic reconstruction of the inner plexiform layer in the mouse retina. Nature 500, 168–174.

Hinz, C., Kobbenbring, S., Kress, S., Sigman, L., Müller, A., Gerlach, G., 2013. Kin recognition in zebrafish, Danio rerio, is based on imprinting on olfactory and visual stimuli. Anim. Behav., Including Special Section: Behavioural Plasticity and Evolution 85, 925–930.

Hinz, R.C., de Polavieja, G.G., 2017. Ontogeny of collective behavior reveals a simple attraction rule. Proc. Natl. Acad. Sci. U. S. A. 114, 2295–2300.

Hirsch, H.V.B., Spinelli, D.N., 1970. Visual Experience Modifies Distribution of Horizontally and Vertically Oriented Receptive Fields in Cats. Science 168, 869–871.

Hollmann, V., Lucks, V., Kurtz, R., Engelmann, J., 2015. Adaptation-induced modification of motion selectivity tuning in visual tectal neurons of adult zebrafish. J. Neurophysiol.

Holt, C.E., Harris, W.A., 1983. Order in the initial retinotectal map in Xenopus: a new technique for labelling growing nerve fibres. Nature 301, 150–152.

Horton, J.C., Hocking, D.R., 1996. An adult-like pattern of ocular dominance columns in striate cortex of newborn monkeys prior to visual experience. J. Neurosci. Off. J. Soc. Neurosci. 16, 1791–1807.

Hua, J.Y., Smear, M.C., Baier, H., Smith, S.J., 2005. Regulation of axon growth in vivo by activity-based competition. Nature 434, 1022–1026.

Huang, L., Maaswinkel, H., Li, L., 2005. Olfactoretinal centrifugal input modulates zebrafish retinal ganglion cell activity: a possible role for dopamine-mediated $Ca^{2+}$ signalling pathways: Olfacto-visual sensory integration. J. Physiol. 569, 939–948.

Hubel, D.H., 1959. Single unit activity in striate cortex of unrestrained cats. J. Physiol. 147, 226-238.2.

Hubel, D.H., Wiesel, T.N., 1968. Receptive fields and functional architecture of monkey striate cortex. J. Physiol. 195, 215–243.

Hubel, D.H., Wiesel, T.N., 1965. Receptive fields and functional architecture in two nonstriate visual areas (18 and 19) of the cat. J. Neurophysiol. 28, 229–289.

Hubel, D.H., Wiesel, T.N., 1963. Receptive fields of cells in striate cortex of very young, visually inexperienced kittens. J. Neurophysiol. 26, 994–1002.

Hubel, D.H., Wiesel, T.N., 1962. Receptive fields, binocular interaction and functional architecture in the cat's visual cortex. J. Physiol. 160, 106-154.2.

Hubel, D.H., Wiesel, T.N., 1959. Receptive fields of single neurones in the cat's striate cortex. J. Physiol. 148, 574–591.

Huberman, A.D., Feller, M.B., Chapman, B., 2008. Mechanisms Underlying Development of Visual Maps and Receptive Fields. Annu. Rev. Neurosci. 31, 479–509.

Hunter, P.R., Lowe, A.S., Thompson, I.D., Meyer, M.P., 2013. Emergent Properties of the Optic Tectum Revealed by Population Analysis of Direction and Orientation Selectivity. J. Neurosci. 33, 13940–13945.

Hunter, P.R., Lowe, A.S., Thompson, I.D., Meyer, M.P., 2013b. Emergent properties of the optic tectum revealed by population analysis of direction and orientation selectivity. J. Neurosci. Off. J. Soc. Neurosci. 33, 13940–13945.

Johnston, J., Ding, H., Seibel, S.H., Esposti, F., Lagnado, L., 2014. Rapid mapping of visual receptive fields by filtered back projection: application to multi-neuronal electrophysiology and imaging. J. Physiol. 592, 4839–4854.

Johnston, J., Lagnado, L., 2015. General features of the retinal connectome determine the computation of motion anticipation. eLife 4.

Jones, J.P., Palmer, L.A., 1987. The two-dimensional spatial structure of simple receptive fields in cat striate cortex. J. Neurophysiol. 58, 1187–1211.

Jusuf, P.R., Almeida, A.D., Randlett, O., Joubin, K., Poggi, L., Harris, W.A., 2011. Origin and Determination of Inhibitory Cell Lineages in the Vertebrate Retina. J. Neurosci. 31, 2549–2562.

Kalueff, A.V., Gebhardt, M., Stewart, A.M., Cachat, J.M., Brimmer, M., Chawla, J.S., Craddock, C., Kyzar, E.J., Roth, A., Landsman, S., Gaikwad, S., Robinson, K., Baatrup, E., Tierney, K., Shamchuk, A., Norton, W., Miller, N., Nicolson, T., Braubach, O., Gilman, C.P., Pittman, J., Rosemberg, D.B., Gerlai, R., Echevarria, D., Lamb, E., Neuhauss, S.C.F., Weng, W., Bally-Cuif, L., Schneider, H., 2013. Towards a Comprehensive Catalog of Zebrafish Behavior 1.0 and Beyond. Zebrafish 10, 70–86.

Kassing, V., Engelmann, J., Kurtz, R., 2013. Monitoring of Single-Cell Responses in the Optic Tectum of Adult Zebrafish with Dextran-Coupled Calcium Dyes Delivered via Local Electroporation. PLoS ONE 8.

Katz, L.C., Shatz, C.J., 1996. Synaptic Activity and the Construction of Cortical Circuits. Science 274, 1133.

Kim, C.K., Miri, A., Leung, L.C., Berndt, A., Mourrain, P., Tank, D.W., Burdine, R.D., 2014. Prolonged, brain-wide expression of nuclear-localized GCaMP3 for functional circuit mapping. Front. Neural Circuits 8.

Kimmel, C.B., 1993. Patterning the Brain of the Zebrafish Embryo. Annu. Rev. Neurosci. 16, 707–732.

Kleiner, M., Brainard, D., Pelli, D., Ingling, A., Murray, R., Broussard, C., 2007. What's new in psychtoolbox-3. Perception 36, 1–16.

Koch, S.M., Ullian, E.M., 2010. Neuronal Pentraxins Mediate Silent Synapse Conversion in the Developing Visual System. J. Neurosci. 30, 5404–5414.

Kuffler, S.W., 1953. Discharge patterns and functional organization of mammalian retina. J. Neurophysiol. 16, 37–68.

Lampl, I., Ferster, D., Poggio, T., Riesenhuber, M., Ferster, D., Poggio, T., 2004. Intracellular measurements of spatial integration and the MAX operation in complex cells of the cat primary visual cortex. J Neurophys 92, 2704–2713.

Lettvin, J., Maturana, H., McCulloch, W., Pitts, W., 1959. What the Frog's Eye Tells the Frog's Brain. Proc. IRE 47, 1940–1951.

Levick, W.R., 1967. Receptive fields and trigger features of ganglion cells in the visual streak of the rabbit's retina. J. Physiol. 188, 285–307.

Li, Y.N., Tsujimura, T., Kawamura, S., Dowling, J.E., 2012. Bipolar Cell-Photoreceptor Connectivity in the Zebrafish (Danio rerio) Retina. J. Comp. Neurol. 520, 3786–3802.

Lister, J.A., Robertson, C.P., Lepage, T., Johnson, S.L., Raible, D.W., 1999. nacre encodes a zebrafish microphthalmia-related protein that regulates neural-crest-derived pigment cell fate. Dev. Camb. Engl. 126, 3757–3767.

Lowe, A.S., Nikolaou, N., Hunter, P.R., Thompson, I.D., Meyer, M.P., 2013. A Systems-Based Dissection of Retinal Inputs to the Zebrafish Tectum Reveals Different Rules for Different Functional Classes during Development. J. Neurosci. 33, 13946–13956.

Maaswinkel, H., 2003. Olfactory input increases visual sensitivity in zebrafish: a possible function for the terminal nerve and dopaminergic interplexiform cells. J. Exp. Biol. 206, 2201–2209.

MacNeil, M.A., Heussy, J.K., Dacheux, R.F., Raviola, E., Masland, R.H., 1999. The shapes and numbers of amacrine cells: matching of photofilled with Golgi-stained cells in the rabbit retina and comparison with other mammalian species. J. Comp. Neurol. 413, 305–326.

MacNeil, M.A., Masland, R.H., 1998. Extreme diversity among amacrine cells: implications for function. Neuron 20, 971–982.

Mangrum, W.I., Dowling, J.E., Cohen, E.D., 2002. A morphological classification of ganglion cells in the zebrafish retina. Vis. Neurosci. 19, 767–779.

Masland, R.H., 2012a. The Neuronal Organization of the Retina. Neuron 76, 266–280.

Masland, R.H., 2012b. The tasks of amacrine cells. Vis. Neurosci. 29, 3–9.

Maturana, H.R., 1960. Anatomy and Physiology of Vision in the Frog (Rana pipiens). J. Gen. Physiol. 43, 129–175.

Maturana, H.R., Frenk, S., 1963. Directional Movement and Horizontal Edge Detectors in the Pigeon Retina. Science 142, 977–979.

McLaughlin, T., Torborg, C.L., Feller, M.B., O'Leary, D.D.M., 2003. Retinotopic Map Refinement Requires Spontaneous Retinal Waves during a Brief Critical Period of Development. Neuron 40, 1147–1160.

Mechler, F., Ringach, D.L., 2002. On the classification of simple and complex cells. Vision Res. 42, 1017–1033.

Meek, H.J., 1990. Tectal morphology: connections, neurones and synapses, in: Douglas, R.H., Djamgoz, M.B.A. (Eds.), The Visual System of Fish. Springer, Dordrecht, pp. 239–277.

Meyer, M.P., Smith, S.J., 2006. Evidence from In Vivo Imaging That Synaptogenesis Guides the Growth and Branching of Axonal Arbors by Two Distinct Mechanisms. J. Neurosci. 26, 3604–3614.

Mueller, T., 2012. What is the Thalamus in Zebrafish? Front. Neurosci. 6.

Mumm, J.S., Williams, P.R., Godinho, L., Koerber, A., Pittman, A.J., Roeser, T., Chien, C.-B., Baier, H., Wong, R.O.L., 2006. In Vivo Imaging Reveals Dendritic Targeting of Laminated Afferents by Zebrafish Retinal Ganglion Cells. Neuron 52, 609–621.

Muto, A., Ohkura, M., Abe, G., Nakai, J., Kawakami, K., 2013. Real-Time Visualization of Neuronal Activity during Perception. Curr. Biol. 23, 307–311.

Nakai, J., Ohkura, M., Imoto, K., 2001. A high signal-to-noise Ca2+ probe composed of a single green fluorescent protein. Nat. Biotechnol. 19, 137–141.

Nawrocki, L., Bremiller, R., Streisinger, G., Kaplan, M., 1985. Larval and adult visual pigments of the zebrafish, Brachydanio rerio. Vision Res. 25, 1569–1576.

Neuhauss, S.C.F., 2003. Behavioral genetic approaches to visual system development and function in zebrafish. J. Neurobiol. 54, 148–160.

Nevin, L.M., Robles, E., Baier, H., Scott, E.K., 2010. Focusing on optic tectum circuitry through the lens of genetics. BMC Biol. 8, 126.

Nevin, L.M., Taylor, M.R., Baier, H., 2008. Hardwiring of fine synaptic layers in the zebrafish visual pathway. Neural Develop. 3, 36.

Niell, C.M., Meyer, M.P., Smith, S.J., 2004. In vivo imaging of synapse formation on a growing dendritic arbor. Nat. Neurosci. 7, 254–260.

Niell, C.M., Smith, S.J., 2005. Functional Imaging Reveals Rapid Development of Visual Response Properties in the Zebrafish Tectum. Neuron 45, 941–951.

Niell, C.M., Stryker, M.P., 2008. Highly Selective Receptive Fields in Mouse Visual Cortex. J. Neurosci. Off. J. Soc. Neurosci. 28, 7520–7536.

Nikolaou, N., Lowe, A.S., Walker, A.S., Abbas, F., Hunter, P.R., Thompson, I.D., Meyer, M.P., 2012. Parametric Functional Maps of Visual Inputs to the Tectum. Neuron 76, 317–324.

Nikolaou, N., Meyer, M.P., 2015. Lamination Speeds the Functional Development of Visual Circuits. Neuron 88, 999–1013.

Northcutt, R.G., Wullimann, M.F., 1988. The Visual System in Teleost Fishes: Morphological Patterns and Trends, in: Atema, J., Fay, R.R., Popper, A.N., Tavolga, W.N. (Eds.), Sensory Biology of Aquatic Animals. Springer New York, New York, NY, pp. 515–552.

Ohkura, M., Sasaki, T., Sadakari, J., Gengyo-Ando, K., Kagawa-Nagamura, Y., Kobayashi, C., Ikegaya, Y., Nakai, J., 2012. Genetically Encoded Green Fluorescent Ca2+ Indicators with Improved Detectability for Neuronal Ca2+ Signals. PLOS ONE 7, e51286.

Olt, J., Allen, C.E., Marcotti, W., 2016. In vivo physiological recording from the lateral line of juvenile zebrafish. J. Physiol. 594, 5427–5438.

Ott, M., Walz, B.C., Paulsen, U.J., Mack, A.F., Wagner, H.-J., 2007. Retinotectal ganglion cells in the zebrafish, Danio rerio. J. Comp. Neurol. 501, 647–658.

Pelli, D.G., 1997. The VideoToolbox software for visual psychophysics: transforming numbers into movies. Spat. Vis. 10, 437–442.

Perrett, D.I., Rolls, E.T., Caan, W., 1982. Visual neurones responsive to faces in the monkey temporal cortex. Exp. Brain Res. 47, 329–342.

Pinelli, C., D'Aniello, B., Sordino, P., Meyer, D.L., Fiorentino, M., Rastogi, R.K., 2000. Comparative immunocytochemical study of FMRFamide neuronal system in the brain of Danio rerio and Acipenser ruthenus during development. Dev. Brain Res. 119, 195–208.

Pitts, W., McCulloch, W.S., 1947. How we know universals the perception of auditory and visual forms. Bull. Math. Biophys. 9, 127–147.

Portavella, M., Vargas, J.., Torres, B., Salas, C., 2002. The effects of telencephalic pallial lesions on spatial, temporal, and emotional learning in goldfish. Brain Res. Bull. 57, 397–399.

Preuss, S.J., Trivedi, C.A., vom Berg-Maurer, C.M., Ryu, S., Bollmann, J.H., 2014. Classification of Object Size in Retinotectal Microcircuits. Curr. Biol. 24, 2376–2385.

Rakic, P., 1976. Prenatal genesis of connections subserving ocular dominance in the rhesus monkey. Nature 261, 467–471.

Ramdya, P., Engert, F., 2008. Emergence of binocular functional properties in a monocular neural circuit. Nat. Neurosci. 11, 1083–1090.

Reichenthal, A., Ben-Tov, M., Segev, R., 2018. Coding Schemes in the Archerfish Optic Tectum. Front. Neural Circuits 12.

Ringach, D.L., 2004. Mapping receptive fields in primary visual cortex: Mapping receptive fields in primary visual cortex. J. Physiol. 558, 717–728.

Roberts, A.C., Bill, B.R., Glanzman, D.L., 2013. Learning and memory in zebrafish larvae. Front. Neural Circuits 7.

Robles, E., 2017. The power of projectomes: genetic mosaic labeling in the larval zebrafish brain reveals organizing principles of sensory circuits. J. Neurogenet. 31, 61–69.

Robles, E., Filosa, A., Baier, H., 2013. Precise Lamination of Retinal Axons Generates Multiple Parallel Input Pathways in the Tectum. J. Neurosci. 33, 5027–5039.

Robles, E., Laurell, E., Baier, H., 2014. The Retinal Projectome Reveals Brain-Area-Specific Visual Representations Generated by Ganglion Cell Diversity. Curr. Biol. 24, 2085–2096.

Rodieck, R.W., Stone, J., 1965a. Analysis of receptive fields of cat retinal ganglion cells. J. Neurophysiol. 28, 833–849.

Rodieck, R.W., Stone, J., 1965b. Response of cat retinal ganglion cells to moving visual patterns. J. Neurophysiol. 28, 819–832.

Rogers, L.J., Miles, F.A., 1972. Centrifugal control of the avian retina. V. Effects of lesions of the isthmo-optic nucleus on visual behaviour. Brain Res. 48, 147–156.

Rombough, P., 2002. Gills are needed for ionoregulation before they are needed for $O_2$ uptake in developing zebrafish, Danio rerio. J. Exp. Biol. 205, 1787–1794.

Rosenthal, G.G., Ryan, M.J., 2005. Assortative preferences for stripes in danios. Anim. Behav. 70, 1063–1066.

Roska, B., Meister, M., 2014. The Retina Dissects the Visual Scene into Distinct Features, in: Werner, J.S., Chalupa, L.M. (Eds.), The New Visual Neurosciences. MIT Press, Cambridge, MA, pp. 163–182.

Ruthazer, E.S., Cline, H.T., 2004. Insights into activity-dependent map formation from the retinotectal system: A middle-of-the-brain perspective. J. Neurobiol. 59, 134–146.

Sajovic, P., Levinthal, C., 1982a. Visual cells of zebrafish optic tectum: mapping with small spots. Neuroscience 7, 2407–2426.

Sajovic, P., Levinthal, C., 1982b. Visual response properties of zebrafish tectal cells. Neuroscience 7, 2427–2440.

Sanes, D.H., Constantine-Paton, M., 1985. The sharpening of frequency tuning curves requires patterned activity during development in the mouse, Mus musculus. J. Neurosci. 5, 1152–1166.

Sanes, J.R., Zipursky, S.L., 2010. Design Principles of Insect and Vertebrate Visual Systems. Neuron 66, 15–36. h

Saszik, S., Bilotta, J., 1999. The effects of temperature on the dark-adapted spectral sensitivity function of the adult zebrafish. Vision Res. 39, 1051–1058.

Saverino, C., Gerlai, R., 2008. The social zebrafish: behavioral responses to conspecific, heterospecific, and computer animated fish. Behav. Brain Res. 191, 77–87.

Schellart, N.A., Spekreijse, H., 1976. Shapes of receptive field centers in optic tectum of goldfish. Vision Res. 16, 1018–1020.

Schellart, N.A.M., 1990. The visual pathways and central non-tectal processing, in: Douglas, R.H., Djamgoz, M.B.A. (Eds.), The Visual System of Fish. Springer, Dordrecht, pp. 345–372.

Schindelin, J., Arganda-Carreras, I., Frise, E., Kaynig, V., Longair, M., Pietzsch, T., Preibisch, S., Rueden, C., Saalfeld, S., Schmid, B., Tinevez, J.-Y., White, D.J., Hartenstein, V., Eliceiri, K., Tomancak, P., Cardona, A., 2012. Fiji: an open-source platform for biological-image analysis. Nat. Methods 9, 676.

Schmidt, A., Bischof, H.-J., 2001. Neurons with complex receptive fields in the stratum griseum centrale of the zebra finch (Taeniopygia guttata castanotis Gould) optic tectum. J. Comp. Physiol. [A] 187, 913–924.

Schmidt, J.T., Buzzard, M., Borress, R., Dhillon, S., 2000. MK801 increases retinotectal arbor size in developing zebrafish without affecting kinetics of branch elimination and addition. J. Neurobiol. 42, 303–314.

Schmitt, E.A., Dowling, J.E., 1999. Early retinal development in the zebrafish, Danio rerio: Light and electron microscopic analyses. J. Comp. Neurol. 404, 515–536.

Schroeter, E.H., Wong, R.O.L., Gregg, R.G., 2006. In vivo development of retinal ON-bipolar cell axonal terminals visualized in nyx:MYFP transgenic zebrafish. Vis. Neurosci. 23, 833–843. h

Schwartz, G.W., Okawa, H., Dunn, F.A., Morgan, J.L., Kerschensteiner, D., Wong, R.O., Rieke, F., 2012. The spatial structure of a nonlinear receptive field. Nat. Neurosci. 15, 1572–1580.

Semmelhack, J.L., Donovan, J.C., Thiele, T.R., Kuehn, E., Laurell, E., Baier, H., 2014. A dedicated visual pathway for prey detection in larval zebrafish. eLife 3.

Shatz, C.J., Stryker, M.P., 1988. Prenatal tetrodotoxin infusion blocks segregation of retinogeniculate afferents. Science 242, 87–89.

Sherrington, C.S., 1906. The integrative action of the nervous system, The integrative action of the nervous system. Yale University Press, New Haven, CT, US.

Simon, D.K., O'Leary, D.D., 1992. Development of topographic order in the mammalian retinocollicular projection. J. Neurosci. 12, 1212–1232.

Simoncelli, E.P., Olshausen, B.A., 2001. Natural image statistics and neural representation. Annu. Rev. Neurosci. 24, 1193–1216.

Smear, M.C., Tao, H.W., Staub, W., Orger, M.B., Gosse, N.J., Liu, Y., Takahashi, K., Poo, M., Baier, H., 2007. Vesicular Glutamate Transport at a Central Synapse Limits the Acuity of Visual Perception in Zebrafish. Neuron 53, 65–77.

Song, P., Matsui, J., Dowling, J.E., 2008. Morphological Types and Connectivity of Horizontal Cells Found in the Adult Zebrafish (Danio rerio) Retina. J. Comp. Neurol. 506, 328–338.

Soto, F.A., Wasserman, E.A., 2014. Mechanisms of object recognition: what we have learned from pigeons. Front. Neural Circuits 8.

Strähle, U., Scholz, S., Geisler, R., Greiner, P., Hollert, H., Rastegar, S., Schumacher, A., Selderslaghs, I., Weiss, C., Witters, H., Braunbeck, T., 2012. Zebrafish embryos as an alternative to animal experiments—A commentary on the definition of the onset of protected life stages in animal welfare regulations. Reprod. Toxicol., Zebrafish Teratogenesis 33, 128–132.

Stuermer, C.A., 1988. Retinotopic organization of the developing retinotectal projection in the zebrafish embryo. J. Neurosci. 8, 4513–4530.

Sun, X.R., Badura, A., Pacheco, D.A., Lynch, L.A., Schneider, E.R., Taylor, M.P., Hogue, I.B., Enquist, L.W., Murthy, M., Wang, S.S.-H., 2013. Fast GCaMPs for improved tracking of neuronal activity. Nat. Commun. 4.

Tallini, Y.N., Ohkura, M., Choi, B.-R., Ji, G., Imoto, K., Doran, R., Lee, J., Plan, P., Wilson, J., Xin, H.-B., Sanbe, A., Gulick, J., Mathai, J., Robbins, J., Salama, G., Nakai, J., Kotlikoff, M.I., 2006. Imaging cellular signals in the heart in vivo: Cardiac expression of the high-signal Ca2+ indicator GCaMP2. Proc. Natl. Acad. Sci. U. S. A. 103, 4753–4758.

Tappeiner, C., Gerber, S., Enzmann, V., Balmer, J., Jazwinska, A., Tschopp, M., 2012. Visual acuity and contrast sensitivity of adult zebrafish. Front Zool, 9, p. 10

Tao, H.W., Poo, M., 2005. Activity-Dependent Matching of Excitatory and Inhibitory Inputs during Refinement of Visual Receptive Fields. Neuron 45, 829–836.

Tavazoie, S.F., Reid, R.C., 2000. Diverse receptive fields in the lateral geniculate nucleus during thalamocortical development. Nat. Neurosci. 3, 608–616.

Temizer, I., Donovan, J.C., Baier, H., Semmelhack, J.L., 2015. A Visual Pathway for Looming-Evoked Escape in Larval Zebrafish. Curr. Biol. 25, 1823–1834.

Thévenaz, P., Ruttimann, U.E., Unser, M., 1998. A pyramid approach to subpixel registration based on intensity. IEEE Trans. Image Process. Publ. IEEE Signal Process. Soc. 7, 27–41.

Thevenaz, P., Ruttimann, U.E., Unser, M., 1998. A pyramid approach to subpixel registration based on intensity. IEEE Trans. Image Process. 7, 27–41.

Thompson, A.W., Scott, E.K., 2016. Characterisation of sensitivity and orientation tuning for visually responsive ensembles in the zebrafish tectum. Sci. Rep. 6.

Tian, L., Hires, S.A., Mao, T., Huber, D., Chiappe, M.E., Chalasani, S.H., Petreanu, L., Akerboom, J., McKinney, S.A., Schreiter, E.R., Bargmann, C.I., Jayaraman, V., Svoboda, K., Looger, L.L., 2009. Imaging neural activity in worms, flies and mice with improved GCaMP calcium indicators. Nat. Methods 6, 875–881.

Tschetter, W.W., Govindaiah, G., Etherington, I.M., Guido, W., Niell, C.M., 2018. Refinement of Spatial Receptive Fields in the Developing Mouse Lateral Geniculate Nucleus Is Coordinated with Excitatory and Inhibitory Remodeling. J. Neurosci. 38, 4531–4542.

Turnell, E.R., Mann, K.D., Rosenthal, G.G., Gerlach, G., 2003. Mate Choice in Zebrafish (Danio rerio) Analyzed With Video-Stimulus Techniques. Biol. Bull. 205, 225–226.

Turner, M.H., Rieke, F., 2016. Synaptic Rectification Controls Nonlinear Spatial Integration of Natural Visual Inputs. Neuron 90, 1257–1271.

Ungerleider, L.G., Mishkin, M., 1982. Two cortical visual systems, in: Analysis of Visual Behaviour. MIT Press, Cambridge, MA, pp. 549–586.

Valente, A., Huang, K.-H., Portugues, R., Engert, F., 2012. Ontogeny of classical and operant learning behaviors in zebrafish. Learn. Mem. 19, 170–177.

Vanegas, H., Ito, H., 1983. Morphological aspects of the teleostean visual system: A review. Brain Res. Rev. 6, 117–137.

Verhaal, J., Luksch, H., 2013. Mapping of the Receptive Fields in the Optic Tectum of Chicken (Gallus gallus) Using Sparse Noise. PLOS ONE 8, e60782.

Vihtelic, T.S., Doro, C.J., Hyde, D.R., 1999. Cloning and characterization of six zebrafish photoreceptor opsin cDNAs and immunolocalization of their corresponding proteins. Vis. Neurosci. 16, 571–585.

Wang, L., Sarnaik, R., Rangarajan, K., Liu, X., Cang, J., 2010. Visual Receptive Field Properties of Neurons in the Superficial Superior Colliculus of the Mouse. J. Neurosci. 30, 16573–16584.

Wässle, H., 2004. Parallel processing in the mammalian retina. Nat. Rev. Neurosci. 5, 747–757.

Wässle, H., Yamashita, M., Greferath, U., Grünert, U., Müller, F., 1991. The rod bipolar cell of the mammalian retina. Vis. Neurosci. 7, 99–112.

Werblin, F.S., 2011. The retinal hypercircuit: a repeating synaptic interactive motif underlying visual function. J. Physiol. 589, 3691–3702.

Westfall, P.H., 2014. Kurtosis as Peakedness, 1905 − 2014. R.I.P. Am. Stat. 68, 191–195.

Wiesel, T.N., Hubel, D.H., 1963a. Effects of visual deprivation on morphology and physiology of cells in the cat's lateral geniculate body. J. Neurophysiol. 26, 978–993.

Wiesel, T.N., Hubel, D.H., 1963b. Single-cell responses in striate cortex of kittens deprived of vision in one eye. J. Neurophysiol. 26, 1003–1017.

Wilson, H.R., Wilkinson, F., 2015. From orientations to objects: Configural processing in the ventral stream. J. Vis. 15, 4–4.

Xiao, T., 2005. A GFP-based genetic screen reveals mutations that disrupt the architecture of the zebrafish retinotectal projection. Development 132, 2955–2967.

Yerkes, R.M., 1903. The instincts, habits and reactions of the frog. Psychol. Rev. Monogr. Suppl. 4, 579–638.

Zhang, M., Liu, Y., Wang, S. -z., Zhong, W., Liu, B. -h., Tao, H.W., 2011. Functional Elimination of Excitatory Feedforward Inputs Underlies Developmental Refinement of Visual Receptive Fields in Zebrafish. J. Neurosci. 31, 5460–5469.